KINETIC STUDY OF DROPLET SWELLING IN BOF STEELMAKING

KINETIC STUDY OF DROPLET SWELLING IN BOF STEELMAKING

BY

ELAINE (XIAO MING) CHEN, B.Eng., M.Sc.

A Thesis

Submitted to the School of Graduate Studies

in Partial Fulfillment of the Requirements

for the Degree

Doctor of Philosophy

McMaster University

DOCTOR OF PHILOSOPHY (2011) McMaster University

(Materials Science and Engineering) Hamilton, Ontario

TITLE: Kinetic Study of Droplet Swelling in BOF Steelmaking

AUTHOR: Elaine (X.M) Chen, B. Eng., (Northeastern University, China), M.Sc., (McMaster University, Canada)

SUPERVISOR: Professor Kenneth Coley

NUMBER OF PAGES: xii, 142

ABSTRACT

Considerable attention has been paid to the reaction between molten iron oxide containing slag and iron droplets or solid carbon due to the critical roles it plays in various metallurgical processes. However, during the last two decades, most of the studies have been carried out on iron droplets, for which the size remains constant. Another important phenomenon, that the droplet will swell has not been paid the same attention. Knowledge of the extent of droplet swelling is essential in predicting residence times in BOF steelmaking. The objective of this study is to develop the understanding for droplet swelling and produce a predictive model that predicts droplet swelling over the range of oxygen steelmaking conditions.

Several workers have observed swelling of high carbon droplets when exposed to oxidizing slags. In the present work, the measurements on swelling rates were made using X-ray fluoroscopy. Comparing the swelling rate with the total volume of gas evolved during the reaction, it is shown that only a small percentage of the gas generated is retained in the droplet to contribute to swelling. The gas generation rate is shown to be controlled by the rate of nucleation of CO bubbles inside the droplet. The critical supersaturation pressure for nucleation is found to be two orders of magnitude less than predicted from theory, which is in keeping with many other studies on nucleation of gases in liquids. However, the effect of surface tension, temperature and saturation pressure shows quantitative agreement with theory.

In order to predict the droplet swelling rate, CO bubble escape rate has to be known. In this research, the escape mechanism has been proposed; it is the film rupture around the iron droplet surface. The rupture rate is mainly influenced by viscosity, surface tension and bubble

size. For a given experimental condition, the calculated film thickness is 1.5 μm at the maximum drop diameter, assuming the bubble radius is 0.3 mm. The CO escape rate is 2.51 cm^3/s, it agrees well with 1 to 12 cm^3/s when gas escapes from steelmaking slags considering the differences of surface tensions and viscosities between metal and slag.

ACKNOWLEDGEMENTS

I am greatly indebted to my supervisor, Dr. Kenneth Coley for his guidance and encouragement throughout my master and PhD studies. I can't begin to describe my gratitude for the many learning opportunities that he provided me with. Professors Gordon Irons and Nikolas Provatas are greatly appreciated for their helpful suggestions as members of my supervisory committee.

I wish to thank many faculties, researchers, staff and graduate students in the department of Materials Science and Engineering for their assistance in the course of this work. I am particularly grateful to Dr. F. Z. Ji. I will always remember with gratitude the many times when he assisted in checking the experimental setup. A sincere note of gratitude is extended to Professor Mansoor Barati for his helpful discussions. The financial support of McMaster Steel Research Center and Natural Science and Engineering Research Council are gratefully acknowledged.

I am also grateful for the support and encouragement of my husband (Chun-Gang Kong) throughout my graduate study and thanks to my son (Xiang-Shen Kong) for his understanding.

This thesis is dedicated to my parents: Xian-Yong Chen and Yu-Qin Zhou.

TABLE OF CONTENTS

LISTS OF FIGURES

Chapter 1 Introduction

Chapter 2 Literature Review

Chapter 3 Experimental Works

Chapter 4 Reaction Kinetics of Metal Droplets and Slags

Chapter 5 Kinetic Model for Metal droplets and Slag Reactions

Chapter 6 Bubble Escape Rate

LISTS OF TABLES

Chapter 2 Literature Review

Chapter 3 Experimental Works

Chapter 4 Reaction Kinetics of Metal Droplets and Slags

Chapter 1

INTRODUCTION

1.1 Motivation for this study

Considerable attention has been paid to the reaction between molten iron oxide containing slag and iron droplets due to the critical roles it plays in various metallurgical processes. [1]-[23] In BOF steelmaking, the metal droplets are ejected into the slag layer from the metal bath, which creates a gas-slag-metal emulsion and thus generates large interfacial reaction areas that increases the refining rate greatly. [1]-[3] In the new bath smelting reduction processes, the quick reaction rate could be realized only at a huge amount of metal droplets ejected in the slag. [21]-[23] In electric arc furnace (EAF) steelmaking process, the reaction of metal droplets with slag causes slag foaming, which decreases heat losses and improved the heat transfer efficiency. [24][25] Driven by such important applications, extensive studies have been carried out on the kinetics for metal droplets reacting with iron oxide containing slags. The reaction between iron droplet and molten iron oxide containing slag can be expressed by reactions:

$$(Fe_2O_3)_{slag} + \underline{C} = 2(FeO)_{slag} + CO_{(gas)} \quad (1.1)$$

$$(FeO)_{slag} + \underline{C} = Fe + CO_{(gas)} \quad (1.2)$$

Using X-ray Fluoroscopy, Mulholland et al. [3] firstly observed a gas halo around metal droplet when it reacted with FeO containing slag, see the following Figure 1.1. The proposed possible rate determining steps could be in sequence:

1. Mass transfer of Fe^{2+} and O^{2-} in the liquid slag phase;
2. Chemical reaction at slag gas interface ($CO + FeO = Fe + CO_2$);
3. Gas phase transport in gas halo;
4. Chemical reaction at carbon gas interface ($CO_2 + C = 2CO$).

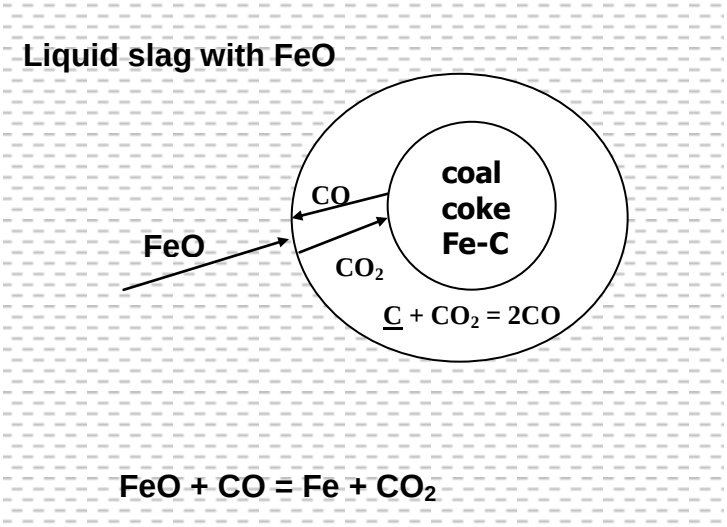

Figure 1.1 − Reaction Mechanism for Droplet with FeO containing slags.

Empirical equations and mathematical models have been established for each of these individual steps, which are well understood. However, another important phenomenon, the droplet will swell when it reacts with iron oxide containing slag has not been paid the same attention, see Figure 1.2.

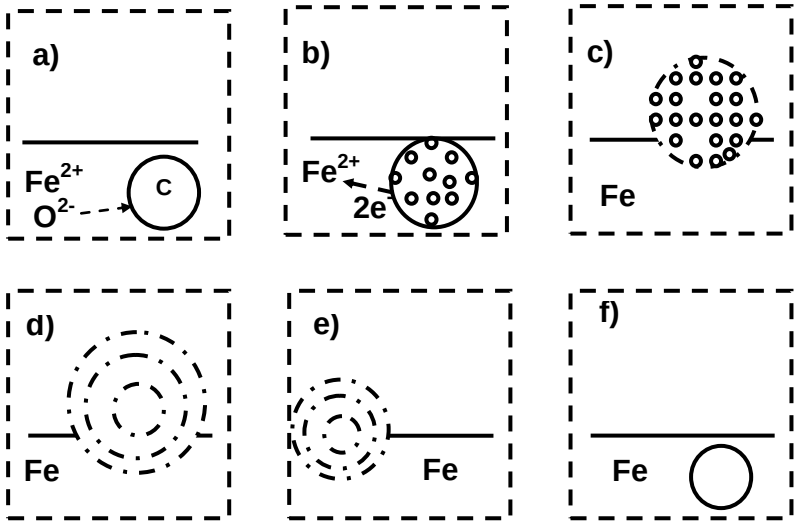

Figure 1.2 – Metal droplet swells during reaction.

The swelling of droplet is due to CO nucleation inside the metal droplets. Whether or not CO bubbles will nucleate inside the metal depends on the balance between the diffusion rate of oxygen transfer from the slag into the bulk of the metal and the rate of the mass transfer of carbon from the bulk to the surface. If the oxygen supply rate is higher than carbon diffusion rate, there is a possibility for CO nucleation inside the metal which causes droplet swelling.

Knowledge of the extent of droplet swelling is essential in predicting residence times in BOF steelmaking [26]-[27]. In BOF furnace, the number, size and residence time of droplets in the slag are critical factors which determine decarburization rate. Physical and mathematical models have been developed for the generation rate of droplets and their size distribution for BOF steelmaking process [28]-[31]. More recently, Brooks et al. [27] developed a model which predicts the trajectory and residence time of metal droplets in the slag considering the bloating of the droplets. They found that the trajectory of the droplets changed after they became bloated. The bloated droplets have less density, which prolongs the residence time of droplets in the slag and decreases the carbon content low enough before it returns to the metal bath.

By using an X-ray Fluoroscopy (XRF) Technique, Molloseau and Fruehan [14]-[15] observed that the droplet expanded and increased to maximum size of over 2 times its original diameter under critical conditions. Earlier works carried out by Meyer et al. [1] and Kozakevitch [2] showed the intensive swelling happened after 8 to 10 min blowing. Other works [17]-[19] also showed that the droplet sizes were more than the original ones. The swelling of droplets changes the droplet's trajectory in the slag and extends their residence time. However, to date, very few studies have been done on the measurement of swelling rate of the droplets in the slag, and there is insufficient data available to predict swelling rates. This is the motivation for this study.

1.2 Objectives of This Study

The overall objective of this study is to develop the understanding for droplet swelling and produce a predictive model that predicts droplet swelling over the range of oxygen steelmaking conditions. The detailed objectives are as follows:

(1) To obtain consistent kinetic data for the reaction over a range of experimental conditions (slag, metal compositions and temperatures);
(2) To understand the detailed mechanism for gas generation and escape from the metal droplets;
(3) To develop a comprehensive model that explains the measurements of the gas generate rate and droplets' swelling rate qualitatively and quantitatively.

1.3 Organization of the Thesis

The thesis of "Kinetic Study of Droplet Swelling in BOF Steelmaking" consists of literature review, experimental results and theoretical analysis on three parts: CO gas generation inside the metal, droplets swelling and gas escape from the metal. Chapter 1 describes the motivation for this study, the detailed objectives and organization of this thesis. Chapter 2 provides a review on the studies of the reaction between metal droplets and molten slags, including the reaction kinetics, and the studies on the swelling rates of metal droplets. Chapter 3 shows the experimental setup and the materials used in this

study. Chapter 4 is the experimental measurements on the reaction rates and the droplet's swelling rates. Based on the results, in Chapter 5, a mathematical model is derived for CO generation rate. Chapter 6 is the calculations on CO escape rate from the metal droplet. In chapter 7, a summary of findings is presented and some conclusions are obtained. The future works are also proposed. The raw data are given in Appendix A, the error analysis is shown in Appendix B, and a list of publications from the research work is provided in Appendix C.

Chapter 2

LITERATURE REVIEW

In this chapter, the first section introduces the decarburization reactions in BOF steelmaking furnace and the aspects related to the metal droplets, including their generation, size distribution and the residence time in the slag. The second deals with the metal droplets slag reaction kinetics and the influences of metal compositions on the reaction rate. The third section concerns the swelling of Fe-C-S droplets in the slag. The fourth part brief introduces the foaming behavior of slags. At last, it gives the summary on literatures and detailed objectives in this study.

2.1 Aspects of Metal Droplets in BOF Furnace

In BOF furnace, the decarburization happens mainly in three zones as shown in Figure 2.1 [25]: under the oxygen jet, in the gas-slag-metal emulsion and within the metal bath.

1. Directly under the oxygen jet;

$$\underline{C} + \frac{1}{2} O_2 = CO \quad (2.1)$$

$$\underline{C} + CO_2 = 2CO \quad (2.2)$$

2. In gas-slag-metal emulsion, foam, or at the slag-metal interface;

$$[Fe] + \frac{1}{2} O_2 = (FeO) \quad (2.3)$$

$$(FeO) + \underline{C} = [Fe] + CO \quad (2.4)$$

3. Within the metal bath;

$$\underline{C} + \underline{O} = CO \quad (2.5)$$

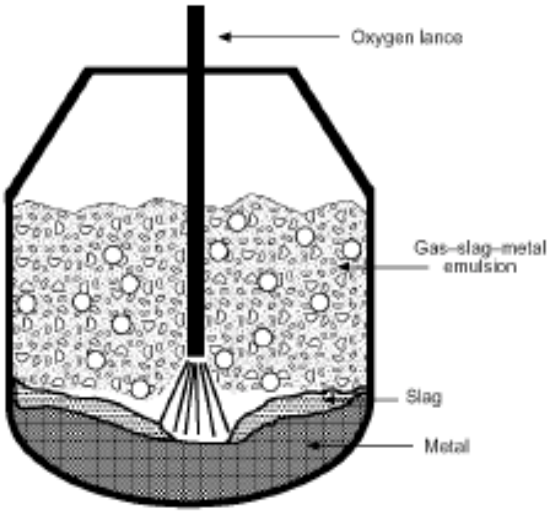

Figure 2.1 − Physical state of a refining period. [25]

There has been an argument among the workers about the significance of slag metal emulsion. Some workers [1][2] estimated about 60%-80% of decarburization was

done in slag metal emulsion, and carbon content was decreased to a very low value before returning to the bath, others argued only 20% of carbon was removed through the emulsion, and the reminder was in metal bath. Price [32] even did not believe that slag metal emulsion was a necessary condition for the removal of carbon. The significance of slag metal emulsion could be verified only after metal droplet's generation rate, size distribution and the residence time could be predicted. The number and size of the droplets determine the total interfacial area for the reaction, and residence time is the available time for the droplets to react with the slag.

2.1.1 Generation Rate of Metal Droplets

A gas jet impinging on a liquid surface, a depression forms in the liquid surface due to the momentum of the gas jet. The deflected gas flowing along the depression surface exerts a shear force on the liquid surface and drives the surface liquid flow. If the jet momentum is very slow, there is no droplet formed on the surface because the dense phase has a tendency of self adjustment to keep the force balance. If the gas flow rate is increased, droplets will be generated at the edge of the depression, see Figure 2.2 [33].

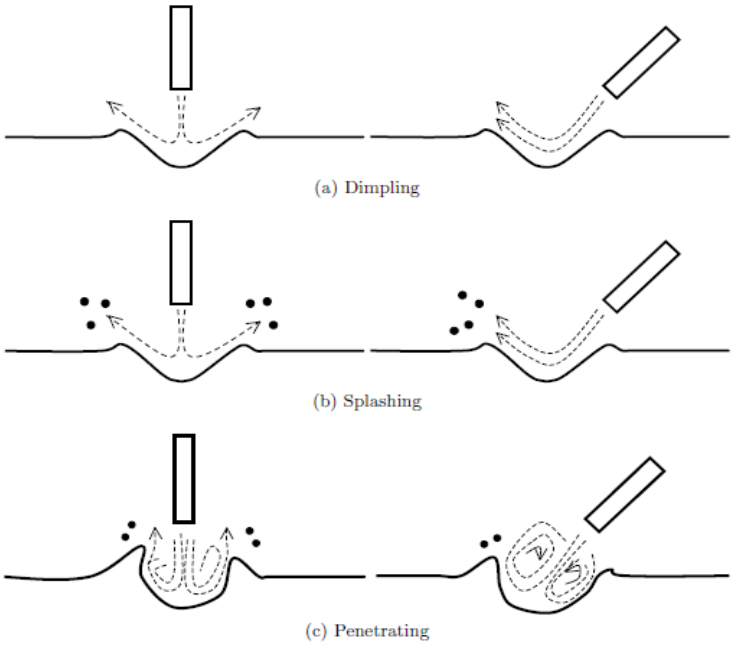

Figure 2.2 − Three depression patterns of vertical and declined jets (a) Dimpling stage: Shallow and stable depression (b) Splashing: droplet generation (c) Penetrating: reduced splashing and deeper cavity. [33]

There are two factors dominated the generation of droplet. One is external factor, which is the momentum intensity of the gas jet. Another factor is internal, which involves the properties of the liquid from which droplets are ejected, such as density, viscosity and surface tension. Noticing Weber number has the similarity criterion, He and Standish [30][31] used it to describe droplets generation rate. The web number is expressed by the following equation,

$$We = \frac{\rho_g u_G^2}{(\rho_l g \sigma)^{1/2}} \tag{2.6}$$

where:

We: nominal Weber number, represent a ratio of inertia forces to the square root of surface tension and buoyancy forces;

$u_{G:}$ jet velocity;

ρ_g, ρ_l: densities of gas and liquid, respectively; σ: surface tension.

Based on He and Standish's work, Li and Harris [34] predicted the onset of splashing according to Kelvin–Helmholtz instability criterion. The splashing occurs at $\frac{\rho_g u_G^{\ 2}}{2\sqrt{\rho_L g\sigma}} = 1$. The physical meaning of the left hand term of equation is how many times the critical Kelvin-Helmholtz instability criterion is exceeded, based on this observation, Subagyo et al. [28] named the dimensionless parameter N_B as the blowing number, which is used to describe the metal droplet generation, where, $N_B = \frac{\rho_G u_G^2}{2\sqrt{\sigma g \rho_L}}$. Figure 2.3 shows the droplet generation rate as a function of blowing number. Using an asymptotic solution approach, Subagyo et al. [28] derived the following empirical correlation:

$$\frac{R_B}{R_G} = \frac{(N_B)^{3.2}}{[2.6\times10^6 + 2.0\times10^{-4}(N_B)^{12}]^{0.2}} \tag{2.7}$$

Where: R_G is the volumetric flow of blown gas in normal cubic meters per seconds and R_B is the droplet generation rate.

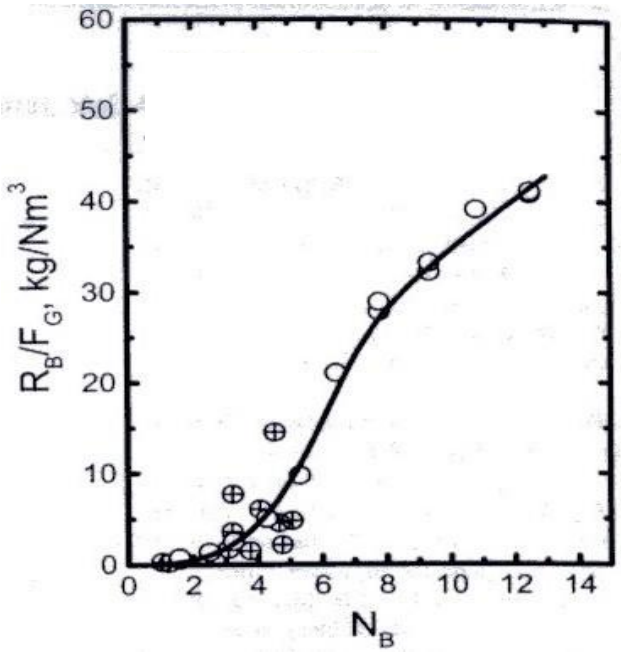

Figure 2.3 – Metal droplet generation rate as a function of blowing number. [28]

2.1.2 Size Distribution

Besides the knowledge of the amount of metal drops generated from the metal bath, the size distribution is also critical for the evaluation on the significance of gas slag metal emulsion. The size of drops produced due to interaction between an oxygen jet and molten pig iron has been studied by many investigators by collecting droplets either outside or inside of converter, or through experimental measurement. Table 1 gives the summary on droplet size distribution from different methods. [29]

Table 2.1 − Drop Size in BOF Steelmaking. [29]

Investigators	Experimental Technique	Sampling technique	Percentage of metal droplet to total metal, %	Droplet size, mm
Schoop et al.	Plant measurement (200t converter)	Bath sampling	1.0	0.05-2.0
Meyer et al.	Plant measurement (230t BOF)	Splashing sampling	6.8-78	0.15-3.36
Price	Plant measurement (90t converter)	Bath sampling	1-15	1.0-2.0
Kozakevitch	Plant measurement	Bath sampling	40	-
Koch et al.	Hot model, (6t converter)	Bath sampling	6.7-8t/s	0.3-0.5
Urguhart and Davenport	Laboratory study	Small scale (1/50) of BOF for hot model, and oil-water system for cold model	45% for water in emulsion, 50% for iron in emulsion	0.1-3.0
Standish and He	Cold model Experiment	Glycerine-Hg and water model	30% for Hg in emulsion	1-5
Turner and Jahanshahi	Cold model Experiment	Glycerol-Hg	25% for Hg in emulsion	-
Koria and Lange	Hot model experiment	Pig iron and oxygen blowing		0.04-70

Koria and Lange [35][36] designed a physical model to simulate the industrial converters. Their model met the requirement on the geometric and dynamic similarities. According to the experimental results, see Figure 2.4, they found that the size distribution

of metal droplets follows the Rosin-Rammler-Sperling (RRS) distribution function, $R = 100\exp[-(d/d')^n]\%$, Where: R: cumulative weight of drops retained on sieve with holes of diameter, %; d: upper limit of class diameter or drop size; d´: characteristic parameter of distribution function.

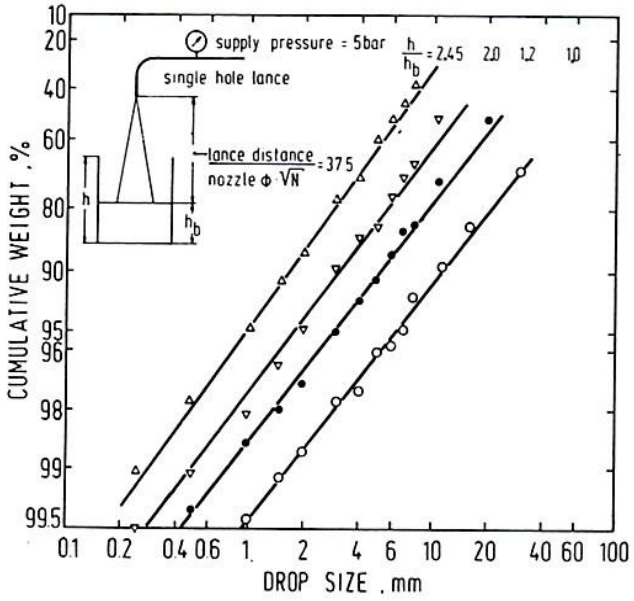

Figure 2.4 − Effect of the vessel height in relation to bath height on the sizes of experimental found drops and their distribution. [35]

Subagyo et al. [28] further developed an empirical equation for characteristic parameter of distribution based their experimental measurements, $d' = 12.0(N_B)^{0.82}$, where, N_B is blowing number. The empirical equation is in reasonable agreement with both Subagyo and Lange, see Figure 2.5.

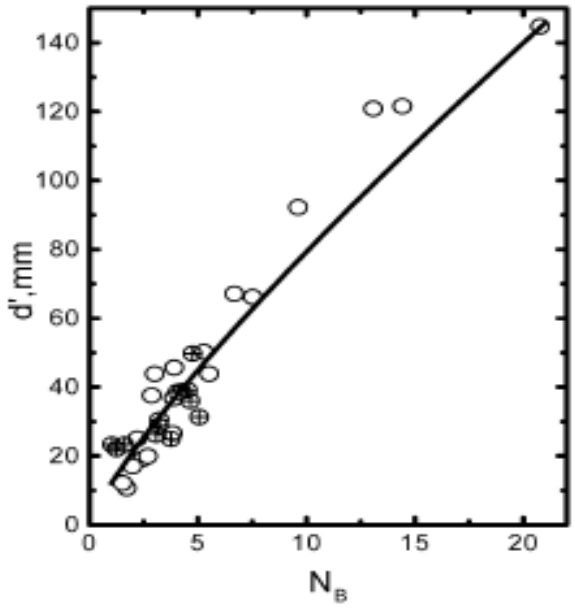

Figure 2.5 − The effect of the blowing number on the RRS distribution parameters of generated metal droplets. [28]

2.1.3 Residence Time

Discrepancies exist regarding the residence time of metal droplet in the slag, it changes from 0.25s to 120s. Price [32] estimated a value of 2 min ± 0.5 min by using of radioactive gold isotope tracer technique in an industrial scale converter. Kozakevitch [2] pointed out that the length of a droplet in the slag being probably less than 1.5 min. Urquhart et al. [37] observed the residence time was about 0.25s at their room temperature experiments. Considering the big discrepancies, Subagyo [26] tried to develop a mathematical model to predict the residence time of metal droplets in the emulsions based on the principles of accelerated moving bodies in a moving fluid. Their model did

not succeed because there was no consideration given on the chemical reaction inside the metal. More recently, Brooks et al. [27] continued their work and successfully predicted the residence time at different conditions. See Figure 2.6 and 2.7. The residence time is less than 1 second without consideration on the droplet's swelling. It could be prolonged to more than 60 seconds considering C and O chemical reaction inside the metal droplet, which causes the droplet's swelling. The swollen droplets have less density, which prolongs the residence time of droplets in the slag.

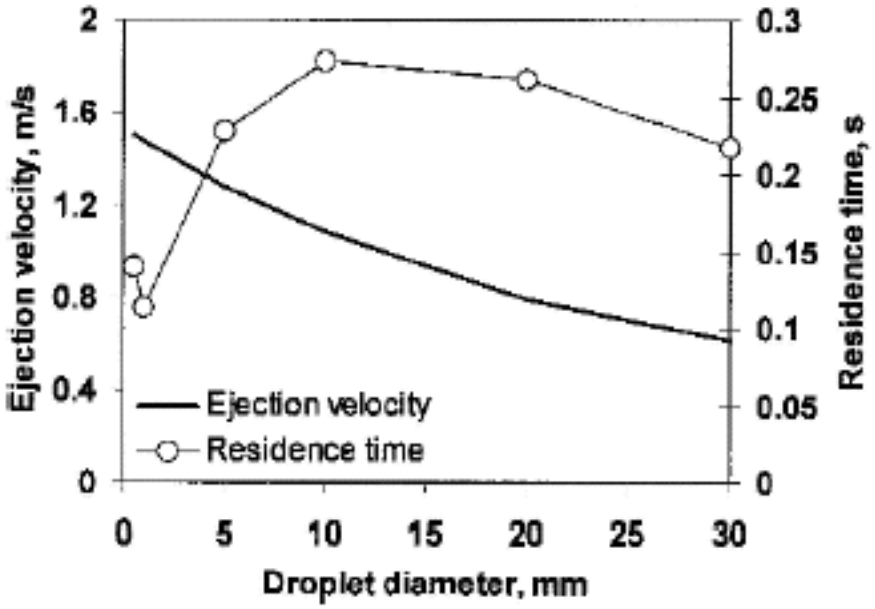

Figure 2.6 − The residence time for droplet without swelling.[27]

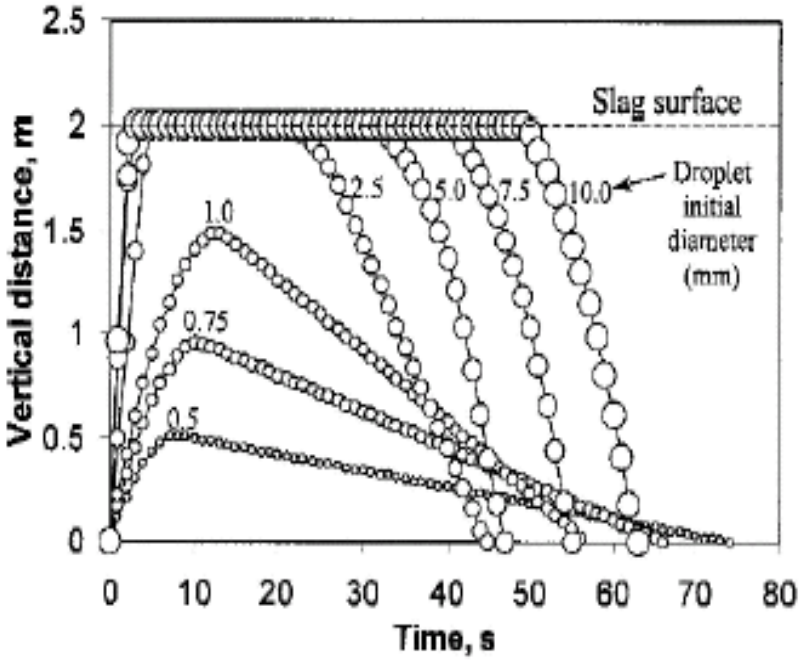

Figure 2.7 − The residence time of droplet with swelling. [27]

2.2 Metal Droplets Slag Reaction Kinetics

2.2.1 Mathematic Models for the Individual Rate Determining Steps

Using X-ray Fluoroscopy, Mulholland et al. [3] firstly observed a gas halo around metal droplet when it reacted with FeO containing slag, see Figure 1.1. Some workers regarded the gas layer around the droplet as continuous; others argued that it is discontinuous because of the poor wetting of gas bubbles by the metal. [7] Based on the proposed reaction mechanism, the possible rate determining steps are:

(1) mass transfer of Fe^{2+} and O^{2-} to gas slag interface;

(2) gas slag reaction: $CO + FeO = Fe + CO_2$;

(3) gas diffusion: diffusion of CO_2 away from gas slag interface to gas metal interface and diffusion of CO away from gas metal interface to gas slag interface;

(4) gas metal reaction: $CO_2 + \underline{C} = 2CO$

2.2.1.1 Liquid Phase Mass Transport Control

Paul et al. [20] concluded that, the reduction of FeO by carbon in liquid iron is controlled by mass transfer of FeO in the slag plus chemical reaction at gas metal interface in the case of slag containing mass contents of less than 5% FeO. Min et al. [21][22] also found that the rate-determining step is the mass transfer at a low FeO contents. Fruehan et al. [16] studied the reduction of FeO from smelting slag by solid carbon; they found that the reduction rate increased with the rotation speed of carbon rod. Their experiments were conducted using a rotating carbon rod immersed in a slag from the system $CaO\text{-}SiO_2\text{-}Al_2O_3\text{-}FeO$, where the content of FeO was less than 10 wt pct. They found that under these experimental conditions, the reaction rate increased with the content of FeO, and also increased with the rotation speed of the carbon rod at a given FeO content. The measured reaction rate ranged from, $3.25*10^{-7}$ $mol.cm^{-2}.s^{-1}$ at 2.1 pct

FeO under static conditions to $3.6*10^{-6}$ mol.cm^{-2}.s^{-1} at 9.5 pct FeO for a rotating rod experiment.

A mass transfer model was proposed, the mass transfer of FeO from the bulk of slag to the reaction site is the rate determining step,

$$J_{FeO} = \frac{m_s \rho_s A(pctFeO - pctFeO^S)}{100 mw_{FeO}} \quad (2.8)$$

where, m_s: mass transfer coefficient in the slag (cm/s);

ρ_s: density of the slag (g/cm^3);

A: emulsified droplet surface area (cm^2) at it becomes stable;

pct FeO: FeO content of the bulk slag;

pct FeO^S: FeO content at the droplet surface (approximately zero at this mechanism);

mw_{FeO}: molecular weight of FeO.

2.2.1.2 Gas Slag Interfacial Chemical Reaction

Gas slag interfacial chemical reaction has been paid many attentions; recently Coley's group [38] conducted the study on the reaction kinetics between CO-CO_2 and iron oxide containing slags. They found that the apparent rate depends on the slag composition, oxidation state and temperature, see Figure 2.8 and 2.9. The dependence on the oxidation state suggests that the rate determining step is the formation of single

charged CO_2^-. The mathematical equation has been developed, and it fits a wide range of experimental conditions.

$$k_a = 2.67\times10^{-4}(C_{Fe})^2 \frac{1}{x(1+x)^2}\exp(\frac{-(475.7-452.4\Lambda)}{RT}) \qquad (\text{mol.cm}^{-2}.\text{atm}^{-1}.\text{s}^{-1}) \qquad (2.9)$$

Where:

k_a: is the apparent rate constant;

C_{Fe} is the total iron concentration in the bulk in mol pct;

$x=Fe^{3+}/Fe^{2+}$;

Λ is the optical basicity of oxide.

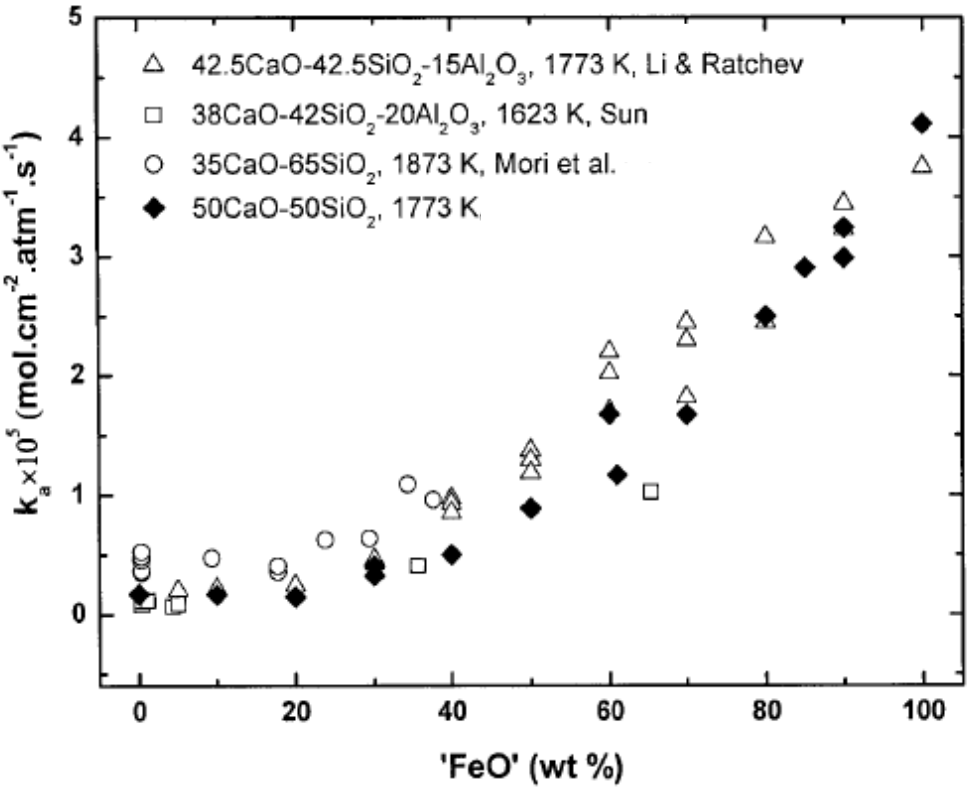

Figure 2.8 − Apparent rate constant of oxidation and reduction reaction as a function of iron oxide content at unit CO2/CO [38]

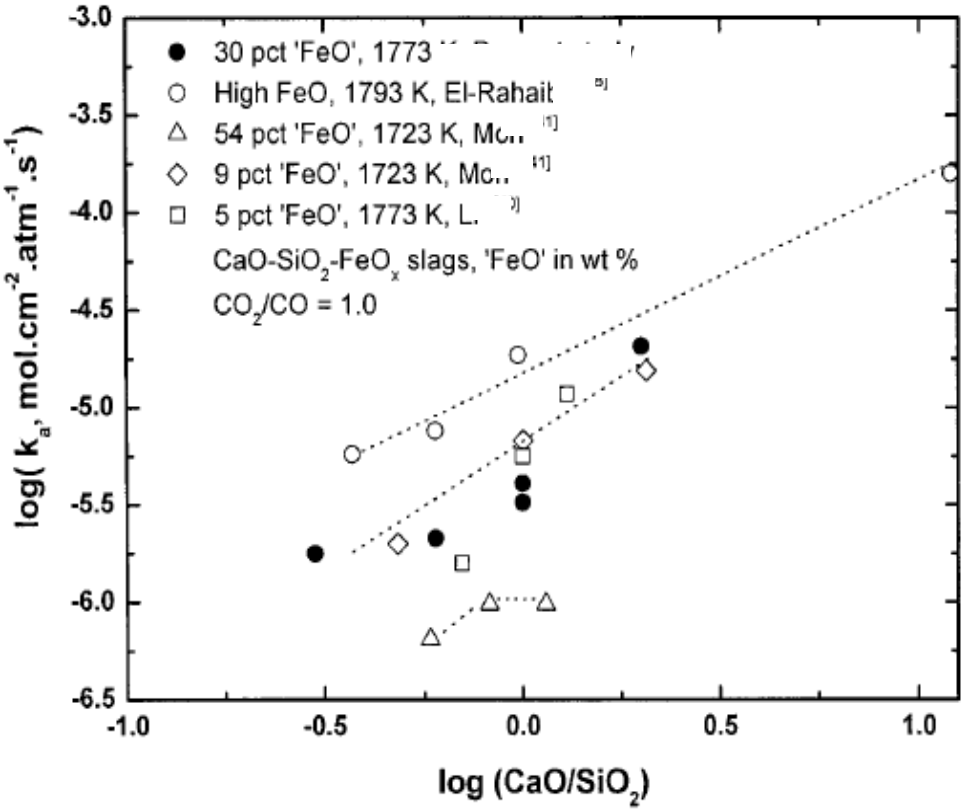

Figure 2.9 − Dependence of the apparent rate constant on the slag basicity at unit CO2/CO [38]

2.2.1.3 Gas Metal Reaction

Sain and Belton [39] measured the rate of the chemical reaction of CO_2 with carbon dissolved in liquid iron, i.e. decarburization of liquid iron. They eliminated the effect of mass transport in the gas by using very high gas flow rates (20-40 l/min), which forces the system into a regime of interfacial reaction control. They demonstrated that the surface active element, sulfur, decreased the reaction rate greatly and concluded that the dissociation of CO_2 was the rate controlling step. Later Cramb and Belton [40] measured

the rate of dissociation of CO_2 on liquid iron using a $^{14}CO_2$-CO isotope exchange method. The rates were similar to that for decaburization confirming that the dissociation of CO_2 was the rate controlling step. Mannion and Fruehan [41] confirmed Sain and Belton's findings, and also found similar effects with other surface active elements, such as, selenium, and tellurium. Min et al. [21] developed a rate equation to calculate the reaction rate,

$$Rate = k_{CO_2} A_m K_1 C[pctFeO] \tag{2.10}$$

where, k_{CO2} is the rate constant for reaction (2.2), mole/cm^2.s.atm,

A_m is surface area of metal drop,

K_1 is equilibrium constant for reaction (1.1),

C constant relating to pct FeO to the activity of FeO.

2.2.1.4 Gas diffusion

A gas halo is produced immediately after the injection of carbon or metal droplets. If its thickness is more than a few millimeter, it is possible that gas phase mass transfer is the rate determining step. [22] Min and Fruehan used the following equation to calculate the rate of CO_2 transfer in the gas halo, [21]

$$(CO_2)_{g\text{-}s} \rightarrow (CO_2)_{g\text{-}m}$$

$$J_{CO_2} = \frac{m_g}{RT} \ln \frac{1 + P^s_{CO_2}}{1 + P^m_{CO_2}} \tag{2.11}$$

where:

$(CO_2)_{g\text{-}s}$ and $(CO_2)_{g\text{-}m}$ are CO_2 at the gas-slag and the gas-metal interfaces, respectively. $P^m_{CO_2}$ and $P^s_{CO_2}$, are equilibrium CO_2 partial pressures of gas metal and gas slag reactions. m_g is the gas phase mass transfer coefficient.

Gas slag and gas metal reactions should be in equilibrium if the mass transfer of CO/CO_2 gas is the rate determining step. The value of m_g can be roughly estimated by,

$$m_g = \frac{D_{Diff}}{z}$$

Where,

z is the thickness of the gas halo (millimeter)

D_{Diff} is the diffusivity (cm^2/s)

Paramguru et al. estimated that the rate constant for gas diffusion is about $5*10^{-7}$ to 10^{-6} $mol.cm^{-2}.s^{-1}$ based on the assumption of a stagnant gas layer. [11]

2.2.2 Measurements on the Reaction Rates

Each of the individual rate determining steps has been studied by designing the experiments so that the reaction was forced into the control of the pre-determined mechanism. For example, the studies on the gas slag interfacial chemical reaction by isotope exchange method. As pioneers, Belton and his co-workers developed the application of the isotope exchange method in studying kinetics of gas-slag/metal reactions. In the last 3 decades, the technique has been employed to measure the

interfacial rate of CO or CO_2 dissociation on the surface of different slags and metals. These workers increased the gas flowrate high enough to eliminate the mass transfer as the rate limiting step. It becomes more complicated when the reaction rate determining step has not been pre-determined. The followings are the discussions on these measurements on the reaction rates.

Gare et al. [5] firstly used CVPI technique (Constant Volume Pressure Increase) to measure reduction rate of FeO from the slag. This technique involves the measurement of the pressure increase in a sealed reaction vessel caused by the evolution of CO gas. 1mole of CO produced equals to 1 mole of FeO reduced from slag, see reaction (1.1).

$$(FeO)_{slag} + \underline{C} = Fe_{(l)} + CO_{(gas)} \qquad (1.1)$$

The slag compositions used in their experiment were: $CaO/SiO_2/Al_2O_3$ = 47/38/15 with 13 wt % of total iron as FeO or Fe_2O_3. They measured the change of carbon content with time; the reduction rate was determined by calculating the slope of the curves. For 16.7% FeO slag, at T=1773K, the measured initial rate is 1.92×10^{-5} moles/s. Their experimental results are shown in table 2.2.

Table 2.2: Decarburization rates for metal-carbon droplets. [17]

Initial C, wt %	Temperature, K	Slag type	Decarburization rate	
			Fast external decarburization period (moles/s)	External-internal nucleation period (moles/s)
4.2	1773	Ferric	11.08×10^{-5}	2.3×10^{-5}
3.68	1813	Ferric	10.51×10^{-5}	1.8×10^{-5}
2.85	1813	Ferric	8.82×10^{-5}	1.6×10^{-5}
1.92	1813	Ferric	4.52×10^{-5}	1.0×10^{-5}
4.2	1773	Ferrous	1.92×10^{-5}	

Murthy et al. [17] also used this technique to determine the reaction rate of FeO reduction from similar slags, their slag compositions are: $47CaO\text{-}41SiO_2\text{-}12Al_2O_3$. This time they measured the total moles of CO produced during the reaction. See Figure 2.10 for their experimental results.

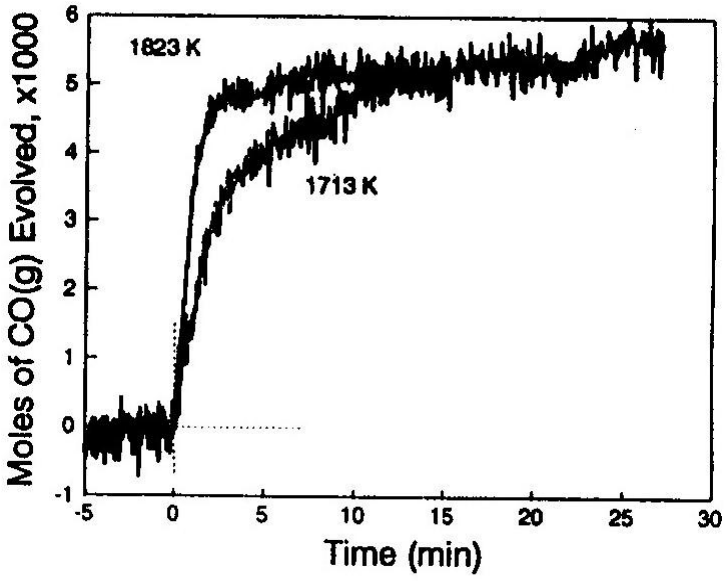

Figure 2.10 − The total moles of CO evolved with time for 8.1 wt pct FeO at T=1713K and 1823K. [17]

2.2.2.1 Effect of FeO content

Murthy et al. [17] found that the dependence of the reduction rate on FeO content is linear, $r = 0.1114+8.351 \times 10^{-3}$ (% FeO). Min [21] determined the reaction rate by measuring the instantaneous flow rate, also found the rate is proportional to the FeO content. See Figure 2.11 for the relationship between the rate constant and FeO content. The temperature is 1673K, $B = CaO/SiO_2 = 1$, [C] = 4.2%, [S] = 0.001%.

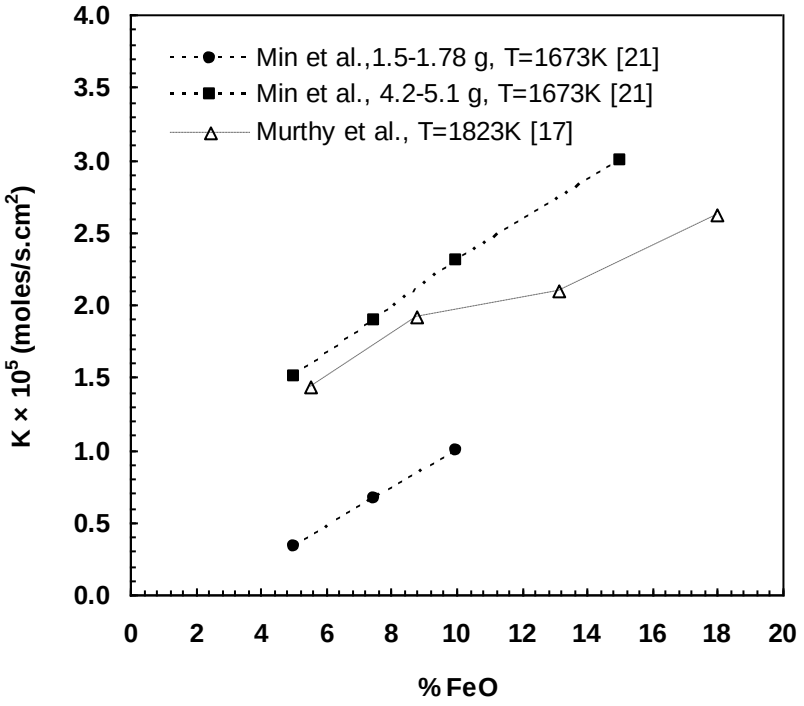

Figure 2.11 − The rate constant as a function of FeO content.

A different phenomenon was observed by Molloseau et al. [14][15] when they measured the rate of FeO reduction from steelmaking type slag, wt pct CaO/ pct SiO_2=1.2, MgO=12.0 wt pct, and FeO content from 3-35 wt pct. Figure 2.12 is a comparison of their experimental results with others. They found that the reduction rate increased by one order when FeO content is 10%, increased two orders when FeO is 20%. At 1713K, the initial rate was 3.3×10^{-6} moles/s for 3 wt pct FeO in the slag, it increased to 3.0×10^{-5} and 2.0×10^{-4} moles/s for 10 and 20 wt pct FeO, respectively.

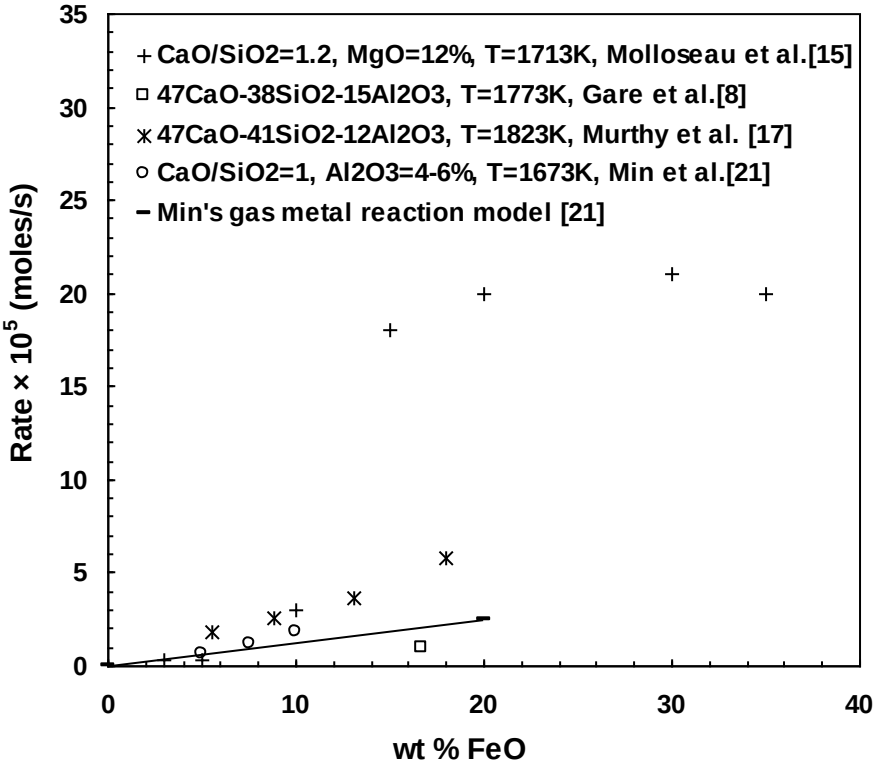

Figure 2.12 − Dependence of the rate of CO evolution on FeO content in the slag.

In Figure 2.12, the straight line represents gas metal reaction model. From the figure, it can be seen that at FeO content >10%, this model could not be applied to explain Molloseau's results. Woolly and Pal [42] studied the reduction rate of ferric and ferrous oxide from calcia-silica-alumina slag by carbon in liquid iron, and found that when most of iron oxide is in form of ferrous, the rate determining step is the mass transfer of FeO to the slag metal interface.

The calculate m_s was 1.3×10^{-3} and 3.0×10^{-3} cm/s for 10% and 20% FeO in the slag. These data seems to be agreed with Ibl and Venczel's [14] penetration model in the range of 1.3×10^{-3} to 1.3×10^{-2} cm/s.

$$m_s = \sqrt{\frac{12Dv(1-B)}{\pi d_b}} \tag{2.12}$$

D: diffusivity (cm^2/s), equals to 7.7×10^{-6} cm^2/s at T=1713K according to Agarwal and Gaskell's model [43]:

$$\log D = \frac{-5450\pm620}{T} - 1.93\pm0.37 \tag{2.13}$$

v: gas evolution rate (cm^3/cm^2s);

B: degree of surface coverage, 0.9;

d_b: average diameter of bubble (cm), 0.1cm.

Molloseau et al. [15] explained the significant increase of reduction rate in term of emulsification. At the higher oxygen potential (FeO in the slag is above 10%), the metal droplet was reported to become "emulsified", this leads to the larger interfacial reaction area, and thus accelerates the decarburization rate greatly. However, when temperature increases to 1763K, the same trend of effect of FeO content on the reaction rate could not be found, see Figure 2.13.

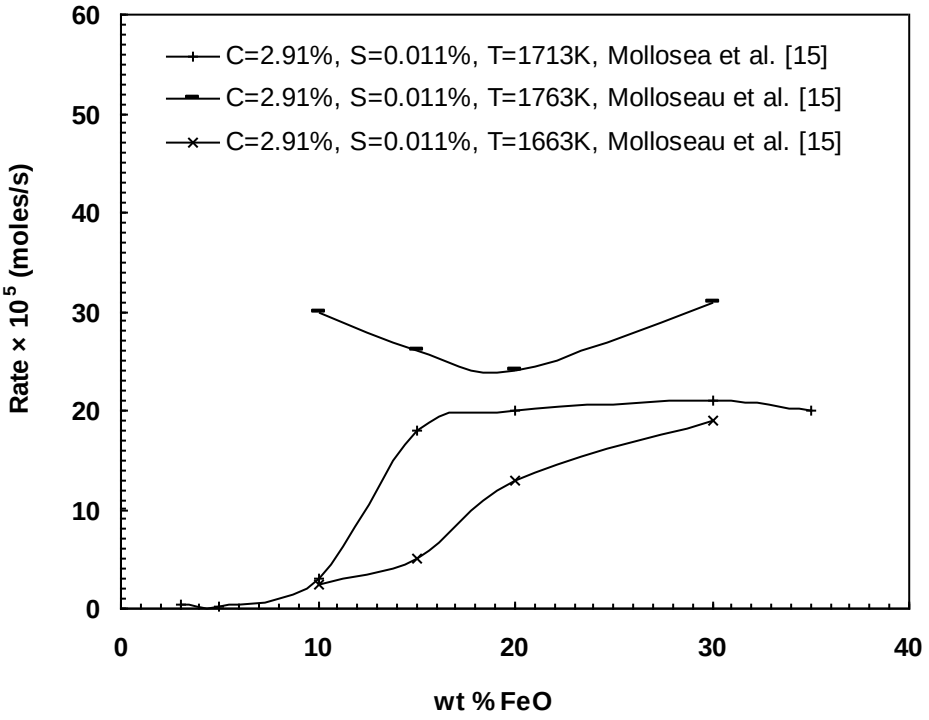

Figure 2.13 − Dependence of CO evolution rate on FeO content.

2.2.2.2 Sulphur Content

Min et al. [21] found that reaction rate decreased greatly with sulfur content, and obeyed this following equation at T=1723K, $k_{CO_2} = \frac{1.5\times10^{-6}}{[pctS]} + k'_{CO_2}$ where: k'_{CO_2} is the residual rate at very high sulphur content.

Murthy et al. [17] revealed that the rate was not influenced by sulfur content. Molloseau et al. [14][15] observed that the rate increased at sulfur content increasing from

0.003 to 0.011 wt pct, it decreased at sulfur increasing from 0.011 to 0.42 wt pct, see Figure 2.14. Disagreement exists among these workers.

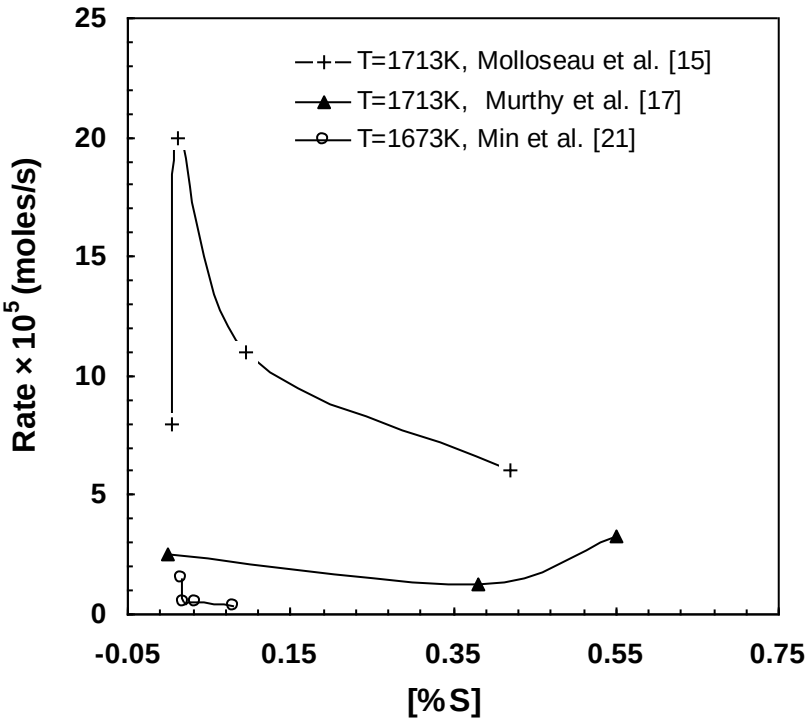

Figure 2.14 − Effect of Sulfur content on reaction rate.

Sulfur affects the decarburization rate in two ways [6]: on the one side, sulfur being surface active, segregates to the surface and leads to poisoning of the reaction, thus decreases the reaction rate, so called "site blockage model" [44]. On the other side, sulphur decreases the surface (interfacial) tension of droplet, increases the interfacial reaction area for metal droplet and slag, and thus improves decarburization rate. Cramb and Jimbo [45] found that surface tension of Fe-C droplet decreases greatly when sulphur content increased from 0–0.025%, which intensifies droplet emulsification, and thus increase the decarburization rate. However, at higher sulphur content, the surface tension

does not decrease significantly with the sulphur content, and it segregates on the reaction site, and block the decarburization reaction. This could be applied to explain Molloseau and Fruehan's finding. For Min and Murthy's experiment, the emulsification of the droplets was not observed, so site blockage model could be applied.

2.3 Swelling of Fe-C Droplets in the slags

When metal droplet reacts with iron oxide containing slags, it will swell at some specific conditions. The drop's swelling prolongs its residence time in the slag significantly and thus decrease the carbon to the very low value before it falls back to the metal bath. However, there are very little studies on this reaction phenomenon.

2.3.1 Measurement on Swelling Rate

Droplet swelling was observed by Molloseau and Fruehan using the X-ray Fluoroscopy technique. Figure 2.15 shows their measurements on the droplet size change with time at T=1713K. [14] They found that it took about 8 s for the droplet to achieve its maximum surface area reacting with slag containing 10% FeO, and after 9 s it became stable. For 20% FeO in the slag, it took 1.6s for the droplet to expand to its largest size, and 2s was stable at this size. Figure 2.16 shows X-ray images from Molloseau's work.

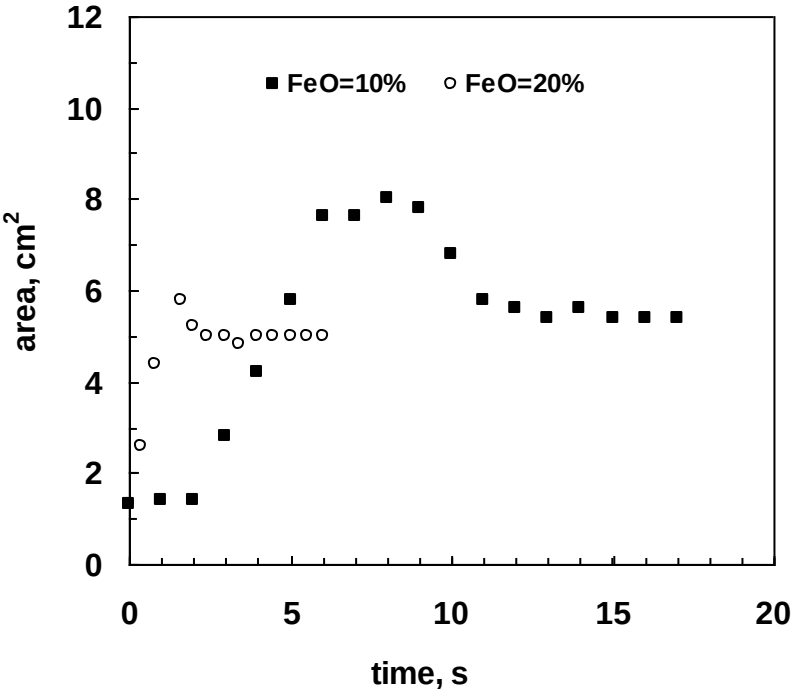

Figure 2.15 – Droplet surface area change with time at 1713K. [14]

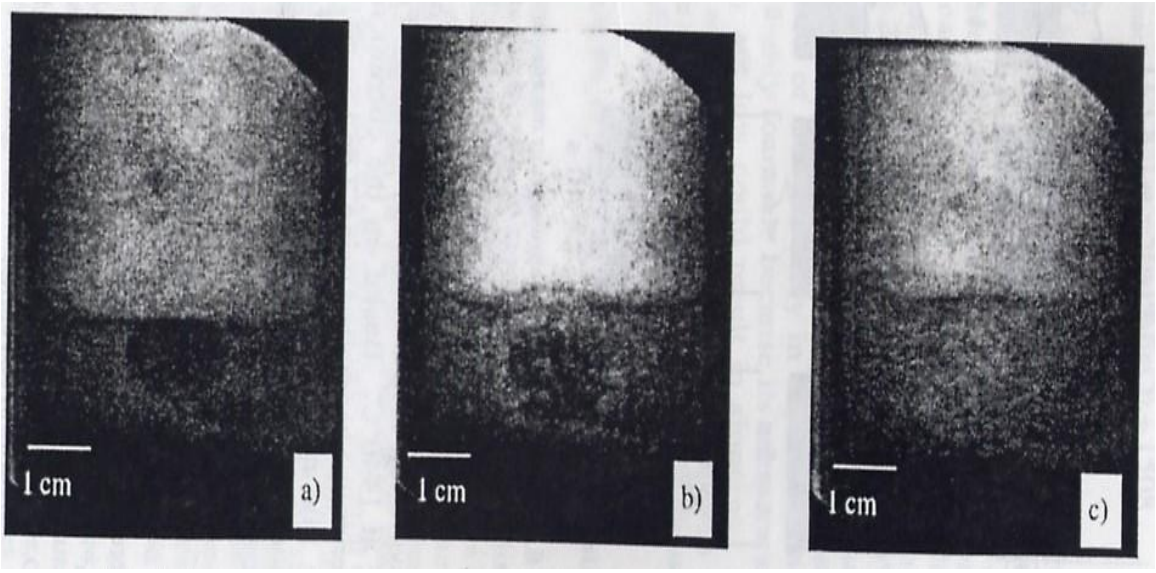

Figure 2.16 − X-ray images of a 1 gram Fe-C-S droplet (2.91%C, 0.011%S) reacting with a slag containing 20 wt % FeO; a) at t = 3s, b) t = 6s, c) t = 8s [14].

The swelling of droplets was also observed by Murthy et al. [17]. They found that droplet became larger after reacting with the slag for some time.

Table 2.3 − Surface area after reacting 30s [17].

Temperature, K	*%FeO of Slag*	*Droplet weight, g*	*Surface Area, cm^2*
1823	5.5	1	1.27
1823	8.78	1	1.34
1823	13.12	1	1.71
1823	18.0	1	2.2
1823	13.12	2	3.34
1773	13.12	2	3.09
1713	13.12	2	3.06
1658	13.12	2	4.09
1598	13.12	2	4.23

More recently, Brooks et al. [27] proposed five stages for the size change with the time during the decarburization, see Figure 2.17. They suggested that the size of the droplets depended on factors, such as, decarburization rate, CO escape rate, threshold decarburization rate and steady stage decarburization rate. At the initial stage, $r_c^{esc} = r_c$, the droplet remained its original size. Usually, this stage is very short. When $r_c > r_c^{esc}$, more CO generated inside the metal, droplet begins to swell until $r_c^{esc} = r_c$. After expanding to its maximum diameter, droplet shrinks until reaching its original diameter.

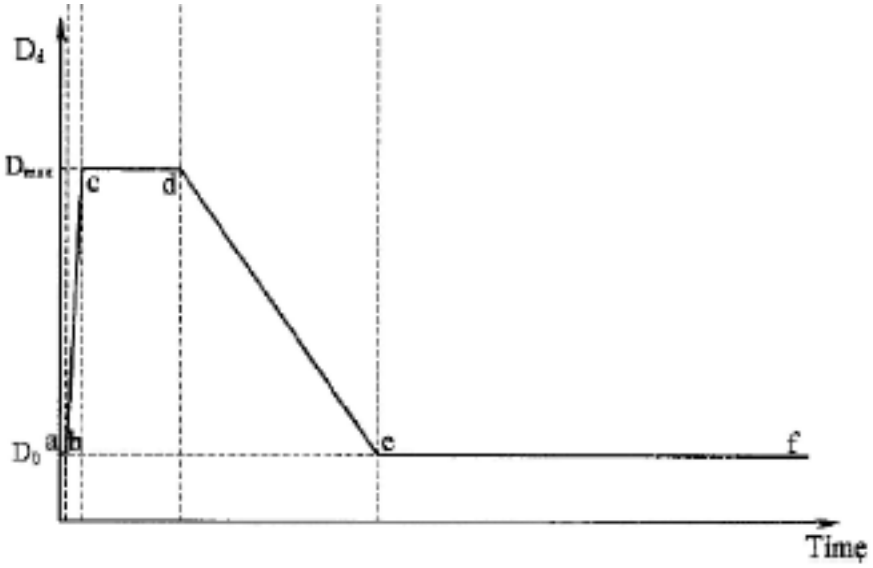

Figure 2.17 − Dependence of swelling rate on time. [27]

2.3.2 CO Nucleation inside the Metal Drop

A similar phenomenon, called "boiling" is observed when droplets pass through oxidizing gases (such as mixtures of CO and CO_2, or O_2) [46]-[59]. Baker et al. first [46]-[48] observed iron droplet's swelling when passing through a gas mixture of oxygen and helium. The droplets were observed to explode due to CO nucleation inside the metal. A supersaturation of 5×10^4 atm [52][59] was calculated for CO nucleation, which is two orders higher than the experimental measurements. The high supersaturation pressure required by classical nucleation theory predicts that the observed homogeneous nucleation of CO bubbles inside metal is impossible. Various explanations have been proposed. Early work by Levine [60]-[62] investigated the effect of the surface active element, oxygen, which will

decrease the surface tension and the work needed for the formation of an embryo inside the melt. However, even if oxygen decreases the surface tension from 1.6 N/m to 1 N/m, the calculated supersaturation pressure is still extremely high (25000 atm) [63]. Gare et al. [8] proposed that the nucleation was heterogeneous due to entrainment of gas in the molten droplet when it fell through furnace at the start of the experiment. The entrained gas acted as a gas nucleus for heterogeneous nucleation. Robertson and Jenkins [51] proposed that the nucleation is neither homogeneous nor heterogeneous, and invoked vortex nucleation. They also mentioned that oxygen has a large effect on interfacial turbulence thus benefiting CO nucleation.

2.3.2.1 Nucleation Rate Equation

The phenomenon of nucleation has attracted much attention and few decades ago, efforts had been paid on the derivation of the nucleation rate. [64]-[75] The theoretical expression for the nucleation rate consists of two parts: the pre-exponential and the exponential:

$$J_n = N \exp[\frac{-\Delta G_{(r)}}{kT}] \tag{2.14}$$

Where:

J_n is the nucleation rate, $cm^{-3}s^{-1}$;

N is the number of liquid molecules per unit volume;

$\Delta G_{(r)}$ is the free energy change for formation of the embryo of radius r.

The pre-exponential has small effect on the nucleation rate. The change of an order of magnitude in the pre-exponential is equivalent to a change of about 1% in the exponential. Equation (2.12) is for the rate of homogeneous nucleation of bubbles from a supersaturated solution. The nucleation is heterogeneous with the occurrence of impurities, and the rate is expressed as:

$$J_n = N \exp\left[\frac{-\Delta G_{(r)} \Phi(\theta)}{kT}\right] \tag{2.15}$$

where Φ is a function of the contact angle, θ.

In order to calculate the nucleation rate, after a series derivations and abbreviations, the nucleation rate could be expressed by:

$$J = N\left[\frac{2\sigma}{\pi MB}\right]^{\frac{1}{2}} \exp\left[\frac{-16\pi\sigma^3}{3kT[P_{ve} - P_L]}\right] \tag{2.16}$$

Where,

N: is the number concentration of embryos in the liquid;

σ is surface tension at liquid gas interface;

ΔH is heat of formation of one gas molecule;

M is the mass of one molecule;

T is temperature, in Kelvin,

k is Boltzman constant;

P_{ve} is the pressure in the vapor bubble at equilibrium;

P_L is liquid pressure.

2.3.2.2 Factors that Influence the Nucleation Rate

From the nucleation equation, it can be seen that the most important factor influencing the nucleation rate is supersaturation pressure; it is cubic in the exponential in the nucleation rate equation. Kaddah and Robertson [52]-[54] calculated the critical supersaturation pressure, S_x, in order to decide if boiling will occur, where, $S_x = P - P_g$, P_g is the ambient pressure and P is the CO pressure equilibrium with dissolved carbon and oxygen. When the supersaturation pressure is larger than the critical supersaturation pressure, boiling will happen. They developed the following partial differential equation for supersaturation of CO in molten iron drops,

$$\partial S/\partial t^* = \partial^2 S/\partial r^{*2} + (2/r^*)\partial S/\partial r^* + 3G[O^*(D^*-1)/D^* + (2r^*/3)\partial O^*/\partial r^*] \quad (2.17)$$

$$G = F \cdot O_{satn} \cdot C_0 \cdot K_4 \quad (2.18)$$

Where:

S: supersaturation ($P-P_g$),

t^*: dimensionless time (Td_0/a^2),

r^*: dimensionless radial coordinate (r/a),

O^*: dimensionless oxygen concentration, (O/O_{satn}),

D^*: D_0/D_c, $F = n_C a/(D_C \cdot C_0)$.

(1) Oxygen Potential

Oxygen potential affects droplet swelling through the decrease the critical supersaturation pressure, see Figure 2.18. The critical supersaturation pressure decreases greatly when oxygen concentration in the metal increased to 0.04 wt%. This seems to explain Molloseau's and Min's observations [15][21][22]. They found that the iron droplet remained as a single spherical drop when the FeO content of the slag was less than 10 wt pct. It became "emulsified" when its content was more than 10 wt pct in the slag.

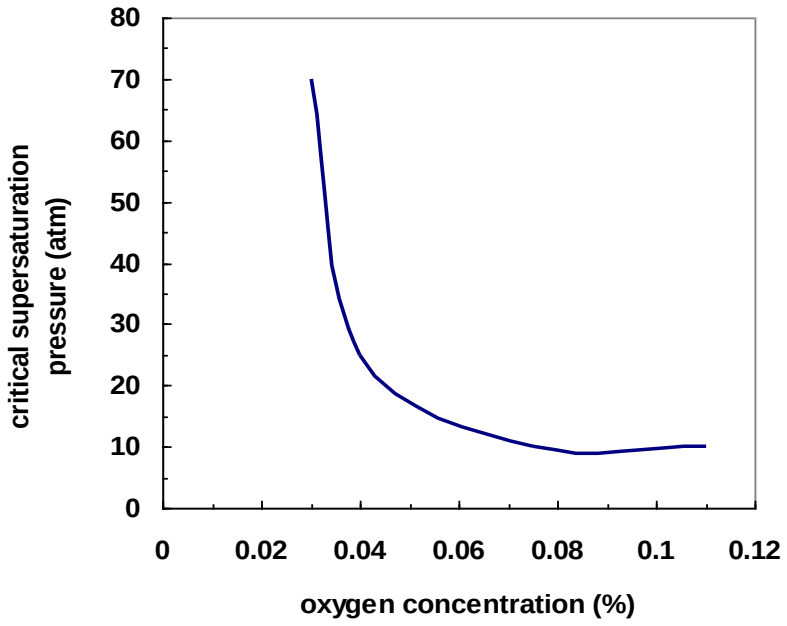

Figure 2.18 − Dependence of critical supersaturation pressure on oxygen concentration. [51]

(2) Carbon Content

The maximum supersaturation pressure $S_x = O_{satn} \cdot C_0 \cdot K_4$ increases with the initial carbon content, especially in the range 0-1%. If the initial carbon is very low, the supersaturation pressure could not be high enough, so boiling could not happen.

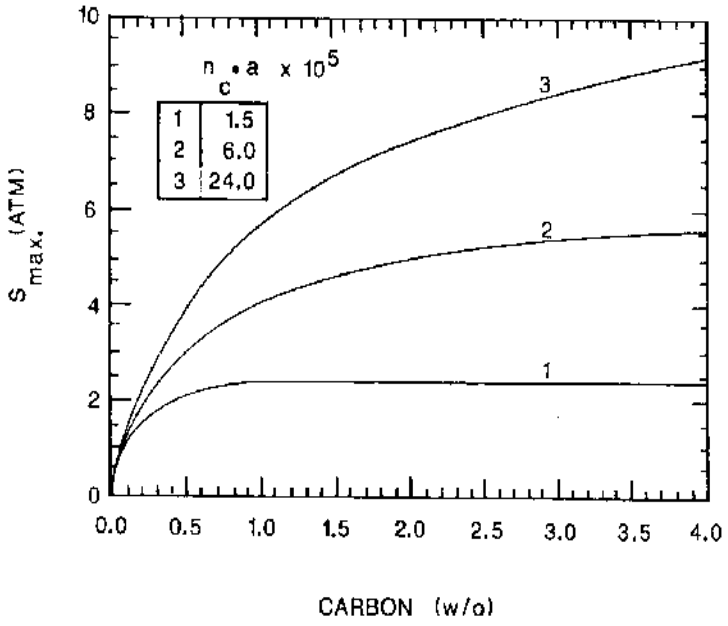

Figure 2.19 − Dependence of maximum supersaturation pressure on carbon content [76].

(3) Si and Mn Effect

It has been observed that Si and Mn delay the oxidation of carbon when passing an iron carbon droplet through oxidizing gases. Recently, Sun et al. [76] developed a mathematic model to calculate the compositions of the iron droplet as a function of reaction time. Their calculated results are shown in Figure 2.20. From this figure, it can be seen that Si and Mn compete with carbon for oxygen in the slag, making less oxygen available for the nucleation and growth of CO gas bubbles, thus prevent droplet swelling.

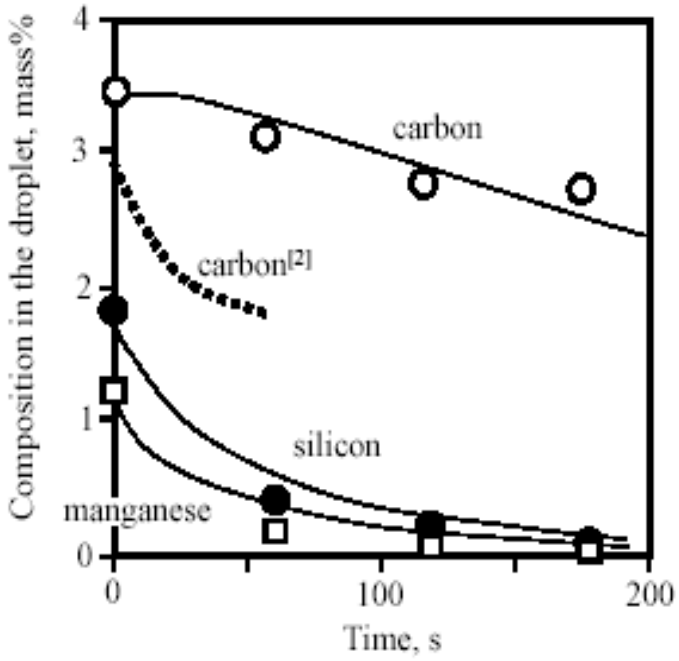

Figure 2.20 – Variations of compositions of the droplet with time during slag-drop reaction at 1773K [76].

2.3.3 Bubble Growth Rate

Conceptually, bubble evolution consists of various stages: nucleation, growth, rise and bursting. Once a bubble nucleates inside the metal, it will grow. There are two regimes for the bubble growth: inertially dominated growth and chemical growth. For the inertially dominated mechanism, the pressure inside the bubble is higher than that of the surrounding liquid and the temperature within the bubble is essentially equal to that of the surrounding liquid. The growth under this mechanism is limited by the rate at which the surrounding liquid can be pushed out of the way and the bubble radius versus time can be calculated from Rayleigh's equation.

The continuity and momentum equations in the liquid surrounding a growing spherical vapor bubbles are given by:

$$\frac{\partial(r^2 u)}{\partial r} = 0 \tag{2.19}$$

$$\frac{\partial u}{\partial r} + u\frac{\partial u}{\partial r} = -\frac{1}{\rho}\frac{\partial P}{\partial r} + \frac{u}{\rho}\left(\frac{\partial^2 u}{\partial r^2} + \frac{2}{r}\frac{\partial u}{\partial r} + \frac{2u}{r^2}\right) \tag{2.20}$$

By simplification and integration with boundary conditions u(0,t) = $\frac{dR}{dt}$ and u(∞,t)=0, also, $P_v - P(R) = \frac{2\sigma}{R}$, the extended Rayleigh Equation is expressed:

$$\frac{P_v - P_\infty}{\rho} = R\frac{d^2 R}{dt^2} + \frac{3}{2}\left(\frac{dR}{dt}\right)^2 + \frac{2\sigma}{\rho R} \tag{2.21}$$

where, R is bubble radius, P_∞ is ambient pressure in liquid surrounding bubble, P_V is bubble pressure, ρ is density of liquid surrounding bubble, σ is surface tension at bubble/liquid interface.

Grezl et al. [7] found that bubbles grew very rapidly to a limiting radius depending on the initial bubble pressure and radius. When the initial pressure is 100 atm, the bubble grew from $5.507*10^{-7}$ m to maximum size of $5*10^{-6}$ m after $\Delta t = 5*10^{-6}$ s, see Figure 2.21.

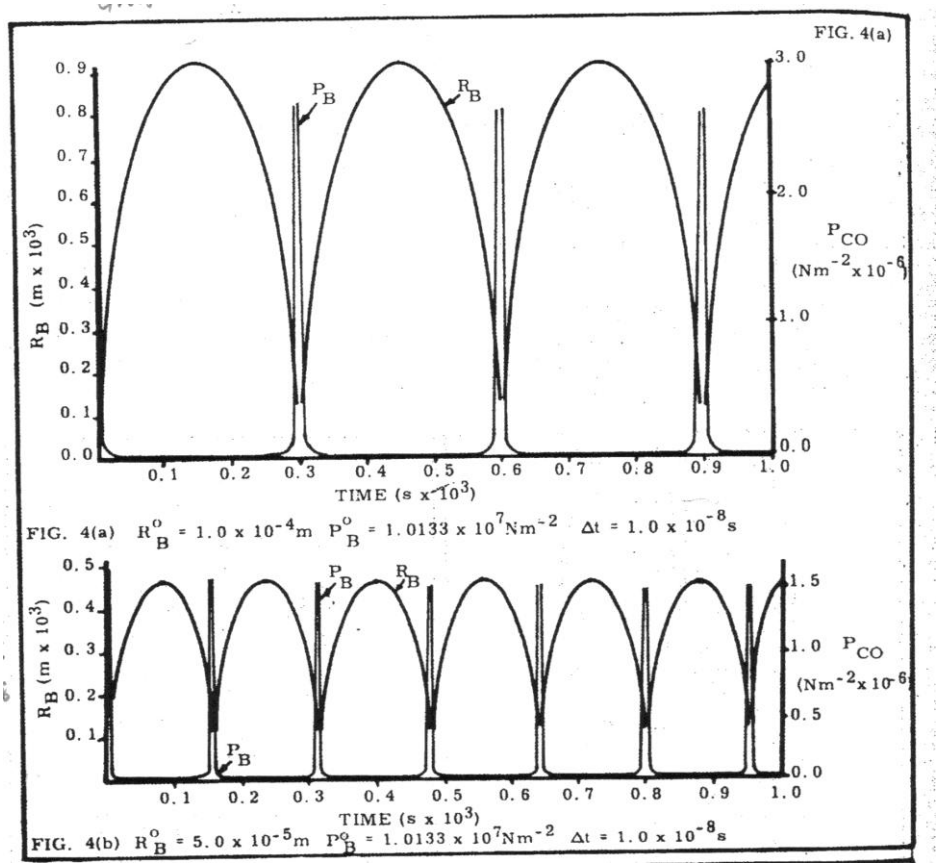

Figure 2.21 – Bubble growth [7].

2.4 Foam

Foaming in metallurgical processes has been studied by several workers due to the critical roles it play. [77]-[87] For example, in BOF steelmaking, the metal droplets are ejected into the slag layer from the metal bath, which creates a gas-slag-metal emulsion and thus generates large interfacial reaction areas that increases the refining rate greatly. In EAF steelmaking process, the reaction of metal droplets with slag causes slag foaming, which decreases heat losses and improved the heat transfer efficiency. Foams are defined as dispersed gases in a continuous liquid phase and divided into two categories: sphere

foam and polyhedron foam. Sphere foams contain large amount of liquid (>25%), gas volume fraction is less than 75%, the bubbles in sphere foams are spherical, like beer foam. The bubbles in polyhedron foam are polyhedral, with very thin liquid lamellae separating them, like "soap bubble foam". See Figure 2.22. At the top, the foam is very dry, the gas volume fraction is about 91%, and the bubbles are polyhedral. At the bottom, the foam is wet, the bubbles are spherical, and the gas volume fraction is about 74%.

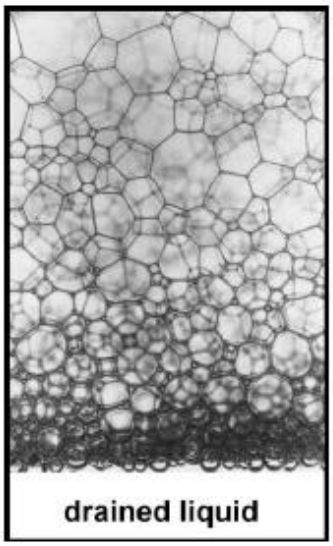

Figure 2.22 – A foam after drainage, at equilibrium. [88]

2.4.1 Steady Foam

The foaminess also known as foaming index, Σ (in seconds, the time an average bubble exists in the foam before bursting) is the most characteristic quantity which can be obtained from dynamic foam measurement, and is defined as: [88]

$$\Sigma = \frac{h_0}{u} \tag{2.22}$$

Where; h_o is the height of the foam at steady state,

u: the gas blowing velocity (m/s).

When gas is injected into the liquid at a constant rate, the foam height initially increases with a constant linear velocity, then the velocity decreases, and after a time a constant height h_o is reached. Σ is independent of the gas flow rate, of the shape and dimensions of the measuring tube, and of the amount of liquid presented, it depends on the physical properties of the liquid, such as the viscosity, surface tension and density of the liquid, and the bubble diameter.

Fruehan and his group have studied the foam behavior of slags [77]-[83]. Using dimensional analysis, they obtained the following relation for bath smelting type of slags (CaO-SiO2-Al2O3-FeO):

$$\sum = 115 \frac{\mu^{1.2}}{\sigma^{0.2} \rho d^{0.9}} \tag{2.23}$$

Where: ρ is the density (kg/m^3),

μ is the viscosity (Ns/m^2),

σ is the surface tension (N/m),

d is the bubble diameter (m).

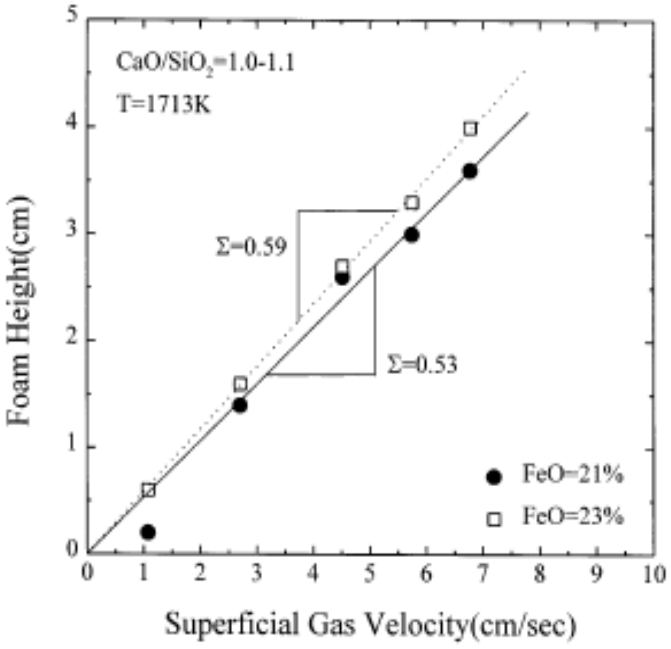

Figure 2.23 – Foam height of CaO-SiO2-FeO-MgO slags as a function of superficial gas velocity at 1713K. [74]

They studied the influences of bubble size, FeO content, slag basicity, TiO_2 and temperature on foam index. The dependence of foam index on FeO content is through the influence of FeO on the slag viscosity. The higher FeO content in the slag, the lower slag viscosity, therefore the lower foam index. Usually, slag viscosity decreases with basicity, so foam index should decrease. But with the increase of slag basicity, at the critical value, solid particles form like 2CaO.SiO2, and leads to the increase of slag viscosity, and increases foam index. TiO2 increase slag viscosity and therefore increases foam index. They also found the dependence of foam index on temperature: $\log\Sigma = \frac{6610}{T} - 3.90$.

2.4.2 Dynamic Foam

In most of the cases, foam height changes with the time due to gas flowrate changes. Under this circumstance, the foam volume changes with time. Seetharaman [87] defined the foam volume change as,

Rate of change of foam volume

= rate of gas generation or injection

– rate of volume change due to bubble rupture

The above relationship is very similar to that proposed in the current work for droplet swelling rate as a balance between gas generation and escape.

The rate of volume change due to bubble rupture = kNv_b, v_b is the average volume of a bubble, N is the total number of bubbles, and k is the rate constant for bubble decay.

$$\frac{dh}{dt} = k_1 Q_g - k_2 h \tag{2.24}$$

Where k_1 and k_2 are the formation and rupture constants of foam, respectively. When the system is in the steady state,

$$\frac{dh}{dt} = 0$$

The steady state foaming is an ideal case. In real steelmaking process, due to the reduction of FeO, the slag chemistry can change dramatically, causing dynamic foaming, where the foaming index changes with time. See Figure 2.24.

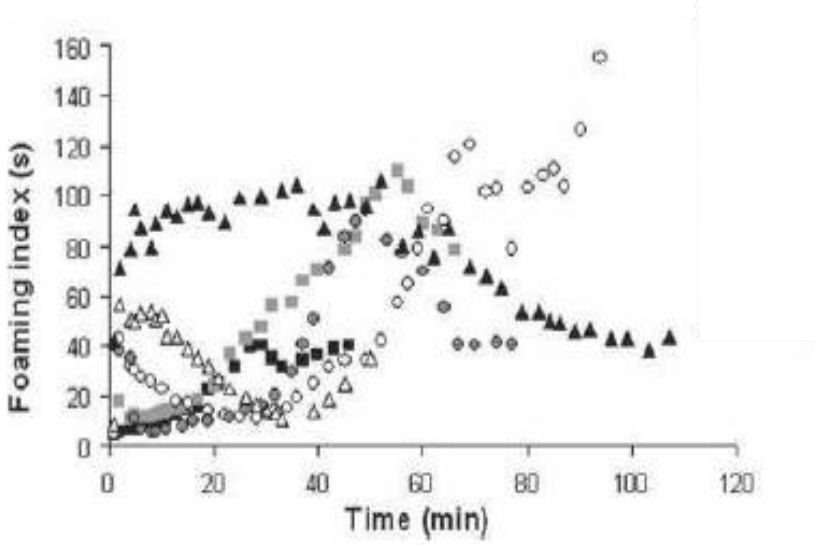

Figure 2.24 – Foaming index for different slags. [87]

2.5 Summary

It has been shown that the residence time of metal droplets is important in oxygen steelmaking. Recent work has shown that swelling of droplets due to CO evolution can have a major influence on residence time. There have been several studies, on the reaction of iron carbon droplets with slag, in general and droplet swelling in particular. However, as yet there is insufficient data to predict quantitatively the swelling behavior of droplets. The aim of the current work is to elucidate the mechanism of swelling, and to develop a model that can predict swelling behavior as a function of conditions.

Chapter 3

EXPERIMENTAL WORKS

There are several methods to measure the decarburization rate for iron droplets. One is to quench the crucible containing slag and metal after the desired reaction time, and calculate the reaction rate through analyzing the chemical compositions of the samples. Using this method, an accurate reaction time is very hard to control, especially when the reaction time is only few seconds. Another method involves measuring the instantaneous flowrate of gas evolved from the reaction. Even when the volume of the furnace is designed to be very small, the mixing of reacted gases is still not avoided. So in this study, the constant volume pressure increase technique is used. This technique measures the pressure increase caused by gas evolution from decarburization reaction, the measured pressure is converted to moles of CO evolved through the calibration before each experiment.

The reaction behavior of iron droplets could be obtained by high speed cinematographic camera or X-ray Fluoroscopy. In this study, the live x-ray fluoroscopy technique is used.

The experimental works involve two measurements, one is the reaction kinetics between metal droplets and slags using constant volume pressure increase technique (CVPI), other measurements are the droplets' swelling rate using X-ray Fluoroscopy. In this chapter, the details of the experimental arrangement, materials and procedures will be introduced.

3.1 Preparation of Metal Pellets and Slag Sample

Pig iron was prepared in a molybdenum disilicide elements heating furnace under Ar (200ml/min) atmosphere. Pre-calculated amount of iron chips (Alfa Aesar, 99.98%, 1-2mm), graphite rod (99% C) and FeS were introduced into the furnace by an alumina crucible (Vesuivus McDanel, O.D = 35mm, Height = 64mm) by considering some amount of the yield loss of carbon and sulfur. The mixture of iron chips, graphite rod and FeS was heated slowly overnight. Once the pre-pointed temperature is achieved, waiting an hour for the homogeneity, then a quartz tube (I.D = 5mm) with a rubber bulb was used to pipette out the sample. Samples were quenched in water, polished the surface and then sectioned into 0.5g, 1g, 1.5g and 2g small piece. The compositions of the metal pellets used in this study were analyzed by Carbon-sulfur determinator (LECO), see table 3.1.

Table 3.1 – Metal Pellets Compositions (wt %)

Metal Pellets	*C*	*S*
1	3.71	0.0063
2	2.87	0.01
3	2.75	0.02
4	2.64	0.022
5	2.70	0.027
6	2.13	0.046
7	2.62	0.06
8	2.94	0.194
9	2.69	0.3

Slag samples were prepared by mixing high grade of FeO, CaO, SiO_2 and MgO well, and used directly in the experiment. No difference was observed between pre-mixing powder and pre-melt slag by the workers [14].

Table 3.2 – Properties of slag making materials

Materials	*Purity (wt pct)*	*Size*	*Supplier*
FeO	99.5		Alfa Aesar
SiO_2	99.5	-400 mesh	Alfa Aesar
CaO	96 (3.3 % LOI)		Fisher Chemicals
MgO	99		Alfa Aesar

3.2 Experimental Arrangement

The experimental apparatus consisted of three main parts: a furnace, X-ray fluoroscopy, and pressure transducer. See Figure 3.1.

Figure 3.1 − The experimental setup.

3.2.1 The Furnace

Two rectangular holes were cut on the stainless shell of the furnace in order to allow the minimum absorption of X-rays. The furnace is heated by molybdenum disilicide elements, see Figure 3.2. An alumina working tube (I.D = 79 mm, O.D = 89 mm, Height = 762 mm) was installed inside the furnace. Both of the ends of the working tube are sealed with an O-ring and stainless steel end caps, which are water-cooled throughout the experiment. The sealed tube provided a vessel for the measurement of pressure change. The magnesium oxide crucible (OD = 45mm, height = 90mm from Alfa Aesar) containing the slag was placed in the alumina working tube. An alumina dispensing tube (I.D = 11mm, O.D = 17mm) was place inside the working tube, 25 mm above the magnesium oxide crucible. There was a 3/16 inch (4.7mm) diameter hole at the base of the dispensing tube allowing 1g of pellet to melt before entering the slag (see Figure 3.3). Figure 3.2 shows the detailed arrangement inside the furnace. A thermocouple (type B: Pt-6 pct Rh/Pt-30 pct Rh) inserted from the bottom was located close to the sample. The whole system was sealed and the work tube flushed with argon in order to prevent air from penetrating into the reaction area before the experiment. The argon was purified before entering the furnace by passing through the column of "Drierite". Temperature control was achieved using a EUROTHERM controller. The temperature profiles in the working tube were carefully measured, a hot zone 40-mm long was identified in which the temperature varied within $\pm 1^{o}C$ as shown in Figure 3.4.

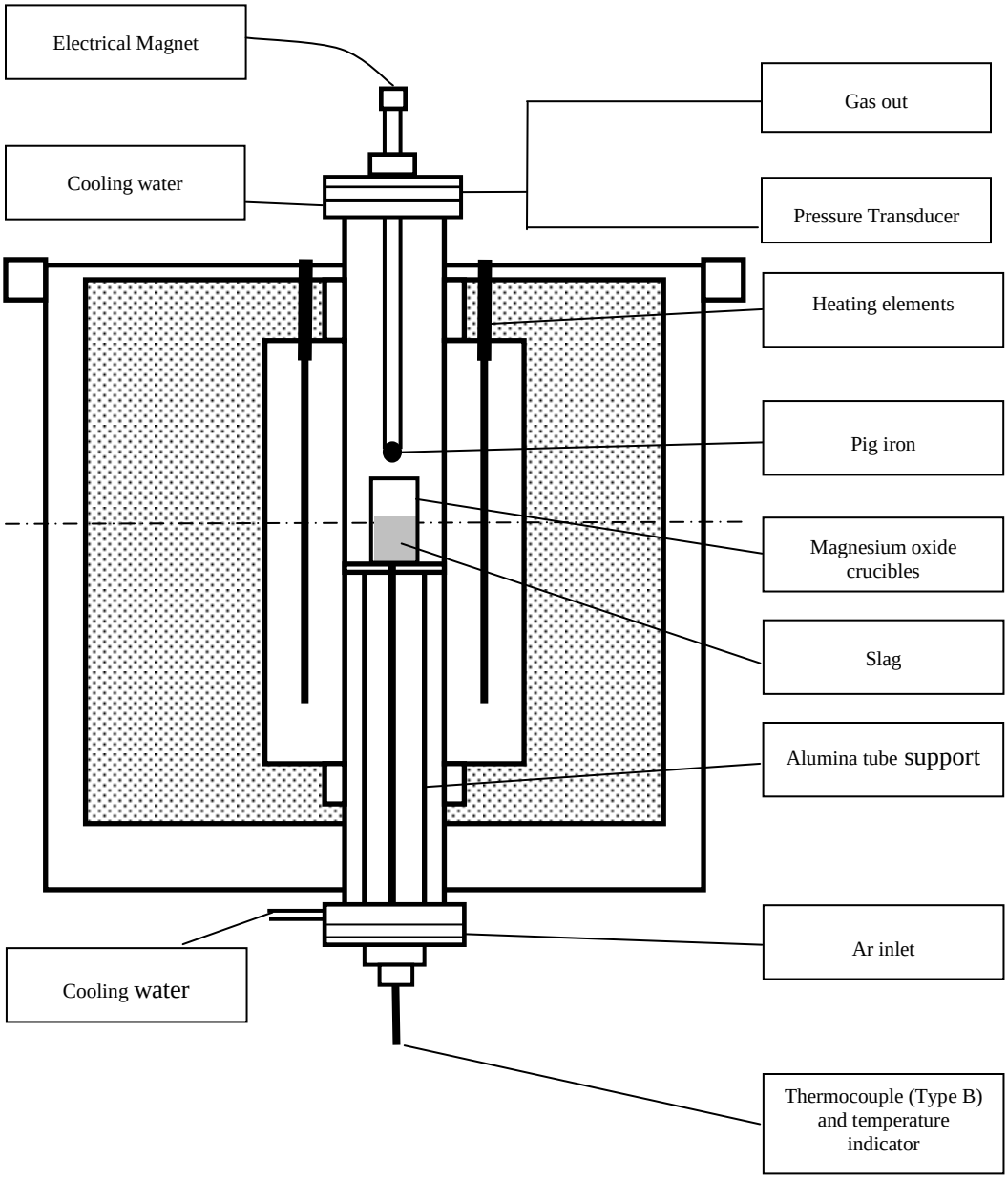

Figure 3.2 − Schematic diagram of the experimental setup.

Figure 3.3 – Details of the dispensing tube.

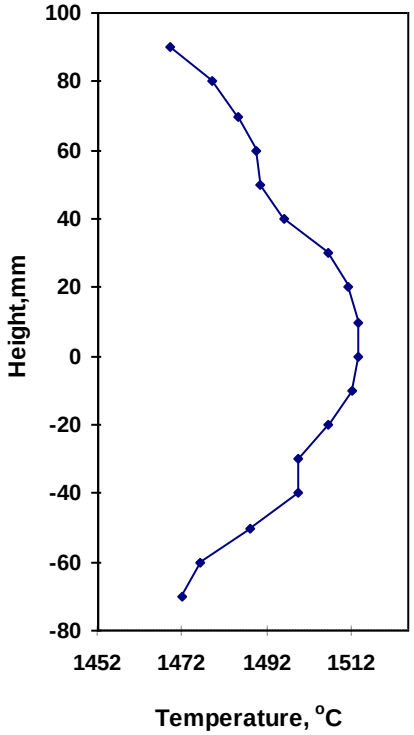

Vertical temperature distribution of the 1730 VY Rapid Temp Furnace at 1500°C.

For temperature±5°C, the uniform temperature zone is about 50mm in height.

For temperature±1°C, the uniform temperature zone is about 40mm in height.

Figure 3.4 − The temperature profile of the furnace

3.2.2 X-Ray Fluoroscopy

X-Ray Fluoroscopy (GE OEC Medical Systems, Inc.) mainly consists of OEC Workstation and movable C-arms. OEC Workstation includes touch-screen, workstation keyboard and Infrared (IR) remote control. The X-ray image was obtained on a 230 mm diameter round fluorescent screen located on C-arms.

3.2.3 Pressure Transducer

A maximum measurable range of 10 inches water of differential pressure transducer (FLW Southeast, Inc, 157C-W050NR, Very Low Pressure Transducer) was used to measure the pressure change due to the gas evolution during the reaction. The set of measurement on the pressure change consists of sensor (pressure transducer), data acquisition system (RS232 Interface and PC). The sensitivity of the pressure transducer is $3*10^{-5}$ atm. The output data is expressed in terms of inch water, which has to be converted to the molar amount of produced CO.

3.3 Calibration for Pressure Transducer

The calibration curve has to be done for the pressure transducer before each experiment. For calibration, the furnace is setup exactly the same as the real experiment, except MgO powder replaces slag in the MgO crucible. Once the desire temperature is reached, 10 ml or 20 ml of air is injected into the furnace each time, and the readings on the pressure transducer are recorded. The calibration curve for T=1773K is shown in Figure 3.5. It can be expressed by $y = ax + c$,

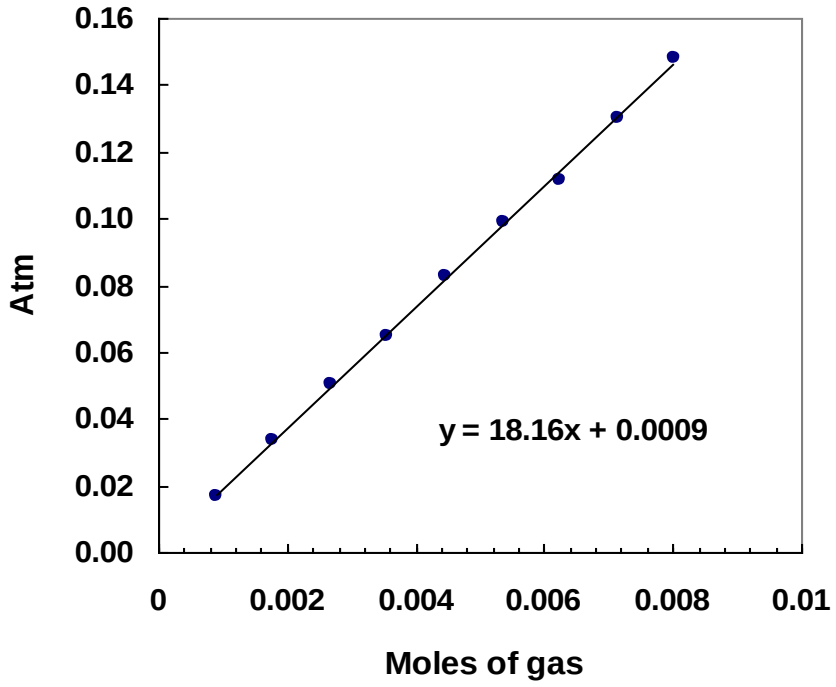

Figure 3.5 − Calibration Curve at T = 1773K.

Table 3.3 – The Calibration for Different Temperatures

T(K)	*a*	*c*
1873	19.258	0.0015
1773	18.160	0.0009
1713	17.604	0.0007
1673	17.369	0.0001
1623	15.237	0.001

3.4 The Experimental Procedure

20g or 60g of a synthetic slag (%CaO/%SiO2 = 1.2, Mg0=12.0 wt %, FeO=20%) was charged into a small (I.D = 32mm, O.D = 38mm, Height = 76mm) or big MgO crucible (Alfa Aesar, O.D = 45mm, Height = 90mm). A calculated amount of FeS was added into the slag to avoid the transfer of sulphur from molten droplet to the slag. The MgO crucible was put into the furnace and heated under an Ar atmosphere (100ml/min). Once the desired temperature was reached, the furnace was sealed. About one gram of pig iron pellet held at the top of the alumina injection tube by an electromagnet. After about 40s, the droplet melted and fell through the 5 mm hole at the bottom of the injection tube. The reaction started immediately, photos were taken by X-ray Fluoroscopy, and gas evolution measured by the pressure transducer and recorded on a PC.

Chapter 4

REACTION KINETICS OF METAL DROPLETS AND SLAGS

This chapter consists of three sections. The first is the preliminary experimental results on CO evolution rate, the second is the observations on the swelling behavior of droplets reacting with slags; and the third is the discussion of the results.

4.1 CO evolution rate

The experimental results for the rate of reduction of FeO from slag by carbon in molten iron with time at T=1713K and T=1773K are given in Figure 4.1. The slag compositions are: CaO/SiO_2=1.2, MgO=12%, FeO=20%, slag weight is 60g.

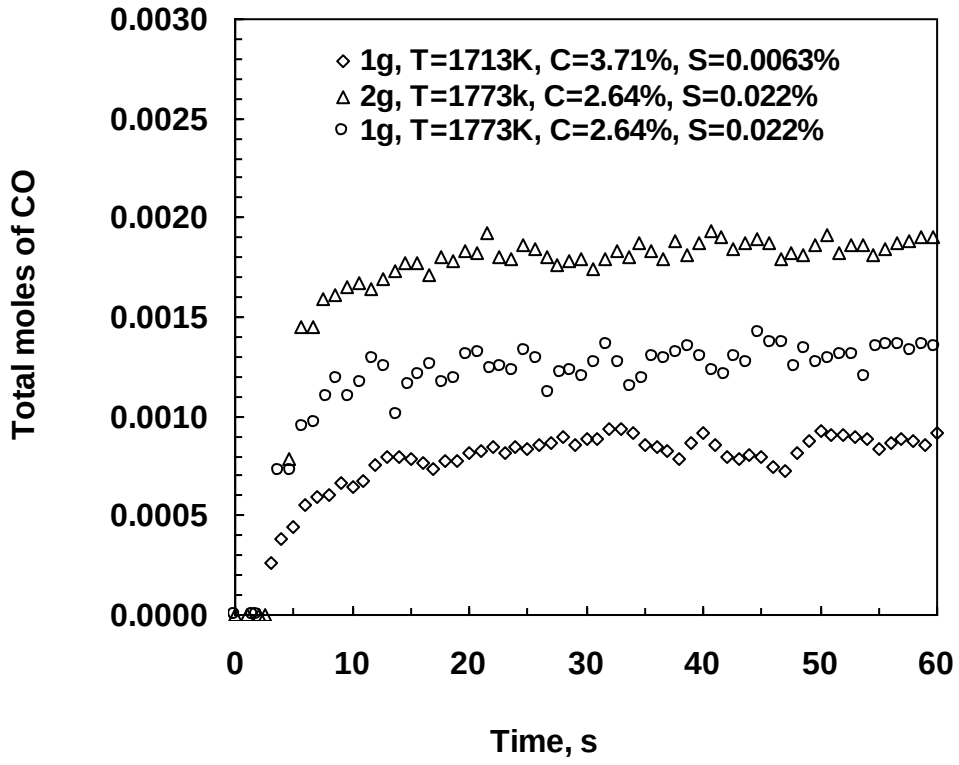

Figure 4.1 − CO evolution with time at T = 1713K and T = 1773K.

The rate is linear with time for the first few seconds. Using linear regression, CO evolution rate is 7.9 $\times 10^{-5}$ moles/s calculated for 1g of droplet, C=3.71 wt%, S=0.0063 wt%. By changing the compositions of droplet, C=2.64 wt%, S=0.022 wt%, the rate increased almost one order, to 20.89 $\times 10^{-5}$ moles/s. When the size of droplet is changed to 2g, the rate increases by two times.

Table 4.1: Reduction rates for 1g and 2g of droplet in 20% FeO containing slag.

Weight (g)	*%C*	*%S*	*Temperature (K)*	*Evolution Rate × 10^5 (moles/s)*
1	3.71	0.0063	1713	7.90
1	2.64	0.022	1773	20.89
2	2.64	0.022	1773	40.57

In order to evaluate the effects of each individual parameter on the CO evolution rate, a complete set of experiments was designed. The dependence of CO evolution rate on its size, temperature, oxygen potential and sulphur content was studied in this work.

4.1.1 The Effect of FeO Content

Keeping metal droplet compositions constant, a wide range of iron oxide, from 3 to 30 wt pct of FeO in the slag, was covered by experiments. In each experiment with fixed FeO content, the temperature varied from 1673K to 1873K. The range of temperature variation was chosen to be higher than the melting point of the slag. Figure 4.2 shows the dependence of CO evolution rate on the iron oxide content expressed as FeO wt pct at T=1673K to 1873K. As can be seen from Figure 4.2, a simple trendline like linear, exponential, or power could not be added in order to fit the experimentally measured data in. The reaction mechanism is needed to be understood in order to find the relationship between the reaction rate and oxygen potentials in the slag.

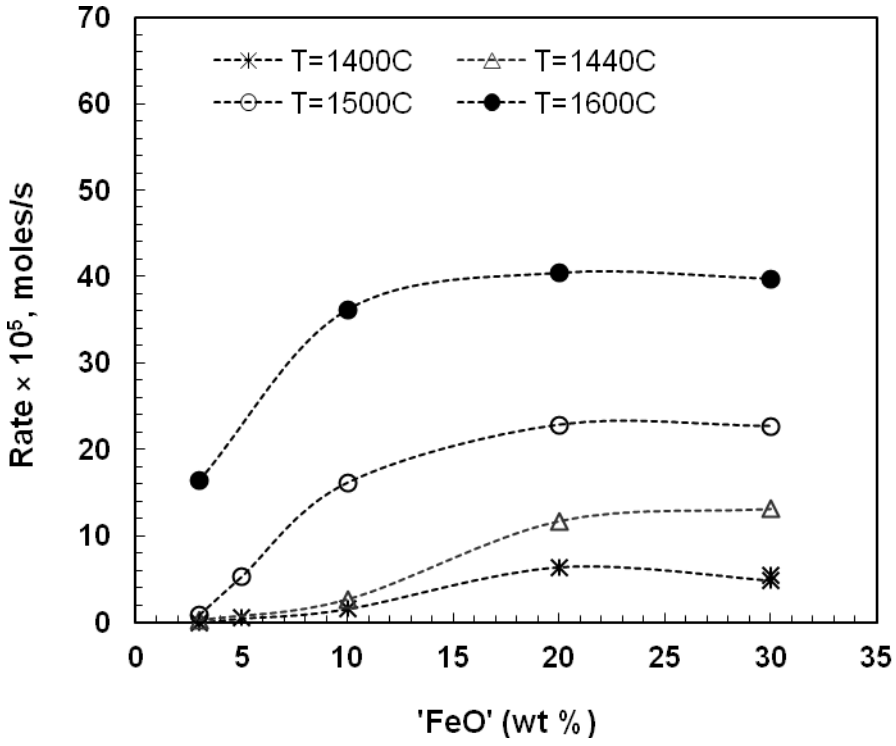

Figure 4.2 − Dependence of CO evolution rate on FeO content.

4.1.2 The Effect of Temperature

The temperature dependence of CO evolution was investigated for slag containing FeO=3, 10, 20, 30%, at fixed metal droplet chemistry. The results are depicted in Figure 4.3.

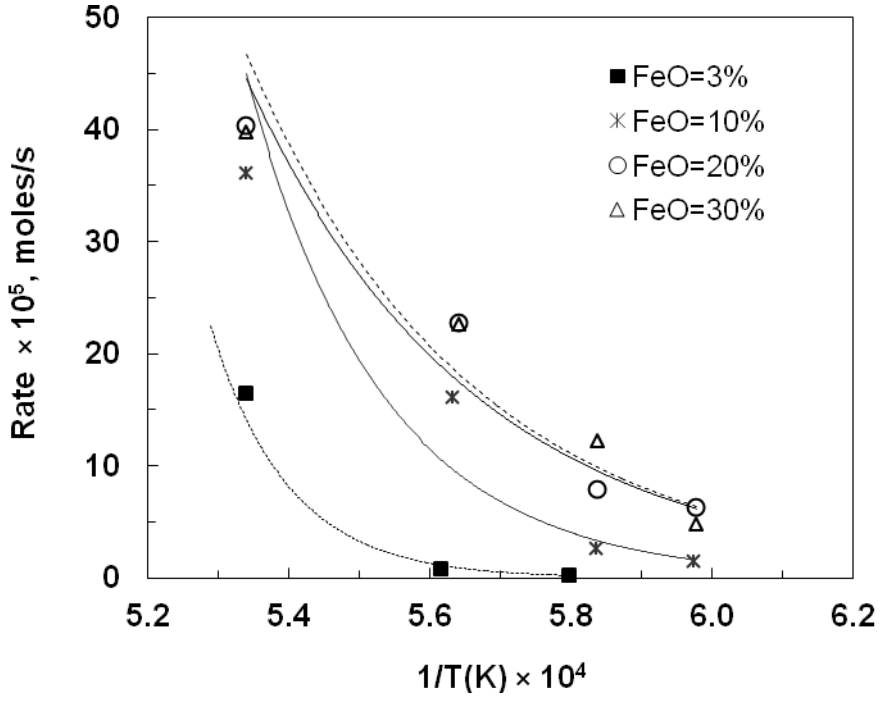

Figure 4.3 − Dependence of CO evolution rate on temperature.

4.1.3 The Effect of Iron Droplet Size

A series of experiments were designed to study the dependence of CO evolution rate on droplet size. For each droplet size, the rate was measured at the common temperature of 1773K. The metal droplet and slag chemistry were kept the same. Figure 4.4 shows the dependence of CO evolution rate on the size of iron pellet, it increases linearly with droplet mass.

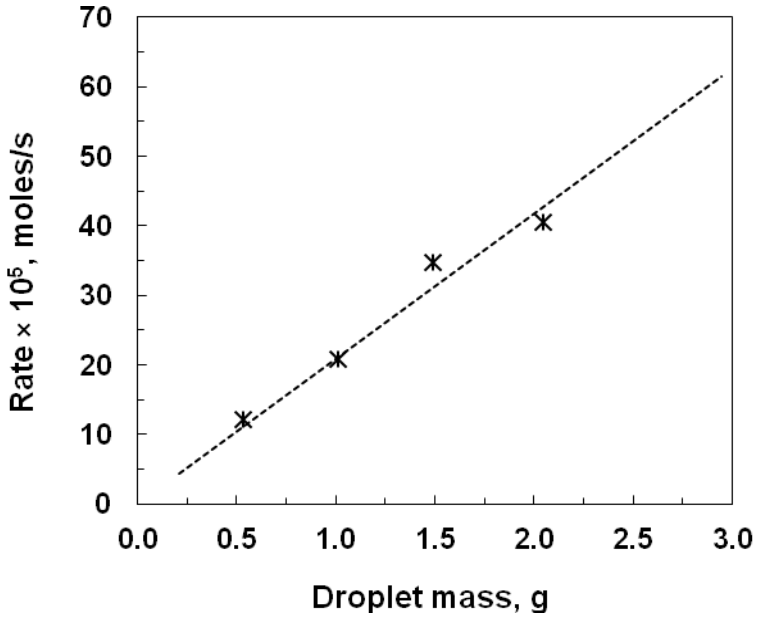

Figure 4.4 − Dependence of CO evolution on iron droplet size at T=1773K.

4.1.4 The Effect of Sulphur Content

At fixed oxygen potential, CO evolution rate was studied at the range of S content from 0 wt pct to 0.3 wt pct at temperatures of 1713K and 1773K. The rate goes through a maximum with respect to sulphur content in the metal about 0.0126%.

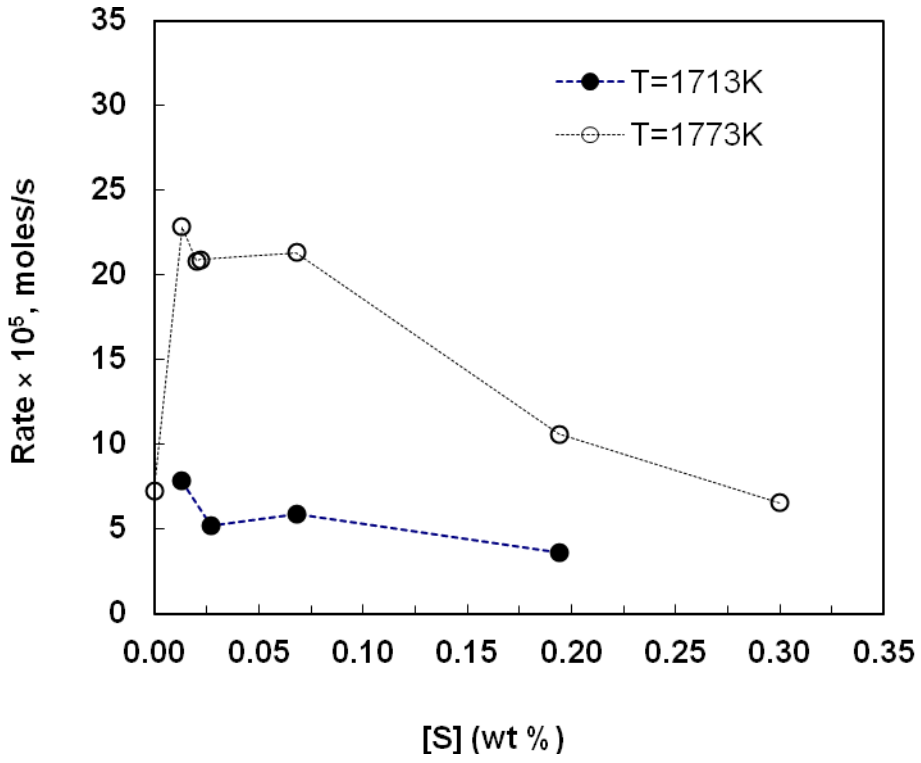

Figure 4.5 − Dependence of CO evolution rate on S content.

Table 4.2: CO evolution rates for 1g of droplet in 20% FeO containing slag at T=1773K.

% C	*% S*	*Evolution Rate ×10^5 (moles/s)*
2.90	0	7.24
2.91	0.013	22.82
2.75	0.02	20.83
2.64	0.022	20.89
2.70	0.0683	21.31
2.94	0.19	10.58
2.69	0.3	6.55

4.2 Droplets Swelling Rate

The main objective in this study is to observe the behavior of Fe-C-S droplet reacting with slag, and measure the swelling rate of droplet. Although the exact behavior of the droplets depends on the precision of experiments, general observations in this study can be described as follows.

4.2.1 Experimental observations

4.2.1.1 Droplet containing C= 3.71%, S=0.0063%

In this experiment, slag compositions are: CaO/SiO_2=1.2, MgO=12%, FeO=20%. Figure 4.6(a) is for the droplet containing C=3.71%, S=0.0063%. On entering the slag, due to the surface tension and fast external decarburization rate, the droplet floated on the surface of the slag rather than falling to the bottom of the crucible. A gas halo was formed around the droplet once it contacted the slag; meanwhile a slag foam was also observed. The diameter of droplets increased to 1.5 times the original. The fast decarburization reaction on slag surface lasted for 4s, then droplets fell back into the slag, after that, the reactive drop still gave off gas so that a maximum 50 mm of foam was observed, while lasted for 15s before it collapsed. Some still photos showing the reaction sequence are shown in the following Figure 4.6 (a).

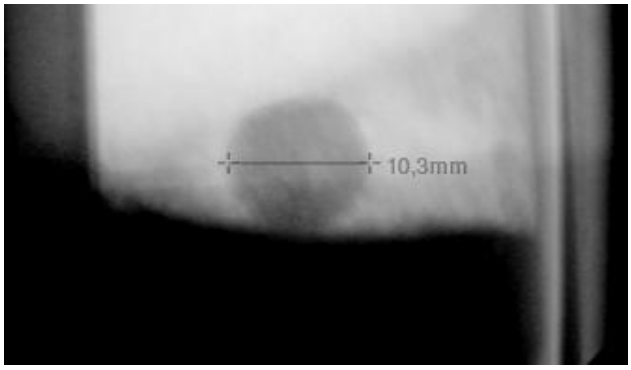

t =1s

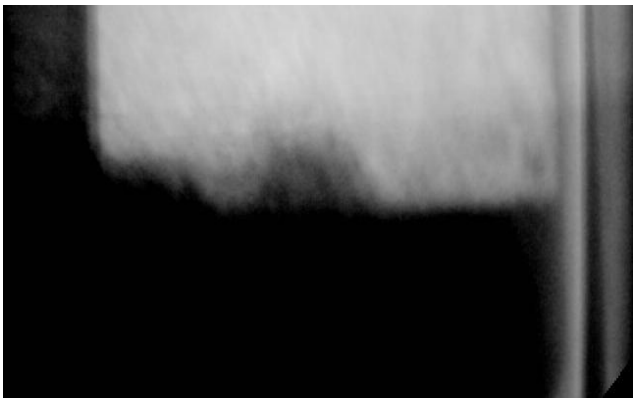

t =4s

Figure 4.6 (a) − X-ray pictures for metal droplet containing C=3.71%, S=0.0063%

4.2.1.2 Droplet containing C= 2.64%, S=0.022%

Faster swelling of droplets in the slag was observed by dropping 1g or 2g of metal with C=2.64%, S=0.022%, see Figure 4.6 (b). After an incubation time of about 1.8s, the droplet diameter became 4 times bigger than the original size for 2g of metal, and 3 times for 1g of metal, then shrunk to 1.5 times the original size, and continued to react with the slag for 2s before falling down to the bottom of the crucible. The still photos in sequence

are shown in Figure 4.6 (b). The swelling rate with time for 1g and 2g droplet is shown in Figure 4.7.

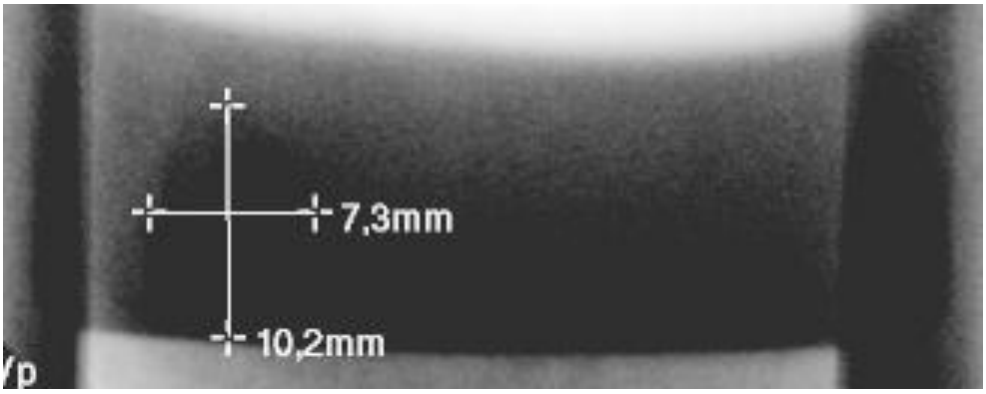

t = 0s

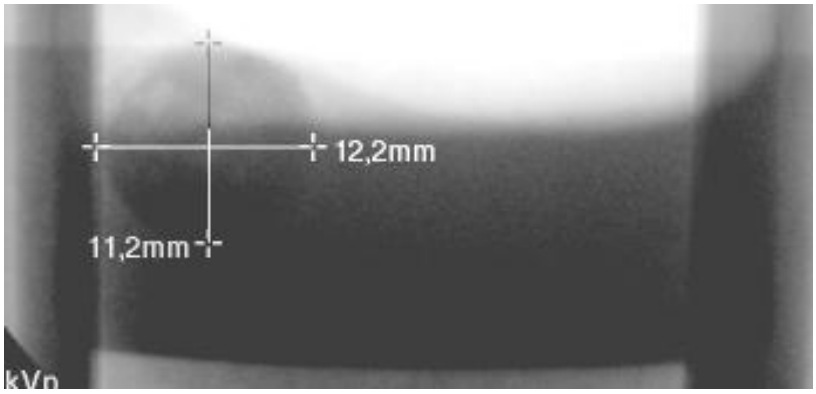

t = 2s

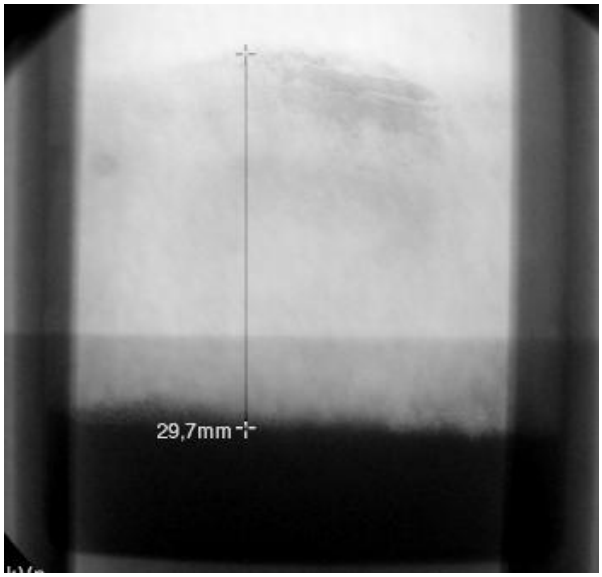

t = 4s

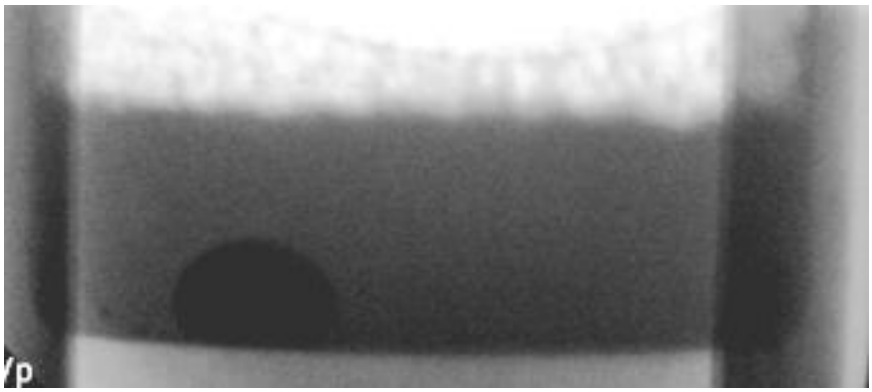

After reaction

Figure 4.6 (b) − X-ray pictures for metal droplet containing C=2.64%, S=0.022%

4.2.2 Swelling rate

The dependence of swelling rate on time for 1g and 2g droplets at FeO=10% and 20% is shown in Figure 4.7, 4.8 and 4.9. It increases with the size of the droplet because the vigorous CO evolution improves the mass transfer coefficient. And the temperature has the same effect. From Figure 4.8, it can be seen that the swelling rate is obviously higher at T=1773K than at T=1713K.

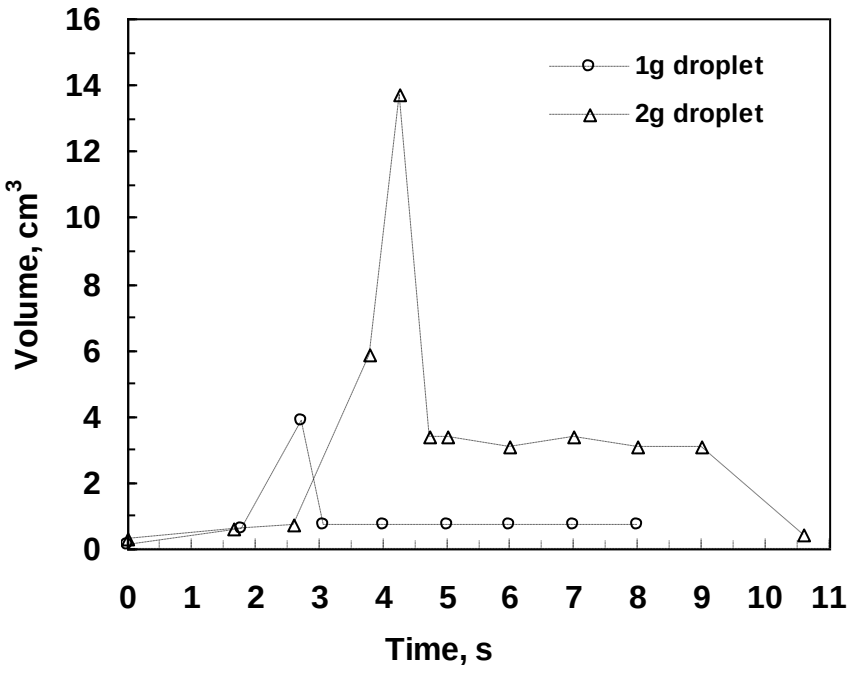

Figure 4.7 – Droplet volume change with time for FeO=10% and 20% at T=1773K.

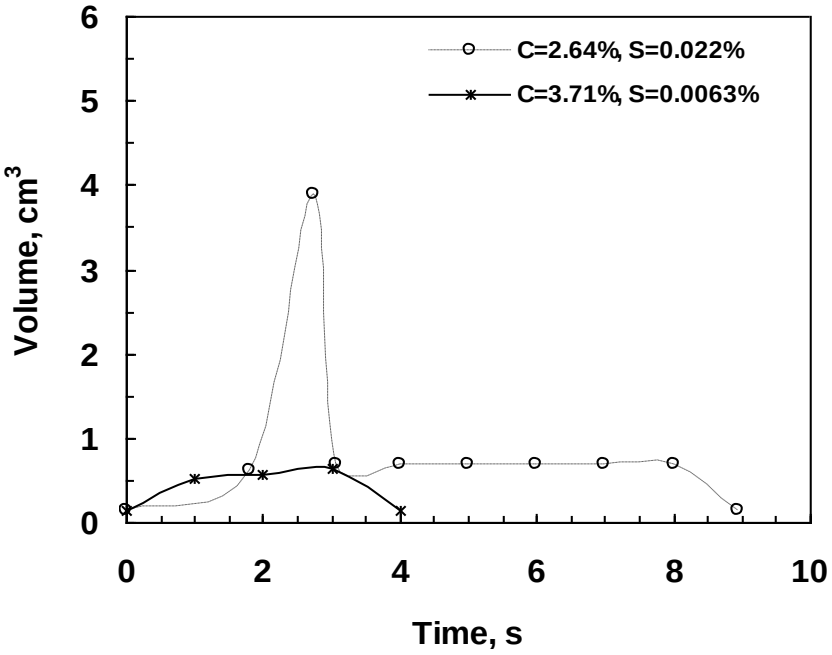

Figure 4.8 − Droplet volume change with time for FeO= 20% at T=1713K and T=1773K.

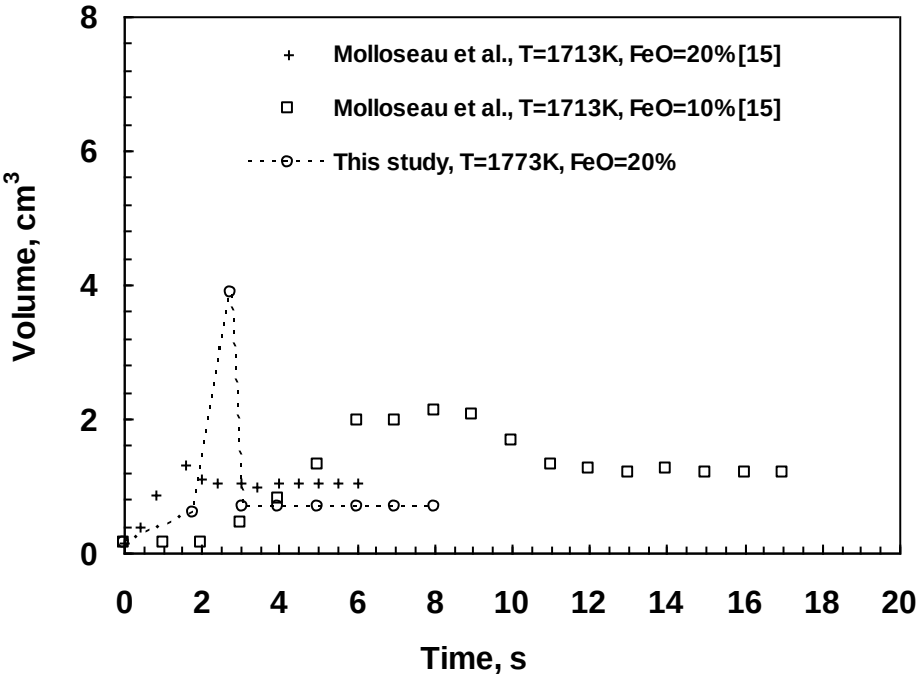

Figure 4.9 - Droplet volume change with time for T=1713K (Molloseau) and T=1773K (this study, C=2.64% and S=0.022%).

4.3 Discussion

4.3.1 Observations on Droplet Swelling

Different phenomena were observed by the workers when metal droplets reacted with FeO containing slags. Mulholland et al. [3] observed a gas halo was formed around the metal droplets and the size of droplets kept constant. The similar phenomenon was found by Min et. al [21] [22] when dropping metal droplet C=2.3 to 4.2 wt pct and S=0.001 to 0.08 wt pct into CaO/SiO2=1, Al2O3=4-6 wt pct slags. Molloseau et al. [14] observed the droplet became emulsified as it reacted with slag containing more than 10% FeO, and metal droplet compositions are C=2.91%, S=0.011%. Once the metal droplets became emulsified, it is still internally connected, and after the reaction was completed, the metal droplet fell back to the crucible as a whole droplet. However, in this study, a different phenomenon was observed.

As shown in Figure 4.6 (b), when the metal droplet fell down into the crucible, there was no gas halo formed around the droplet due to the lower carbon content, and oxygen diffused into metal droplet to achieve supersaturation pressure for CO nucleation inside the metal. With the nucleation of CO bubbles, droplet became bigger and bigger and float out of the slag surface, meanwhile foam was formed. Then the metal expanded explosively as a whole droplet, and did not fragment. With the expansion of metal droplet, the metal films between bubbles started thinning, when the critical thickness reached, the film ruptured; from this moment, CO bubbles escape from the droplet and causing slag foaming. Gas escape rate increases with the CO generation, when gas escape

rate is bigger than the generation rate, the droplet starts shrinking, and finally falls back to the bottom of the crucible.

In summary, there are two distinct regimes of reaction phenomena, one is the formation of gas halo around the droplet, another is the big swelling of droplet, which phenomenon will occur depends on the chemistries of slag and metal droplet as well as temperatures.

Which phenomenon will be observed depends on the carbon and oxygen reaction. There are two reaction sites for carbon and oxygen reaction, one is the surface reaction where carbon is removed at the surface of the droplet, under this circumstance, a gas halo is formed around the droplets and the size of droplet does not change. Another involves the nucleation of CO bubbles inside the metal, in which case the droplet will swell. Whether or not CO bubbles will nucleate inside the metal depends on the balance between the diffusion rate of oxygen transfer from the slag into the bulk of the metal and the rate of the mass transfer of carbon from the bulk to the surface. If the oxygen supply rate is higher than carbon diffusion rate, there is a possibility for CO nucleation inside the metal which causes droplet swelling. Usually, the higher carbon contents benefit for the nucleation of CO bubbles, see reaction (1). But if carbon content in the droplet is too high, such as Min's observation, the surface reaction happens, and the big swelling of droplet would not be observed. In Min's study, FeO in the slag is 2 to 20%.

4.3.2 CO Evolution Rate

Based on the observation of X-ray Fluoroscopy on the reaction behavior of metal droplets reacting with FeO containing slag, it is understood that the CO evolution is due to the nucleation of CO bubbles inside the metal, the following will discuss what are the relationships between CO evolution rates and experimental variables in order to understand the rate determining step.

4.3.2.1 The Effect of FeO Content

Figure 4.10 shows the dependence of CO evolution rate on the iron oxide content in the slag. The dashed line is Min's gas metal reaction model, the smooth line is Murthy's result in which the mass transfer is concluded as the rate determining step. The slag compositions in Min's experiments: CaO/SiO2=1, Al2O3=4-6%, Murthy's compositions: CaO=47%, SiO2=41%, Al2O3=12%. From Figure 4.10, it can be seen that the results of this study and Molloseau did not fit any of these two models; the reaction mechanism exists as others. The measured CO evolution rates in this study are much higher than these in Min and Murthy is because the reaction phenomena are different. As discussed previously, Min and Murthy's observed a gas halo formed around the metal droplet since the higher carbon content and lower sulphur content used in their studies. Usually, the higher carbon content should be benefit for C and O reaction, however, if carbon content is too high, C and O reaction will mainly happen on the droplet surface, and less oxygen diffused into metal droplets. The supersaturation pressure needed for the nucleation of CO bubbles could not be reached.

S has two competing effects on the reaction rate. On the one side, sulfur is a surface active element, it segregates on the surface and leads to poisoning of the reaction, thus decreases the reaction rate, so called "site blockage model". On the other side, sulphur decreases surface (interfacial) tension of droplet, which lowers the energy barrier for CO bubble nucleation in the metal. In both of Min and Murthy's experiments, there is little or no sulphur in the metal, the energy barrier is too big for the formation of CO bubbles.

In this study, the experimental conditions (C=2.91%, S=0.013%) are designed to avoid the formation of gas halo, allowing more oxygen diffusing into the metal droplet and causing droplet a big swelling. Even under the similar experimental conditions, different reaction behaviors could be observed in this study and Molloseau's. As mentioned in Molloseau's work, they observed the droplet becoming emulsified; however, in this study the droplet was found to be expanded and did not fragment, the swelling rates are different, see Figure 4.9. This is the reason for the difference of the results between Molloseau and this study. In this study, the kinetic model was developed for self-consistent explanation for all the observations.

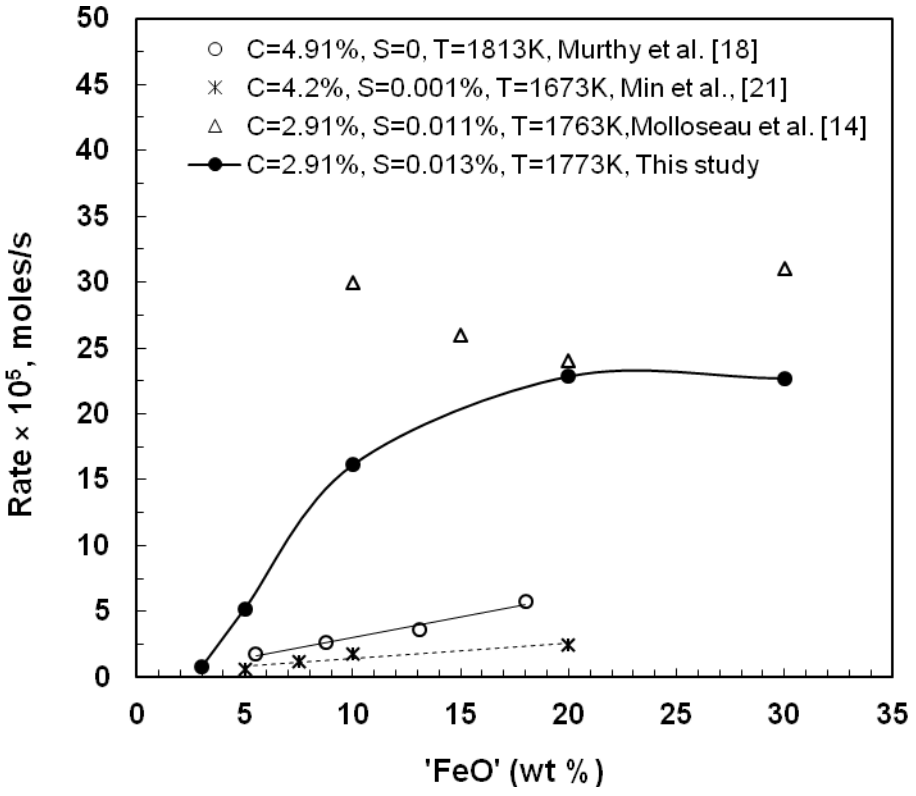

Figure 4.10 − CO evolution rate as function of FeO content in the slag.

4.3.2.2 The Effect of Temperature

CO evolution rate increases exponentially with temperature, the slopes are different from 3 to 20% FeO content in the slag, and it seems unchanged after FeO increased up to 20%. CO evolution rate is exponential to the temperature, see Figure 4.11.

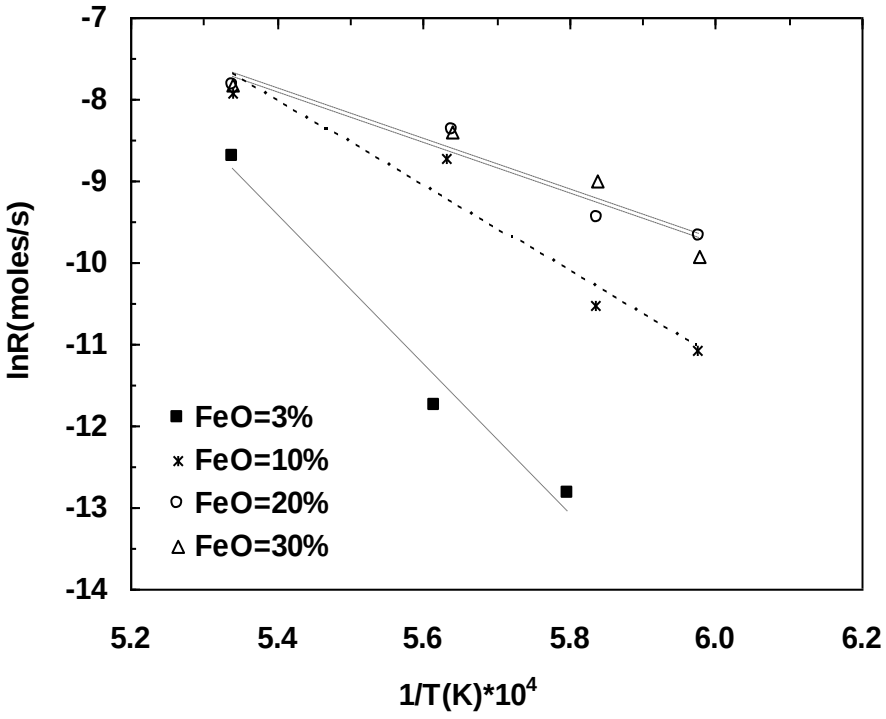

Figure 4.11 − Dependence of CO evolution rate on temperature.

4.3.2.3 The Effect of Iron Droplet Size

Figure 4.3 shows the effect of droplets mass on CO evolution rate. In equation (2.16), the pre-exponential term has little effect on the nucleation rate, the terms inside the exponential, temperature, T, surface tension, σ and supersaturation pressure, ΔP change less than 1%, J may rise by many orders of magnitude. If T, σ and ΔP were kept the same, CO evolution rate should increase linearly with droplet mass, this is in good agreement with our experimental results.

4.3.2.4 The Effect of Sulphur Content

The effect of sulphur on CO evolution rate is quite complicated. On the one hand, it decreases metal surface tension, and reduces the energy barrier for the nucleation, thereby accelerating the decarburization rate. On the other hand, sulfur segregates to the surface and leads to poisoning of the reaction sites. Due to the poisoning of the reaction sites, less oxygen would transfer into the metal droplets, causing a lower supersaturation pressure, which would decrease the CO nucleation rate. Due to two competing effects, a maximum value of CO evolution rate should be observed at specific sulphur content. In this study, at T=1773K, the maximum rate was found at S=0.0126 wt pct, see Figure 4.12. The trend of S effect on CO evolution is similar as Molloseau, however, the magnetite is different. There is no explanation this time other than the experimental technique.

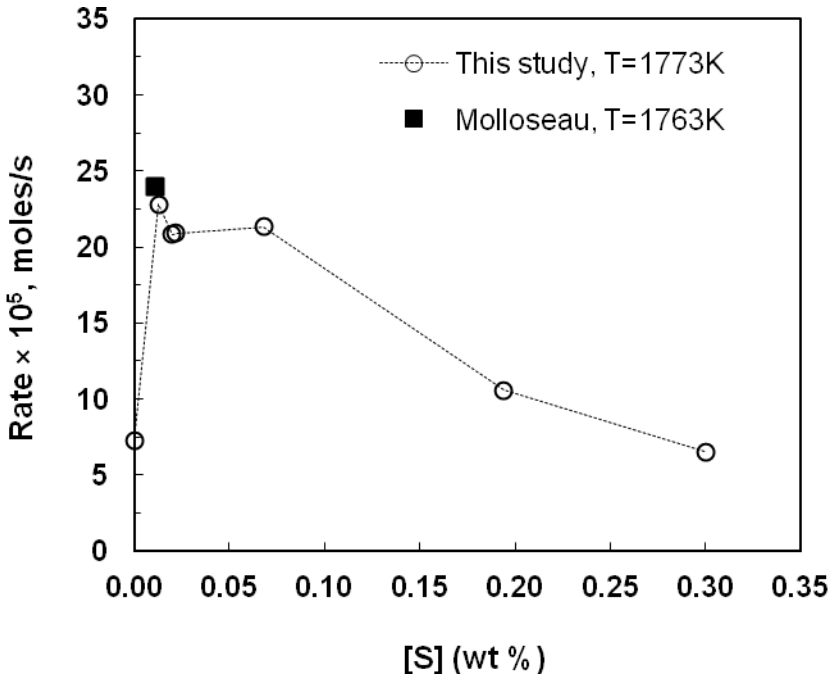

Figure 4.12 − Dependence of CO evolution rate on S content at T=1773K.

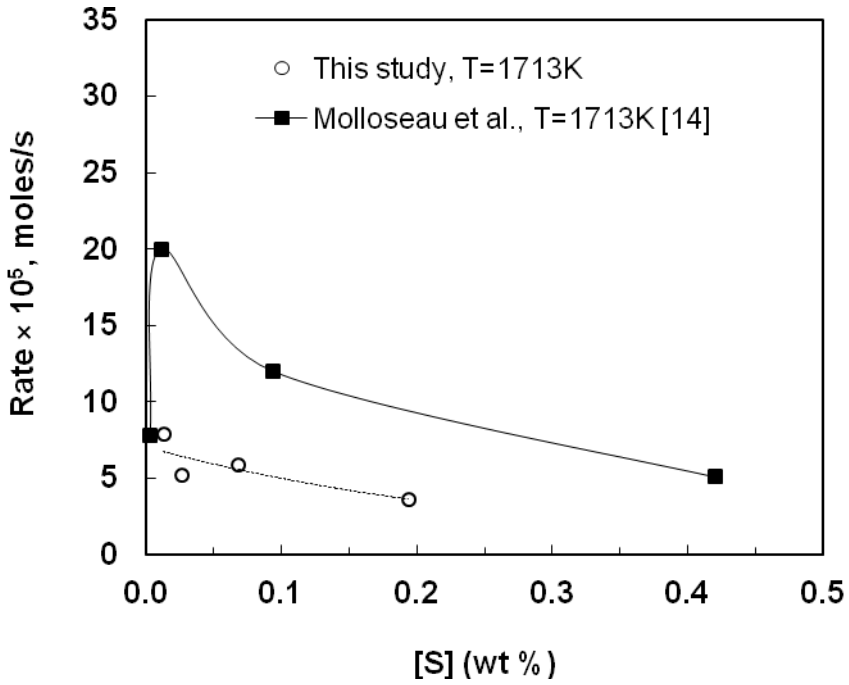

Figure 4.13 − Dependence of CO evolution rate on S content at T=1713K.

4.4 Summary

(1) The reaction phenomenon for metal droplets reacting with MgO-CaO-SiO2-FeO melts depends on metal droplet and slag chemistries as well as temperatures;

(2) CO evolution rate for metal droplet reacting with MgO-CaO-SiO2-FeO melts increases with FeO content, but the relationship is neither linear nor exponential;

Chapter 5

KINETIC MODEL FOR METAL DROPELTS AND SLAG REACTIONS

5.1 Introduction

About two decades ago, L. A. Baker et al. [46]-[48] observed CO bubbles nucleation inside Fe-C droplets when falling through gas mixture of oxygen and helium using rotating prism cine-camera. Noticing the significance of interaction between slag and metal droplets in decarburization in an oxygen steelmaking furnace, Mulholland et al. [3] studied the reaction behavior of Fe-C with Fe_2O_3 containing slag. They found an important reaction phenomenon that there is a gas halo existing around the metal droplet, and the subsequent reactions proceed through gas as intermediate, the size of droplet kept intact. Later Fruehan's group [14]-[15] firstly demonstrated the change in phenomenon form a droplet that keeps intact to one that is emulsified. Although these excellent studies have provided some information on the reaction behavior, very little has been achieved with respect to quantitative prediction of CO bubble nucleation rate inside the metal.

The overall reduction reaction of FeO in liquid slag by C dissolved in the metal droplet can be written as:

$$\underline{C} + \underline{O} = CO_{gas} \tag{5.1}$$

Nucleation of CO bubbles involves the clustering process: carbon and oxygen firstly form a metastable CO cluster, [65]

$$\begin{matrix} C \rightarrow C^* \\ \qquad\quad \rightarrow (CO)^* \\ O \rightarrow O^* \end{matrix} \tag{5.2}$$

As the clustering process proceeds, the liquid metal becomes supersaturated with CO embryos, local fluctuation sets CO embryos growing into bubbles. Kaddah and Robertson [51]-[54] used equation $I = Zw^*(\dot{C}_0 + \dot{C}_C)\exp(-\Delta F / kT)$ to predict the nucleation rate, and a supersaturation of 5×10^4 atm was calculated for CO nucleation, which is two orders higher than the experimental measurements. Until now, the nucleation rate still could not be predicted quantitatively.

As for the kinetics for metal droplets reacting with iron oxides containing slags, discrepancies exist among the workers. For example, Molloseau et al. [14]-[15] found the reaction rate for metal droplet (C=2.91%, S=0.011%) and MgO-CaO-SiO2-FeO (CaO/SiO2=1.2) melts was two orders higher when FeO content was increased from 3 wt pct to 20 wt pct, this was not observed by Murthy et al. [17]-[19], they found that the

dependence of the reduction rate on FeO content in the slag of 47CaO-41SiO2-12Al2O3 is linear for Fe-C droplet C=4.339 wt pct to 4.911 wt pct, the relationship is r = $0.1114+8.351 \times 10^{-3}$ (% FeO). The effects of sulphur on the reaction rate are found to be different by the workers. Min et al. [21][22] applied the site blockage model to explain the decrease of the reaction rate with S from 0.016 wt pct to 0.08 wt pct in the metal, however, Murthy concluded that S had no effect on the reaction rate. Molloseau found the positive effect of S, and the reaction rate goes to the maximum at specific value.

The current and previous work were performed by the present authors on the reaction behavior of metal droplets with MgO-CaO-SiO2-FeO melts in order to, first, qualitatively provide the regimes for distinct reaction behaviors, and second, derive an expression for the CO evolution rate to render nucleation rate predictable.

5.2 REACTION PHENOMENA

There are two distinct regimes for the reaction behavior when metal droplets react with iron oxide containing slags.

5.2.1 The presence of Gas halo

One of the reaction phenomena observed involves the presence of gas halo around the droplet, the size of droplet does not change. This behavior was observed by Mulholland [4] and Min et al. [21] In order to observe this phenomenon, the carbon content in the metal droplet has to be high, C= 4 ~ 5%, and oxygen potential in the slag should be

lower. The lower oxygen potential makes it impossible for enough oxygen diffuse into the metal drop, thus the C and O reaction mostly happens at the surface of the droplet. Under this circumstance, CO bubbles nucleate at the interface between the metal and slag. The energy barrier is quiet small because it is heterogeneous nucleation. In the presence of a gas halo, as shown in Figure (5.1), the possible rate determining steps could be: mass transfer of oxygen in the liquid slag phase, charge transfer by the reaction: $Fe^{2+} + O^{2-} = Fe + O_{ads;}$ chemical reaction at slag gas interface ($CO + O_{ad} = CO_2$), gas phase transport in gas halo, and chemical reaction at metal gas interface ($CO2 + \underline{C} = 2CO$). During the past 20 years, all of these rate determining steps have been given much attention and are well understood. [16][17]

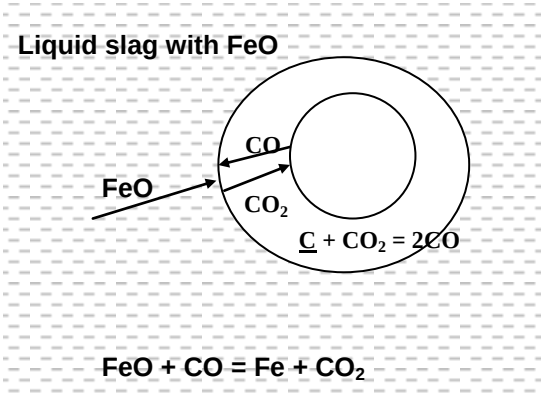

Figure 5.1 − Elementary steps for metal droplets react with slag with the presence of a gas halo.

5.2.2 Droplets have big swelling

When the carbon content in the metal is lower, C and O surface reaction would not proceed very rapidly. If the oxygen potential in the slag is high, oxygen will start to diffuse into the metal droplet, with more O accumulated inside the metal, CO embryos will be formed, and the local fluctuation sets CO embryos growing into bubbles. This process could be broken into few steps: mass transfer of oxygen in the slag phase; charge transfer by the reaction: $Fe^{2+} + O^{2-} = Fe + O_{ads;}$ O diffusion inside the metal; C mass transfer inside the metal; nucleation of CO bubbles; CO escapes from metal droplets, see Figure 5.2. It has to be mentioned that this circumstance is different from the phenomenon of gas slag metal emulsion, the metal droplet was observed to have a big swelling and it is inter-connected. The gas pressure inside the metal droplet is not high enough to break droplet into some tiny pieces. See Figure 5.2 for the droplet's swelling rate.

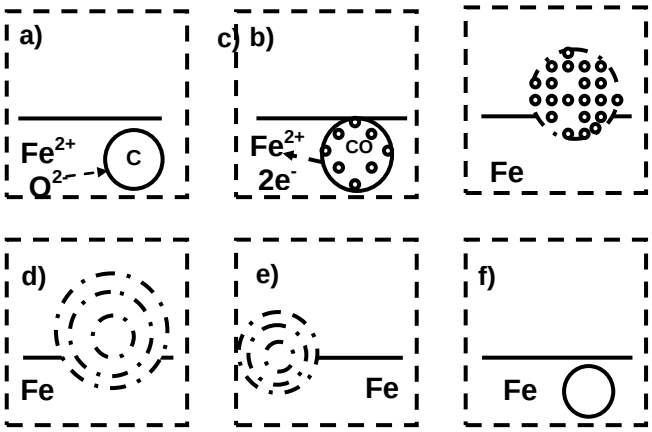

Figure 5.2 − Elementary steps for metal droplets react with slag having big swelling.

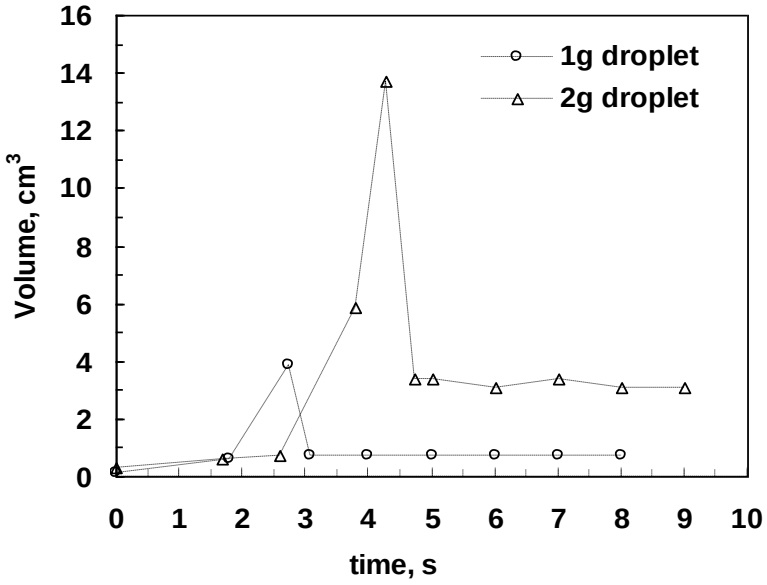

Figure 5.3 – Droplet (weight = 1 g and 2 g) volume change with time at T=1773K.

5.3 KINETIC MODEL

The phenomenon that there is a gas halo present around the drop has been understood very well, however, there is little study on the behavior that the droplet has a big swelling, so in this study, special attentions will be paid to this phenomenon.

5.3.1 Elementary Reaction Steps

(1) Oxygen mass transfer in the slag: corresponding to a) and b) in Figure 5.2, the little swelling part in Figure 5.3. At this stage, oxygen starts to diffuse into the metal drop, there is a very small amount of CO nucleated inside the droplet due to the local fluctuation of embryo density, and caused droplet floating out of the slag surface, there is no foam formed. The increase in the pressure could not be measured due to the limit of

the sensitivity of the pressure transducer. During this incubation period, O mass transfer in the slag is the rate determining step;

(2) Massive CO nucleation inside the drop: rapid CO bubbles nucleation inside the metal due to the buildup of supersaturation pressure. During this stage, the metal droplet has a big swelling, meanwhile slag foam was formed and reached to the highest volume.

Once a bubble nucleated inside the metal, it will grow. There are two regimes for the bubble growth: inertially dominated growth and chemical growth. For inertially dominated mechanism, the pressure inside the vapor space is higher than that of the surrounding liquid and the temperature within the bubble is essentially equal to that of the surrounding liquid. The growth under this mechanism is limited by the rate at which the surrounding liquid can be pushed out to the way and the bubble radius versus time can be calculated from Rayleigh's equation. Grezl et al. [7] found that bubbles grew very rapidly to a limiting radius depending on the initial bubble pressure and radius. When the initial pressure is 100 atm, the bubble grew from $5.507*10^{-7}$ m to maximum size of $5*10^{-6}$ m after $\Delta t = 5*10^{-6}$ s. The bubble growth is so rapid that it is ruled out of the rate limiting step.

The reason that the size of the bubbles trapped in the metal increased with time is because of the coarsening and coalescence, see Figure 5.4. The sample was obtained by

quenching metal droplet into cold water when it was reacting with Fe2O3 containing slag, the pore size left over is about 0.3 mm.

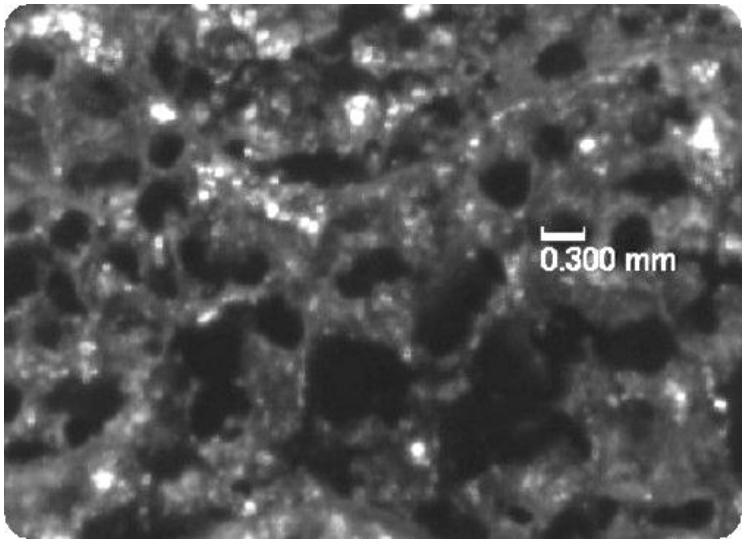

Figure 5.4 − Metal droplets recovered by quenching

CO bubbles as small as 24 Å were produced as predicted previously in this study. At early stage, it is impossible for these minute bubbles escape from the metal droplets because the surface tension is too big to overcome. With CO bubbles nucleated inside the metal, the gas fraction volume increased greatly, see Figure 5.5. The maximum volume fraction for the metal droplet can reach $\varepsilon = 0.96$ (very dry foam) at S=0.022%, and $\varepsilon = 0.84$ at S=0.01%. The thickness of metal films between the bubbles is getting smaller and smaller, finally reaches the rupture point. From this point, CO started to escape from the drop.

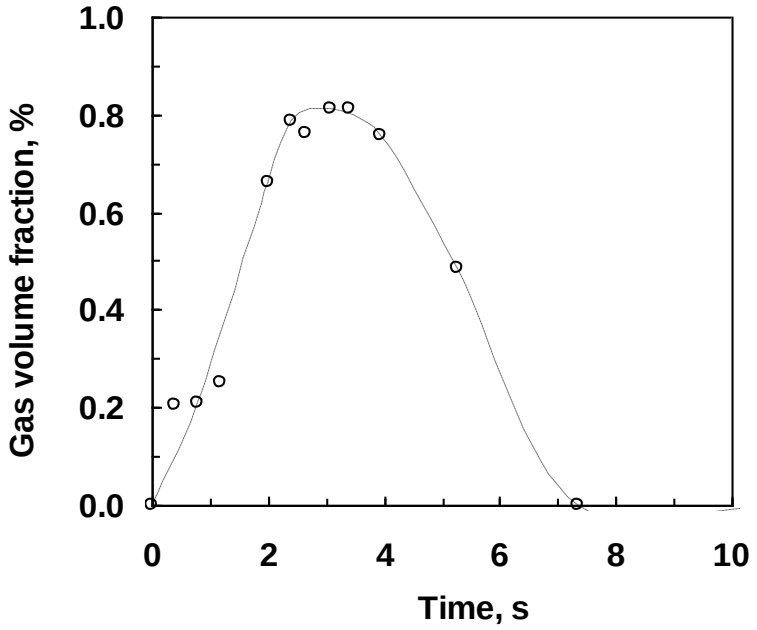

Figure 5.5 − Gas volume fraction change with the time.

CO nucleation as the rate determining step could be successfully applied to explain S effect on the reaction rate. On the one side, sulfur is a surface active element, it segregates on the surface and leads to poisoning of the reaction, thus decreases the reaction rate, so called "site blockage model". On the other side, sulphur decreases surface (interfacial) tension of droplet, which lowers the energy barrier for CO bubble nucleation in the metal. So as observed in this study and Molloseau's work, at specific S content, the reaction rate reached the maximum value.

(3) Fast reaction stops. With the consumption of C and O, there would be no more CO generated inside the metal, droplets started shrinking and fell to the bottom of the crucible as one whole drop. After this, foam still can sustain for a while since C and O

surface reaction happen when drop fell to the liquid slag phase where the oxygen potential is higher.

5.3.2 Kinetic Model

Robertson et al. [52] used this equation, $I = Zw^*(\dot{C}_0 + \dot{C}_C)\exp(-\Delta F / kT)$, to calculate the nucleation rate and defined the concentration of CO embryos in the drop as the sum of C and O. Levine [62] treated it as the total atom inventory, equals to $N_C + N_O + N_{Fe}$. According to the nucleation theory [79], it is the number of liquid molecules per unit volume. In this study, it is CO embryos concentration, which should be related to the chance of a C atom meeting an O atom, therefore it is related to the product of C and O concentrations. However, at very low concentrations of one element this concentration should dominate the value of the product. Therefore, in this study, the number concentration of CO embryos depends on the smaller of the concentration of oxygen or carbon, in the case of a high carbon activity in the metal, it depends on oxygen concentration reached during the incubation time. The X-ray observations showed that for each size of iron droplet, it requires time, τ, to establish the steady stage nucleation conditions. In this study it took about 1.8s for a 1g droplet to rise out of the liquid slag, during this period, oxygen diffused into metal droplet. Taking the oxygen mass transfer co-efficient as $3.8*10^{-3}$ cm/s as proposed by Molloseau and Fruehan [14]-[15], the calculated activities of carbon and oxygen as 6.525 and 0.062, respectively, and the CO pressure at equilibrium as 163 atm.

Considering the phenomenon of CO nucleation is similar to liquid vapor phase change phenomena [66][79] and the nucleation rate is given by:

$$J_s = N_0 \exp[\frac{-\Delta H}{kT}][\frac{3\sigma}{\pi m}]^{\frac{1}{2}} \exp[\frac{-16\pi\sigma^3}{3kT[P_{ve} - P_L]^2}] \quad (5.3)$$

Where: N_0: is the number concentration of CO embryos in the liquid; σ is surface tension at liquid gas interface; ΔH is heat of formation of one CO molecule; m is the mass of one molecule; T is temperature, in Kelvin, k is Boltzman constant; P_{ve} is the pressure in the vapor bubble at equilibrium; P_L is liquid pressure.

Put all of these parameters into equation (5.3), the calculated nucleation rate is:

$$J_s = 2.04*10^{38} \exp[-\frac{2.17}{10^{-6}}] = 0 \quad (5.4)$$

The classical nucleation rate equation predicts no bubble formation, as has also been found by several other workers [22][52]. Heterogeneous nucleation on inclusions is unlikely because the metal is very clean. From the calculation in equation (5.4), it can be seen that the nucleation rate goes to zero because the energy term inside the exponential is too large. This observation led most previous workers to conclude that an extremely high supersaturation pressure (two orders higher than experimental measurements) is needed

for the formation of CO bubbles, this is in keeping with many other studies on nucleation of gasses in liquids[73][74].

Assuming a value for σ of 0.9N/m [92][93], the minimum radius of stable bubble nucleus is $r = 1.97*10^{-7}$ m, which contains about $2.2*10^{7}$ molecules. The large number of molecules makes formation of such nucleus impossible. Levine [61]-[63] proposed that doubly charged chemisorbed oxygen ions in the surface layer of spherical CO embryos decreased the surface tension and thus decreased the energy barrier for nucleation. The reduction magnitude of surface tension is not known, however, we can define surface tension modifying parameter, ψ, where the effective surface tension $\sigma = \psi\sigma_0$. ψ=0.023 was obtained based on one of the measured CO evolution rates, ψ value between 0 and 1 has been shown to be reasonable in several systems [61][73][74]. Re-calculating the bubble radius, $r = 2.64*10^{-9}$m, this bubble would contain 54 molecules. This is consistent with studies of dissolved gas in water where there are typically a few hundred molecules in the critical nucleus [80]. The modified nucleation rate equation is expressed by:

$$J_s = N_0 \exp[\frac{-\Delta H}{kT}][\frac{3(\psi\sigma_0)}{\pi m}]^{\frac{1}{2}} \exp[\frac{-16\pi(\psi\sigma_0)^3}{3kT[P_{ve} - P_L]^2}] \quad (5.5)$$

The CO generation rate can be calculated now:

$$R_G = J_s \cdot (\frac{n_e}{N_A}) \cdot V_0 \quad (5.6)$$

where:

R_G is CO generation rate, moles/s;

J_s is CO nucleation rate, /cm^3s;

V_0 is the original droplet volume, cm^3;

n_e is the number of molecules in an embryo;

N_A is Avogadro number.

5.3.3 Derivation of Optimum Parameters

Equation (5.5) presents a mathematical equation for the CO nucleation rate inside the metal droplet. In order to use this expression to predict CO evolution rate for other similar conditions, the values of parameters in equation (5.5) have to be derived. The kinetic data produced in this study will be used for this purpose, and other parameters are obtained from the literature.

5.3.3.1 Estimation of the number concentration of CO embryos in the metal

The CO embryo number concentration depends on how much oxygen was transferred into the metal during the incubation time; Min's mass transfer model [16] can be employed:

$$J_{FeO} = \frac{m_s \rho_s A(pctFeO - pctFeO^S)}{100 mw_{FeO}} \quad (5.7)$$

where, J_{FeO}: FeO flux (moles/s);

m_s: mass transfer coefficient in the slag (cm/s);

ρ_s: density of the slag (g/cm^3);

A: original droplet surface area (cm^2);

pct FeO: FeO content of the bulk slag;

pct FeO^s: FeO content at the droplet surface (approximately zero at this mechanism);

mw_{FeO}: molecular weight of FeO.

Taking the oxygen mass transfer co-efficient as 3.8*10^{-3} cm/s for 20 and 30% FeO in the slag, 1.3*10^{-3} cm/s as proposed by Molloseau and Fruehan [14]-[15], the oxygen concentration can be calculated.

5.3.3.2 Supersaturation pressure

Supersaturation pressure is CO pressure equilibrium with dissolved C and O atoms in the drop, calculated by

$$P_{ve} = k a_c a_o \tag{5.8}$$

where k is equilibrium constant for the reaction (5.1), $\log k = \frac{1160}{T} + 2$

a_c is carbon activity, $a_c = f_c[\%C]$, $\log f_c = 0.14*[\%C] - 0.34*[\%O] + 0.046*[\%S]$

a_o is oxygen activity, $a_O = f_O[\%O]$, $\log f_o = -0.2*[\%O] - 0.13*[\%C] - 0.133*[\%S]$

The Figure 5.6 shows a comparison between supersaturation pressure calculated using the above method and Robertson's experimental measurements [52].

5.3.3.3 Surface Tension

By fitting results from the authors previous work to Equation (5.5), values of ψ, were found in the range $5.81*10^{-4}$-$2.4*10^{-4}$.

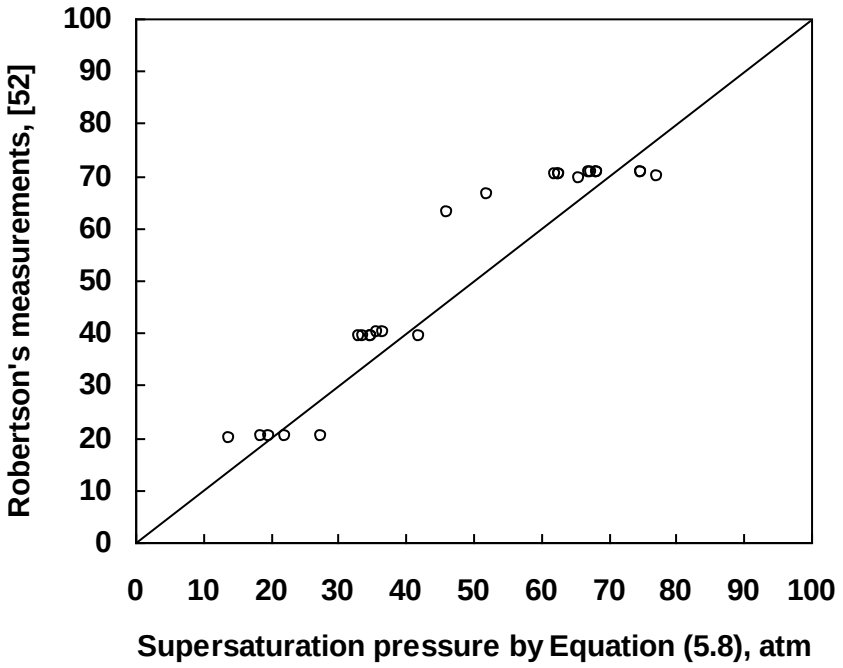

Figure 5.6 − Comparison between predictions and experimental measurements.

5.4 Model Validation

5.4.1 Size Effect

In equation (5.5), the pre-exponential term has little effect on the nucleation rate, the terms inside the exponential, temperature, T, surface tension, σ and supersaturation pressure, ΔP change less than 1%, J may rise by many orders of magnitude. If T, σ and ΔP were kept the same, CO evolution rate should increase linearly with droplet mass, this is in good agreement with our experimental results, see Figure 5.7.

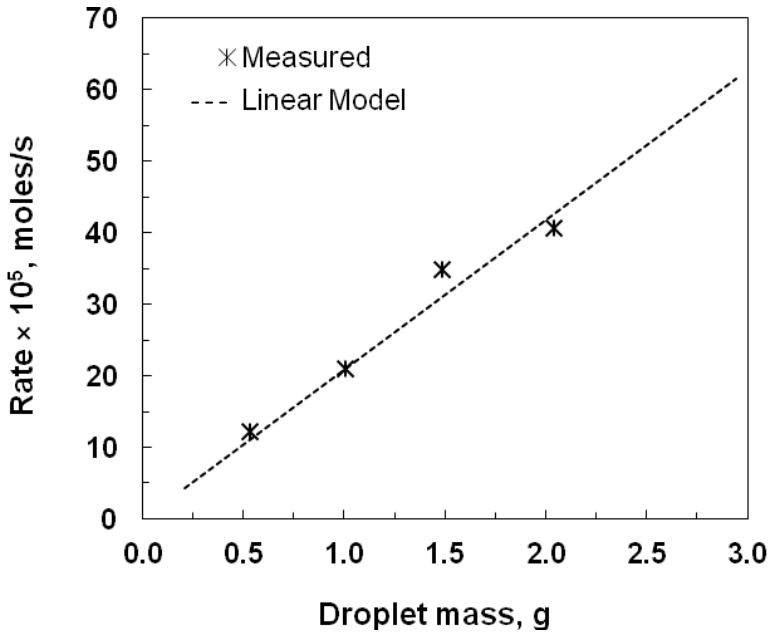

Figure 5.7 − CO evolution rate as function of droplet mass.

5.4.2 Supersaturation Pressure

The dependence of CO evolution rate on supersaturation pressure is complicated. The CO evolution rate is plotted against FeO contents in the slags, see Figure 5.8. As seen, the relationship fits the equation very well.

5.4.3 S Effect

The effect of sulphur on CO evolution rate is quiet complicated. On the one hand, it decreases metal surface tension, and reduces the energy barrier for the nucleation, thereby accelerating the decarburization rate. On the other hand, sulfur segregates to the surface and leads to poisoning of the reaction sites. Due to the poisoning of the reaction sites, less oxygen would transfer into the metal droplets, causing a lower supersaturation pressure, which would decrease the CO nucleation rate. Due to two competing effects, a maximum value of CO evolution rate should be observed at specific sulphur content. In this study, at T=1773K, the maximum rate was found at S=0.0126 wt pct.

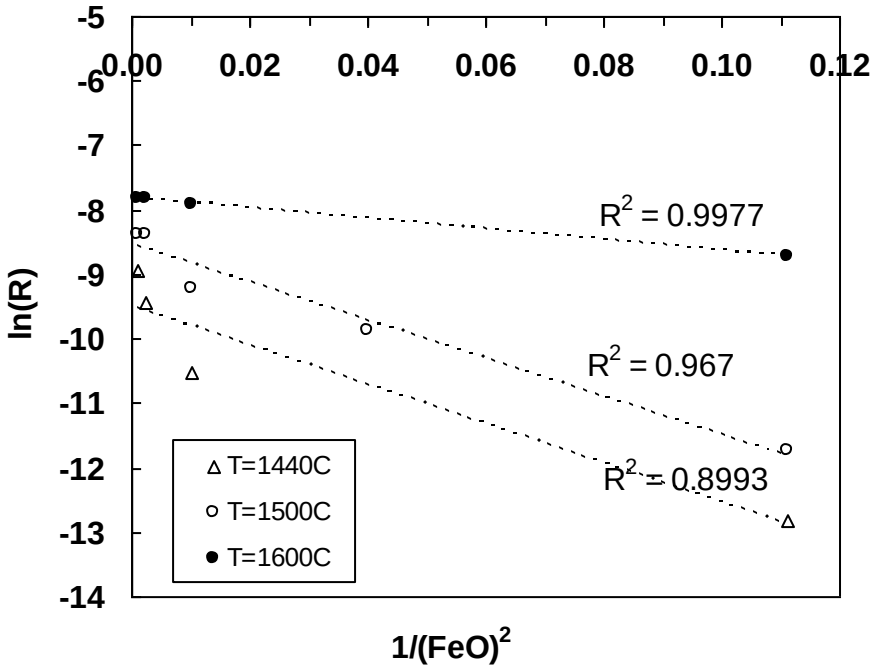

Figure 5.8 − CO evolution rate as function of FeO contents in the slags.

5.4.4 Comparison with Experimental Result

Figure 5.9 shows the comparison between experimental measurements and the calculated values from equation (5.6), taking ψ=0.023, the agreement is excellent for T=1773K and very reasonable for other temperatures, it is possible that a different value of ψ should be used for various temperatures. Molloseau's data could not fit the model well because of the different swelling rate observed in their study.

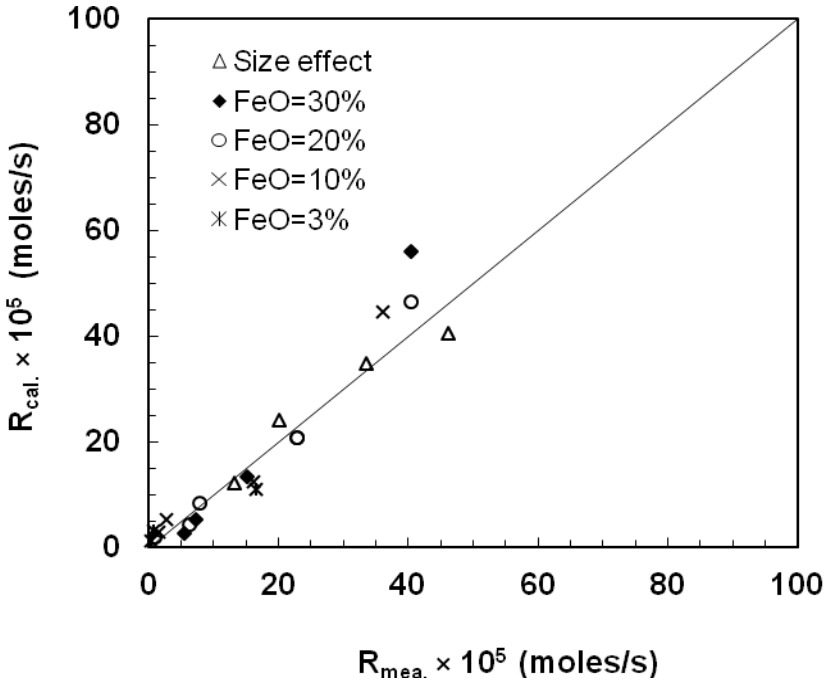

Figure 5.9 − Comparison between theoretical predictions and experimental measurements

The modification number has been kept the same for different temperature at the fixed FeO content in the slag, different number has been used for various FeO contents in the slag. And the following table gives the number of ψ at the range of 3 to 30 wt pct FeO.

FeO, wt pct	*ψ*
3	0.0019
5	0.0029
10	0.0053
20	0.023
30	0.029

5.5 Conclusions

(1) For iron-carbon droplets reacting with oxidizing slag, the dependency of CO evolution rate on original droplet size indicates that the rate determining step is the nucleation of CO bubbles;

(2) Classical nucleation theory shows excellent qualitative agreement with the observed gas generation rates. However, to obtain reasonable quantitative predictions of nucleation rates, the metal surface tension has to be decreased by a factor of about 40. This is consistent with observation of gas nucleation behavior in a number of different systems.

Chapter 6

BUBBLE ESCAPE RATE

The objective of this part of the work is to study the mechanism of CO bubbles escaping from the metal droplets and the droplets swelling rate, the experimental and theoretical analysis were taken on this subject, and the results of which are presented in this chapter.

6.1 Mechanism of Bubble Escape from the Metal Drop

6.1.1 The Growth of Bubbles

The classical nucleation theory, with a modified surface tension term, shows excellent qualitative agreement with the observed gas generation rates; the rate determining step is the nucleation of CO bubbles; at initial stage, the bubbles are tiny and far away from each other, the coalescence is not important. The kinetics of the initial stage of the process is therefore described only in terms of the rates of bubble nucleation and growth. The driving force for the growth is the pressure difference between that inside the bubble and in the liquid. Grezl et al. [7] modified Rayleigh's equation for the bubble growth,

$$R\frac{d^2R}{dt^2}+\frac{3}{2}(\frac{dR}{dt})^2=\frac{1}{\rho_l}(P_V-P_L-\frac{2\sigma}{R}) \quad (6.1)$$

where, R is the bubble radius, ρ_l is the density of liquid surrounding bubble, P_V is the bubble pressure, P_L is the ambient pressure in liquid surrounding bubble, σ is the surface tension at bubble/liquid interface. They also derived the radius change over a time increment Δt,

$$\Delta R=\frac{dR}{dt}\cdot\Delta t+\frac{1}{2}\cdot\frac{d^2R}{dt^2}\cdot\Delta t^2 \quad (6.2)$$

They found that bubbles grew very rapidly to a limiting radius depending on the initial bubble pressure and radius. When the initial pressure was 100 atm, the bubble grew to $0.5*10^{-3}$ m from $5*10^{-5}$ m, $0.9*10^{-3}$ m from $1*10^{-4}$ m after $\Delta t = 1*10^{-8}$ s. In this study, the growth of bubbles from nuclei is not considered because the size of bubble was calculated under equilibrium conditions.

CO bubbles as small as 24 Å were produced as predicted when equilibrated with the supersaturation pressures created by oxygen diffusing into the metal drop. However, these bubbles at a later stage will grow due to coalescence with the new adjacently nucleated bubbles. The size of the bubbles trapped in the metal increased with time; see the following Figure 6.1. The sample was obtained by quenching the metal drop into cold

water when it was reacting with Fe_2O_3 containing slag, the pore size left over is about 0.3 mm.

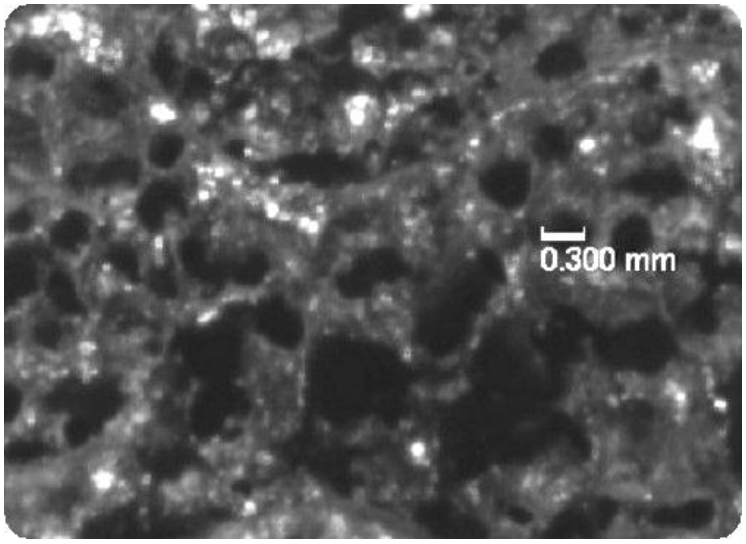

Figure 6.1 − Metal droplets recovered by quenching sample into cold water

6.1.2 Metal Film Thinning

With the continuous nucleation and growth of CO bubbles inside the metal drop, the plateau border channel forms an interconnected network; see Figure 6.2, the continuous phase is the liquid metal film surrounding the bubbles.

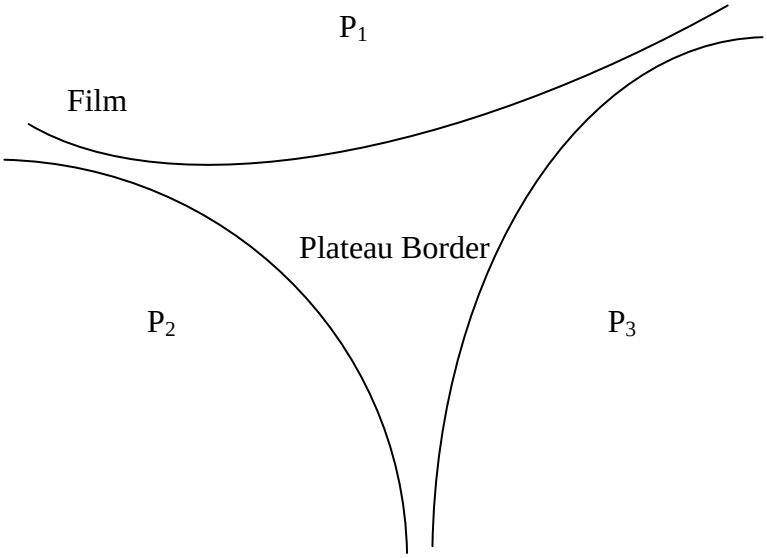

Figure 6.2 – Plateau Border Cross-Section.

Over the years, models have been developed for the drainage of foam; see Figure 6.3 for the drainage of a horizontal film. Sheludko [94] derived an expression for the thinning between two disc surfaces under the influence of a uniform external pressure,

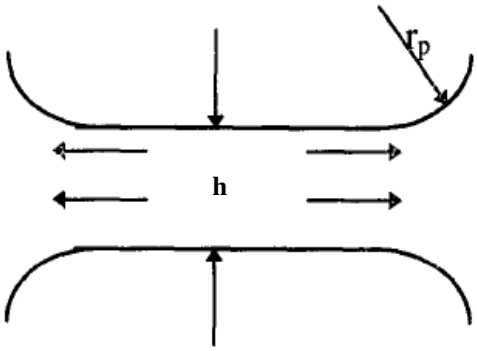

Figure 6.3 − A Draining Film [95]

The change of film thickness with drainage time is given by: [96]

$$u = \frac{1}{6\mu}\left(\frac{h^{12}\Delta P^{8}}{4\sigma^{3} r_{b}^{4}}\right)^{\frac{1}{5}} \tag{6.3}$$

Where, h is the film thickness, μ is the viscosity of the liquid, r_b is the radius of the disk and ΔP is the pressure difference causing the flow, σ is the surface tension.

In case that the film is vertical, the drainage is caused by the gravity, and the thinning equation is given by:

$$u = \frac{\rho g h^{2}}{8\mu} \tag{6.4}$$

Where: h is the film thickness; ρ is the liquid density in the film; and μ is the viscosity of the liquid.

6.1.3 Film Rupture

The point at which rupture happens depends on the disjoining pressure. The disjoining pressure (II) is the repulsive force that arises when the film surfaces are close enough to interact with each other.

$$\Pi = \Pi_{VW} + \Pi_{DL} + \Pi_{SR}$$

Where: Π_{VW} is van der Waals force, Π_{DL} is repulsive force, and Π_{SR} is a short range repulsive force. The film will rupture if the disjoining pressure decreases when the film thickness decreases, see Figure 6.4.

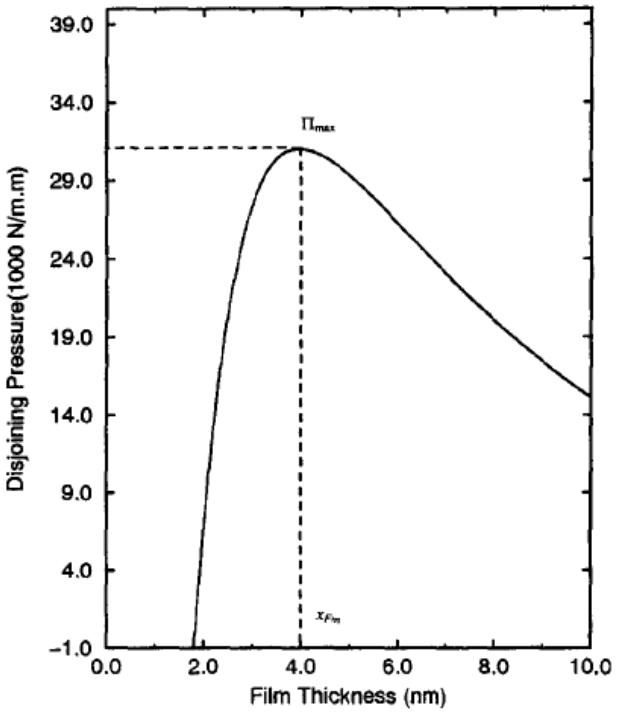

Figure 6.4 – Disjoining Pressure Isotherm [97]

A film can rupture when it is very thick; the stability of the film in this situation will be independent of the disjoining pressure and will be determined primarily by the elasticity of the film and the nature of the mechanical perturbations involved. This mechanism of film rupture is not considered in this study.

6.2 Swelling of Metal Drop during CO Evolution

6.2.1 Gas Volume Fraction Change with Time

The drop diameter increases with swelling. The diameter starts at around 6.51 mm for 1g of metal. When the diameter increased to 8.22 mm, the drop was observed to come out of the slag. At this point the gas volume fraction was around 50%. During CO evolution, the gas volume fraction (defined as, $\varepsilon = \frac{gas\ \ volume}{gas\ \ volume + metal\ \ volume}$) increases with time, see Figure 6.5 and 6.6.

In Figure 6.5, the experimental temperature is T=1873K, and the slag compositions are FeO=30%, CaO/SiO2 = 1.2, MgO=12%, the metal droplet: C=2.87%, S=0.01%. The maximum volume fraction reaches ε = 0.84 at t = 3s. In Figure 6.6, the temperature is T=1773K, slag compositions are FeO=20%, CaO/SiO2=1.2, MgO=12%, the weight of the metal drop is 2 grams, and the metal compositions are: C=2.64%, S=0.022%. The maximum volume fraction reached ε = 0.96 (very dry foam) at t = 3s.

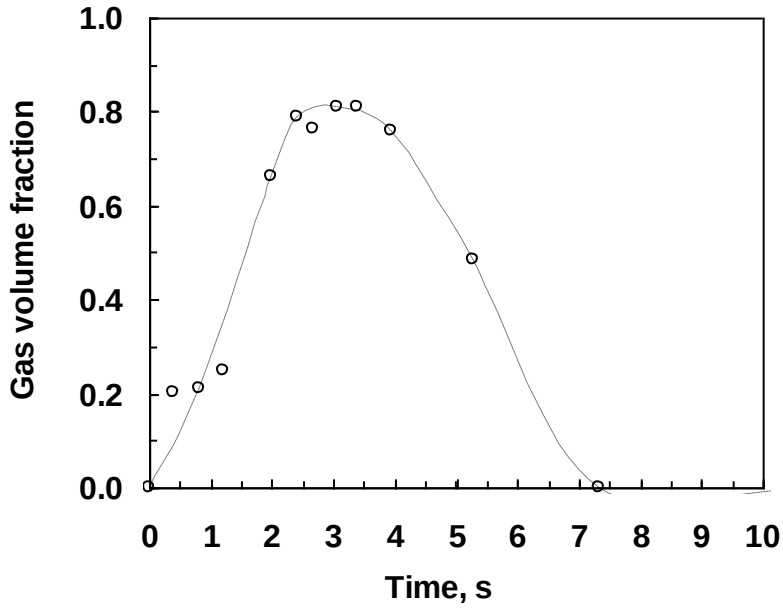

Figure 6.5 – Gas Volume Fraction Change with Time at T=1873K (metal droplet: C=2.87%, S=0.01%).

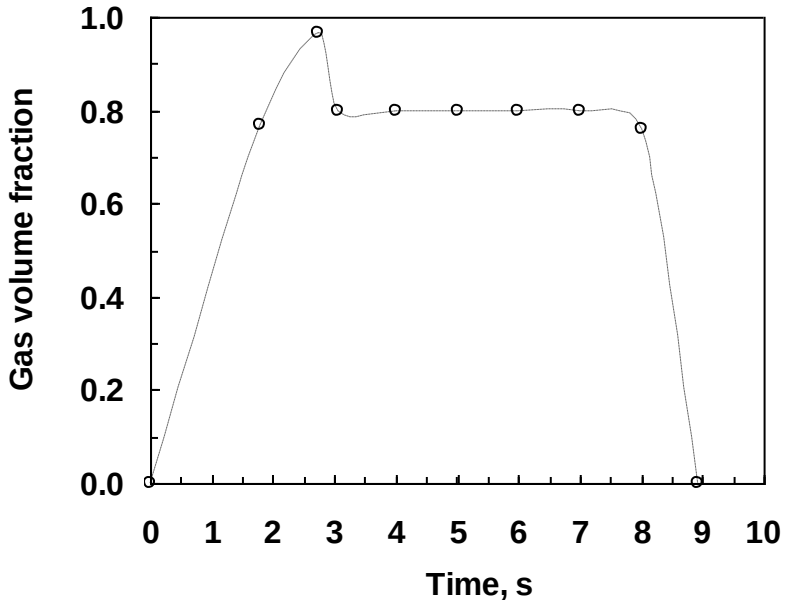

Figure 6.6 – Gas Volume Fraction Change with Time at T=1773K (metal droplet: C=2.64%, S=0.022%).

6.2.2 Metal Drop Swelling Rate

The following figures show the droplet's (weight = 1g) swelling rate and gas evolution with time. In Figure 6.7, the metal droplet: C=2.87%, S=0.01%, FeO=30%. The CO evolution could not be measured during the incubation time of 1.2s; and at this stage, there are no CO bubbles escaping from the metal. CO bubbles started escaping with drop swelling. For example, at t = 3s, the generated CO volume is 27.15 cm3, and the maximum volume of the drop is only 0.88 cm3, most (97%) of CO escaped through the metal surface. After reaching the maximum diameter, the evolution of CO continued for about 3s, and then became very slow, and the drop was observed to shrink back to the original size.

The same phenomenon was observed for metal drop (weight = 1 g) of C=2.62%, S=0.06% reacting with the slag FeO=20% at T=1500C, see Figure 6.8. At t = 2s, the CO volume generated is 105 cm^3, and the volume of the metal drop increased maximally to 4.48cm^3. It took approximately 5s for the CO gas evolution, and then the drop shrunk to the original size.

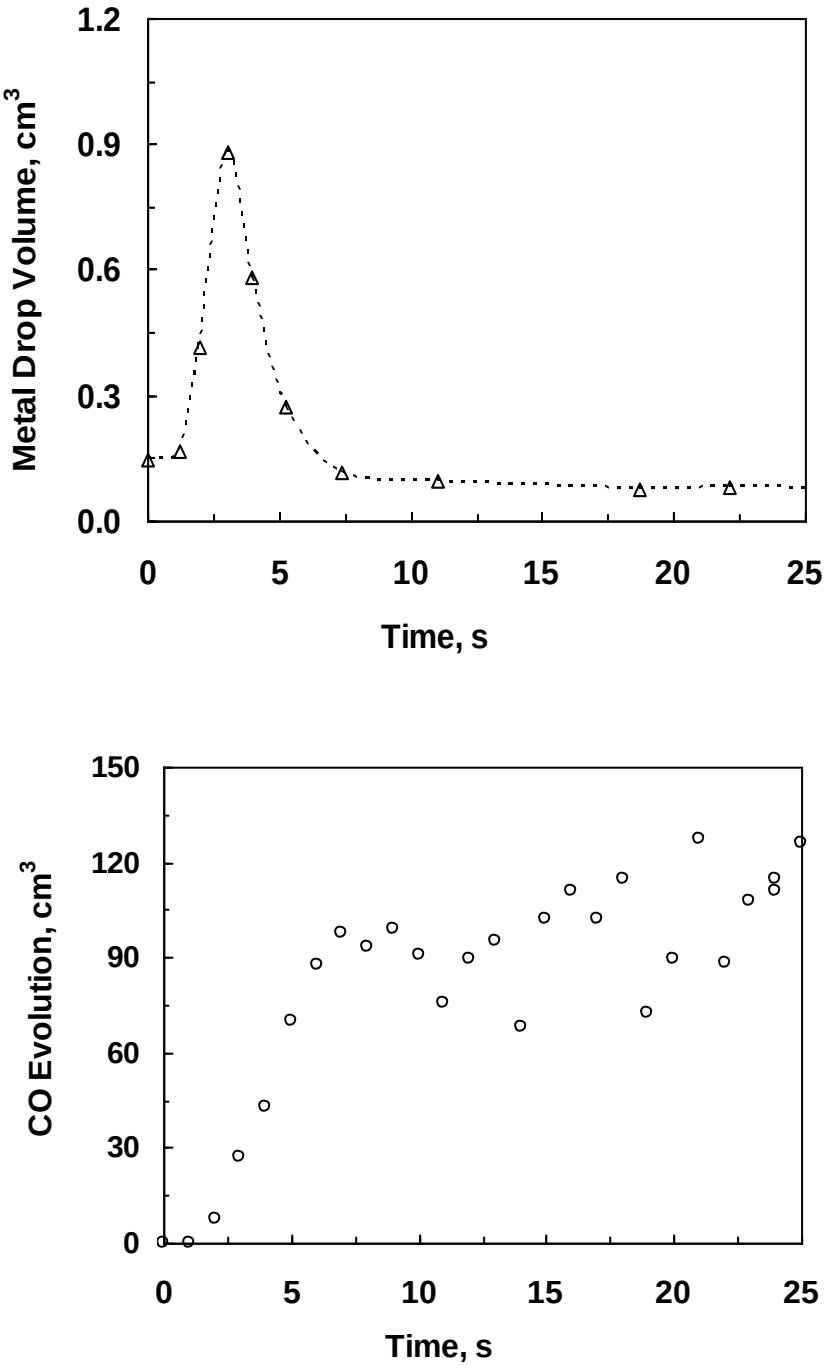

Figure 6.7 – Iron droplet (weight = 1 g) size change and CO gas evolution with time at T=1873K (metal droplet: C=2.87%, S=0.01%).

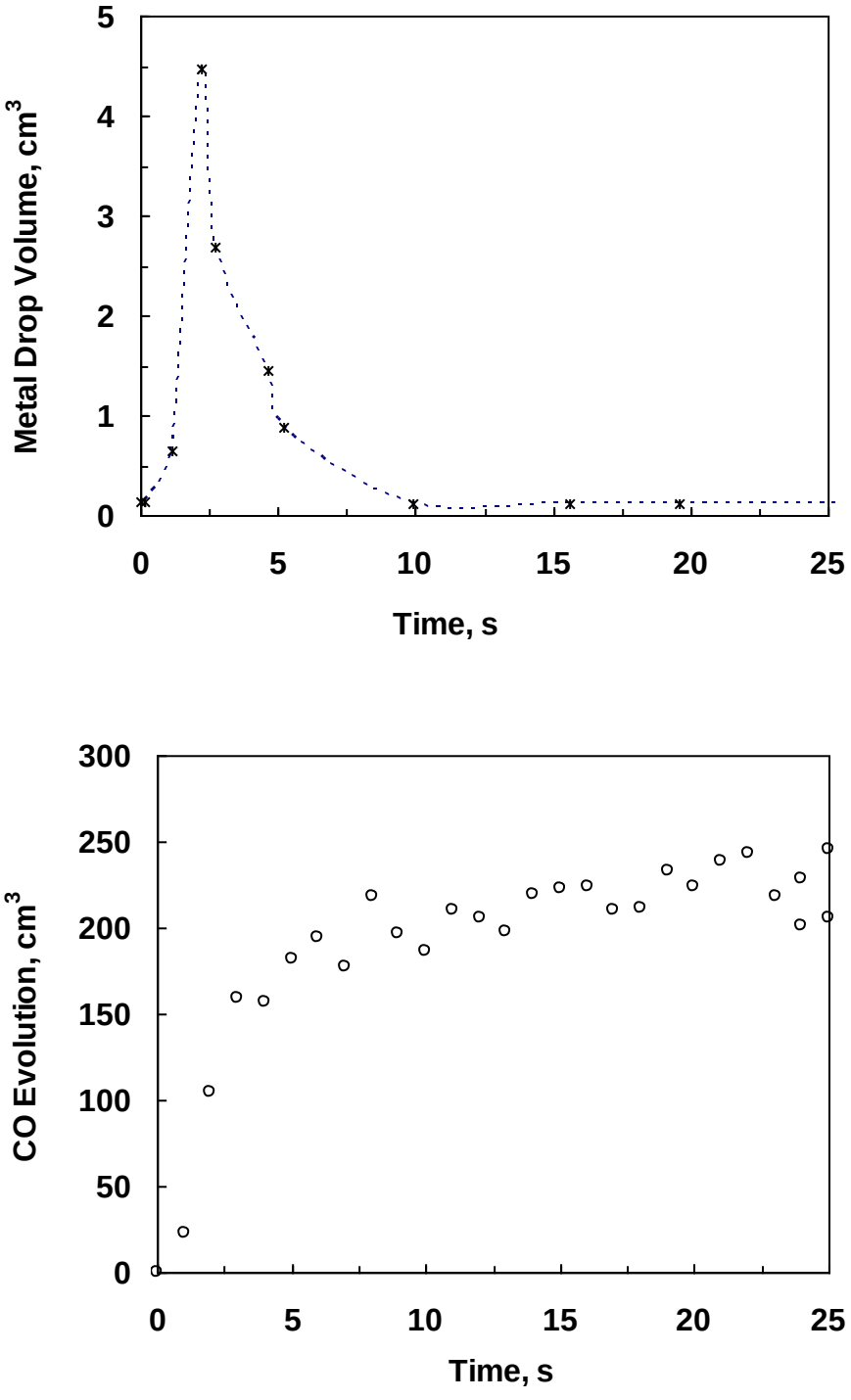

Figure 6.8 – Comparison of droplet size (weight = 1 g) change and CO evolution with time at T=1773K (metal droplet: C=2.62%, S=0.06%).

6.3 Mechanism and Model of Gas Escape from the Drop

As discussed previously, with the generation of CO gases inside the metal, the metal film becomes thinner and thinner, as soon as the thickness of the metal films at the surface decreases to a critical value, the foam begins to collapse, and the gas starts escaping from the drop, see Figure 6.9.

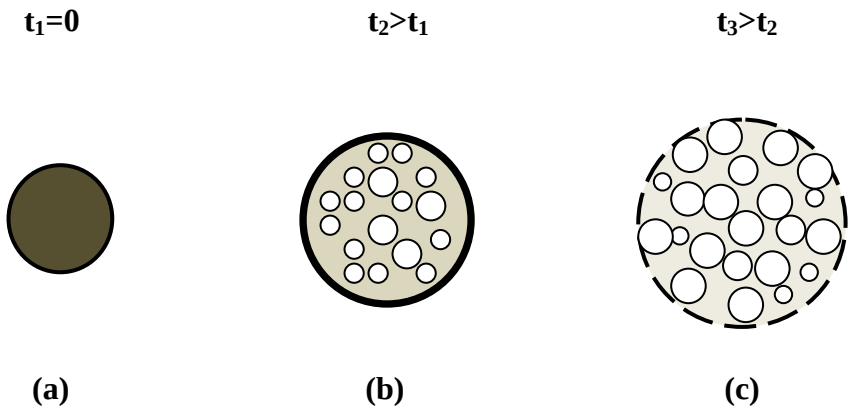

Figure 6.9 – Schematics of gas evolution inside the metal droplet: (a) shows the initial droplet $t_1=0$; (b) and (c) show the droplet at progressively larger times, t_2 and t_3.

Most of the studies on the foam collapse involve the drainage of the liquid in the plateau border. As shown in Figure 6.9, in this study, the gas escape is through the film thinning. The change in the volume due to the drainage from the films to the plateau borders should be: q_{PB}= (number of bubbles per unit volume)*(the number of films per bubble)*(the bubble film area)*(the film thinning rate); [97]

$$q_{PB} = N \cdot a_F \cdot n_F \cdot u \tag{6.5}$$

Where: N is the number of bubbles per unit volume; n_F is the number of films per bubble; A_F is the bubble film area; and u is the film thinning rate. If the gas volume fraction is ε, the gas and liquid ratio should be $\frac{\varepsilon}{1-\varepsilon}$, the foam collapse rate could be,

$$Q_E = \frac{\varepsilon}{1-\varepsilon} \cdot N \cdot a_F \cdot n_F \cdot u \tag{6.6}$$

Where, $a_F \approx 1.152\ r_b^2$, $n_F = 6$, $N = A/(\pi\ r_b^2)$,

$$Q_E = 2.2 \cdot \frac{\varepsilon}{1-\varepsilon} \cdot u \cdot A \tag{6.7}$$

Where A is the instantaneous surface area of the iron droplet, cm^2.

If we define, $$Q_E = k_E A \tag{6.8}$$

Then, $$k_E = 2.2 \cdot \frac{\varepsilon}{1-\varepsilon} \cdot u \tag{6.9}$$

where:

Q_E is CO escape rate, cm^3/s;

k_E is the bubble rupture rate, cm/s;

Knowing the gas escape rate, the metal drop swelling rate could be calculated as follows:

$$\frac{dV}{dt} = Q_G - Q_E \tag{6.10}$$

Where, V is the drop volume, cm^3; Q_G is CO generation rate, cm^3/s; Q_E is CO escape rate, cm^3/s;

$$Q_G = J_s \cdot \frac{n_e}{N_A} \cdot R \cdot T \cdot V_o \tag{6.11}$$

Js is CO nucleation rate, $/cm^3s$; V_o is the original droplet volume, cm^3; n_e is the number of molecules in an embryo; N_A is Avogadro number.

Therefore, the swelling rate equation:

$$\frac{dV}{dt} = J_s \cdot \frac{n_e}{N_A} \cdot R \cdot T \cdot V_o - k_E A \tag{6.12}$$

$$\frac{dV}{dt} = J_s \cdot \frac{n_e}{N_A} \cdot R \cdot T \cdot V_o - 2.2 \cdot \frac{\varepsilon}{1-\varepsilon} \cdot u \cdot A \tag{6.13}$$

Where, $u = \frac{1}{6\mu}\left(\frac{h^{12}\Delta P^8}{4\sigma^3 r_b^4}\right)^{\frac{1}{5}}$

At the maximum diameter, $\frac{dV}{dt} = 0$, thus $Q_G=Q_E$, and the escape rate could be calculated at this point. For example, at T=1500^{o}C, FeO=20%, C=2.64%, S=0.022%, the CO evolution rate is 30.37 cm^3/s, and the drop maximum diameter is 19.5mm; the calculated CO escape rate is k_E=2.51 cm/s. At this moment film thickness h = 1.5 μm, and ΔP=0.03 atm, μ=0.008Pa.s, the calculated bubble radius is 0.3 mm.

6.4 Discussion

When gases are injected or generated in a liquid column, bubbles move up to the top of the liquid due to the buoyancy force. If the liquid is not a foaming liquid, such as water, the gas will escape from the top surface right away. If the liquid is a foaming liquid, the gas will stay in the liquid for a while and coalescence with other bubbles forming a foam on the top. For less stable foams, it is possible to arrive at a steady state where the rate of foam collapse around the top surface becomes equal to the generation rate of gas bubbles and the foam height does not change with time, as observed by the workers.

In this study, bubbles could be held up inside the metal drop before escaping to the surrounding atmosphere because of the very high surface tension, thereby the metal drop swollen. The gas escape rate is determined by the bubble size, the number of the bubbles, the film thickness between bubbles and physical properties of the metal drop.

The number of bubbles and the film thickness in the metal drop are considered to be determined by the gas evolution rate, the bubble size and the metal properties. However, it is difficult to calculate directly the rate of film rupture of a bubble at the top of the foam.

6.4.1 Viscosity Effect on CO Escape Rate

The downward flow in the film of the bubble around the metal drop surface increases with the decrease of liquid viscosity. The viscosity decreases with an increase of temperature, thereby the drainage rate of liquid through the plateau border is higher at higher temperature. In addition, the gas evolution rate is faster at higher temperature, the increase of gas evolution rate will result in a higher gas volume fraction, which increases the escape rate. Figure 6.10 shows the escape rate increases with the temperature for slag containing FeO=30%, and C=2.87%, S=0.01% in the metal.

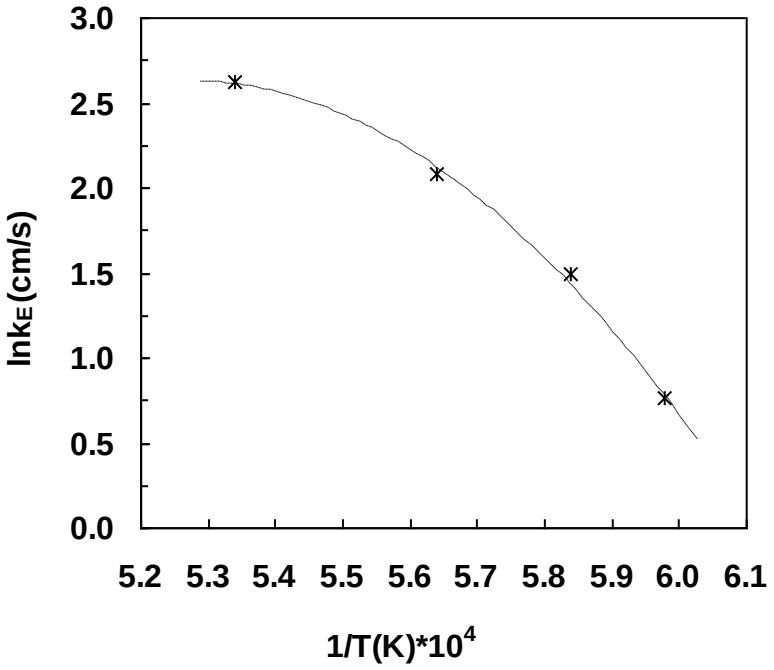

Figure 6.10 – Temperature effect on the gas escape rate at FeO=30% in the Slag.

At T=1500°C, when the drop reached the maximum drop diameter, the gas escape rate is 2.08 cm^3/s, compared with $5cm^3/s$ measured by Gaye et al for gas escaping from slag. This shows better agreement considering that slag has higher viscosity than metal.

6.4.2 Effect of Reaction Rate on the Maximum Volume of the Drop

It is obvious that the CO generation rate will have a significant effect on the maximum volume of the metal drop. Figure 6.11 shows the maximum diameter as a function of CO evolution rate. It is clear that the maximum diameter increases with the gas generation rate.

From the equations of 6.12, it can be seen that both of the drop size and the escape rate become bigger with the increase of the gas generation rate, especially the escape rate. At higher CO generation rate, the escape rate increased greatly due to the coalescence of bubbles and higher gas volume fraction. With bubbles continuous nucleation, the escape rate will be greater than the generation rate, and therefore $\frac{dV}{dt}$ becomes negative, and the drop started shrinking.

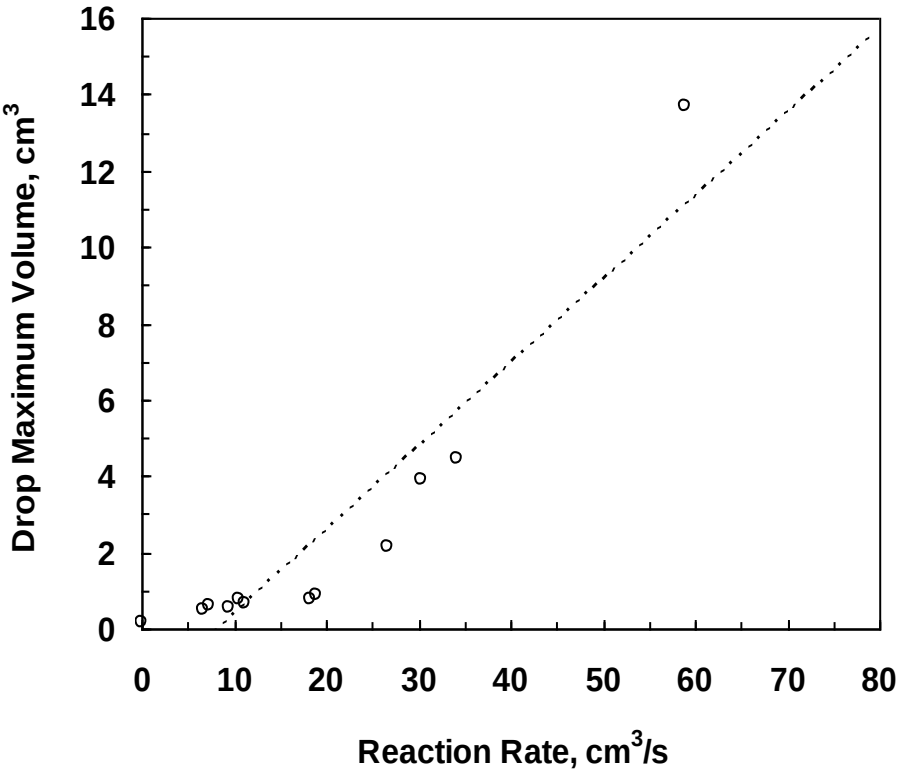

Figure 6.11 – Effect of CO evolution rate on the droplet maximum diameter for FeO = 20% in the slag at T=1773K, metal drop ≈ 1 gram.

6.4.3 Sulfur Effect

The maximum volume of the metal drop increases with CO evolution rate, therefore sulphur has an optimum value with respect to the drop maximum volume because sulphur has the similar influence on the CO evolution rate, see Figure 6.12. The maximum volume increases with S firstly, and then decreases.

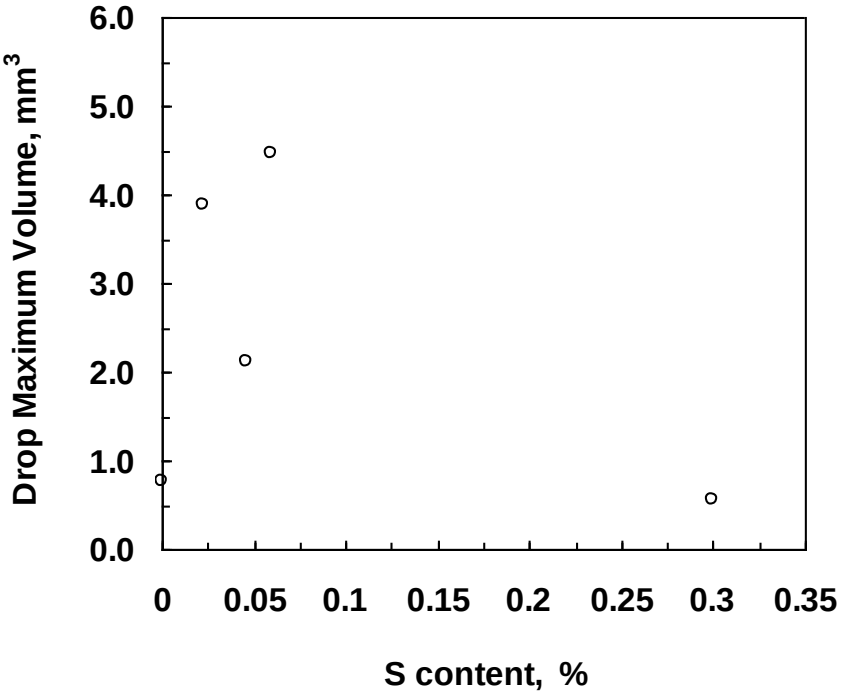

Figure 6.12 – Drop Maximum Volume as Function of S Contents at T=1773K.

6.5 Conclusions

(1) The bubbles escape through the surface due to the thinning of the metal film; As soon as the thickness of the metal film decreases to a critical value, gas bubbles started escaping from the drop;. The rupture rate is mainly influenced by viscosity, surface tension and bubble size.

(2) The maximum volume of the metal drop depends on the gas generation rate, mostly; it increases with the generation rate.

Chapter 7

CONCLUSIONS AND FUTURE WORKS

7.1 Summary and Conclusions

The experimental measurements and the theoretical analysis have been done on the CO gas evolution rate and the swelling rate of Fe-C-S droplet when it reacts with MgO-CaO-SiO_2-FeO melts, and were reported in Chapter 3 to 6. They are summarized in this section of the final chapter.

The approaches used in this study are given in Chapter 3. The measurements on CO evolution rate were made by Constant Volume Pressure Increase (CVPI) technique and the swelling of the droplets was observed by X-ray Fluoroscopy. The experimental results are given in Chapter 4, and can be summarized as follows:

- The reaction phenomenon for metal droplets reacting with MgO-CaO-SiO_2-FeO melts depends on metal droplet and slag chemistries as well as temperatures;
- CO evolution rate for metal droplet reacting with MgO-CaO-SiO_2-FeO melts increases with FeO content, but the relationship is neither linear nor exponential;
- CO evolution rate showed maximum with respect to sulphur.

A kinetic model has been developed in Chapter 5 to explain the results in Chapter 4. The following conclusions can be drawn from Chapter 5:

1. For iron-carbon droplets reacting with oxidizing slag, the dependency of CO evolution rate on original droplet size indicates that the rate determining step is the nucleation of CO bubbles;
2. Classical nucleation theory shows excellent qualitative agreement with the observed gas generation rates. However, to obtain reasonable quantitative predictions of nucleation rates, the metal surface tension has to be decreased by a factor of about 40. This is consistent with observation of gas nucleation behavior in a number of different systems.

Chapter 6 proposes the mechanism of CO gas bubbles escaping from the metal droplets, and the escape rate equation has been derived.

1. The bubbles escape through the surface due to the thinning of the metal film; As soon as the thickness of the metal film decreases to a critical value, gas bubbles started escaping from the drop;. The rupture rate is mainly influenced by viscosity, surface tension and bubble size.
2. The maximum volume of the metal drop depends on the gas generation rate, mostly; it increases with the generation rate.

3. The swelling rate equation could be expressed by: $\frac{dV}{dt} = Q_G - Q_E$, where, $Q_G = J_s \cdot \frac{n_e}{N_A} \cdot R \cdot T \cdot V_o$ and $Q_E = 2.2 \cdot \frac{\varepsilon}{1-\varepsilon} \cdot u \cdot A$

7.2 Future Works

The modeling of the swelling of the metal droplet when it reacts with steelmaking slags has not been fully completed. However, the swelling rate equation have been proposed, and verified at point of maximum swelling. Further works are needed to fully simulate the swelling behavior of the metal droplet.

REFERENCES

1. H. W. Meyer, W. F. Porter, G. C. Smith and J. Szekely, *"Slag-Metal Emulsions and Their Importance in BOF Steelmaking"*, Journal of Metals, 1968, July, pp. 35-42

2. Paul Kozakevitch, *"Foams and Emulsions in Steelmaking"*, Journal of Metals, 1969, July, pp. 57-68

3. E. W. Mulholland, G.S.F Hazeldean, and M. W. Davies, *"Visualization of Slag Metal Reactions by X-ray Fluoroscopy: Decarburization in Basic oxygen steelmaking"*, Journal of the Iron and Steel Institute, 1973, September, pp. 632-639

4. R. Acheson A. W. D. Hills, *"Rate Controlling Mechanisms in Basic Oxygen Steelmaking"*, Physical chemistry of process metallurgy: The Richardson Conference, 1973, pp. 153-163

5. M. W. Davies G.S.F Hazeldean P. N. Smith, *"Kinetics of Reaction between Liquid Iron Oxide Slags and Carbon"*, Physical chemistry of process metallurgy: the Richardson conference, papers presented at the July 1973 conference, pp. 95-107

6. H. Gaye and P. V. Riboud, *"Oxidation Kinetics of Iron Alloy Drops in Oxidizing Slags"*, Metallurgical and Materials Transactions B: 1977, 8B, pp. 409-415

7. K. Grezl, N. A. Molloy, *"Decarburization Reaction Model",* Second Australisian Conference on Heat and Mass Transfer, 1977, pp. 461-468

8. T. Gare and G. S. F. Hazeldean, *"Basic Oxygen Steelmaking: Decarburization of Binary Fe-C Droplets and Ternary Fe-C-X Droplets in Ferruginous Slags"* Ironmaking and Steelmaking, 1981, No. 4, pp. 169-181

9. K. Upadhya, I. D. Sommerville, and P. Grieveson, *"Kinetics of Reduction of Iron Oxide in Slag by Carbon in Iron: Part 2 Effect of Carbon Content of Iron and Silica Content of Slag"*, Ironmaking and steelmaking, 1980, No. 1, pp. 33-36

10. Akira SATO, Goro ARAGANE, Kazushige KAMIHIRA and Shiro YOSHIMATSU, *"Reducing Rates of Molten Iron Oxide by Solid Carbon or Carbon in Molten Iron"*, Transactions ISIJ, 1987, Vol. 27, pp. 789-796

11. R. K. Paramguru, H. S. Ray, and P. Basu, *"Kinetics of Reduction of FeO in CaO-SiO2-FeO Slags Part I: Reduction by Solute Carbon"*,1996, Vol. 23, No. 4, pp. 328-334

12. Jeong-Do Seo and Seon-Hyo KIM, *"Reaction Mechanism of FeO Reduction by Solid and Dissolved Carbon"*, Steel Research, 1998, Vol. 69, No. 8, pp. 307-311

13. David E. Woolley and Uday B. Pal, *"Rate of Reduction of Ferric and Ferrous Oxide from Calcia-silica-alumina Slag by Carbon in Liquid Iron"*, ISIJ International, Vol. 39, No. 2, 1999, pp. 103-112

14. C. L. Molloseau, *"Waste Oxide Recycling during Oxygen Steelmaking"*, PhD thesis, Carnegie-Mellon University, Pittsburgh, PA, 1999

15. L. Molloseau and R. J. Fruehan, *"The Reaction Behavior of Fe-C-S Droplets in CaO-SiO2-MgO-FeO Slags"*, Metallurgical and Materials Transactions B, 2002, 33B, June, pp. 335-344

16. R. J. Fruehan, D. Goldstein, B. Sarma, S. R. Story, P. C. Glaws and H. U. Pasewicz, *"Recent Advances in the Fundamentals of the Kinetics of Steelmaking Reactions"*, Metallurgical and Materials Transactions B, 31B, 2000, October, pp. 891-898

17. G. G. Krishna Murthy, Y. Sawada and J. F. Elliott, *"Reduction of FeO Dissolved in CaO-SiO2-Al2O3 Slags by Fe-C Droplets"*, Ironmaking and Steelmaking, 1993, Vol. 20, No. 3, pp. 179-190

18. G. G. Krishna Murthy, A. Hasham and U. B. Pal, *"Reduction Rates of FeO Dissolved in CaO-SiO2-Al2O3 Slags by Fe-C Droplets"*, Ironmaking and Steelmaking, 1993, Vol. 20, No. 3, pp. 191-200

19. G. G. Krishna Murthy, Ali Hasham and Uday B.Pal, *"Removal of FeO during Foaming of CaO-SiO2-Al2O3 Slags by Low Carbon Iron Melts"*, ISIJ, 1994, pp. 408-413

20. Amitava Paul, Brahma Deo and Narayanasami Sathyamurthy, *"Kinetics Model for Reduction of Iron Oxide in Molten Slags by Iron Carbon Melt"*, Steel Research, 1994, No. 10, pp. 414-420

21. D. J. Min and R. J. Fruehan, *"Rate of Reduction of FeO in Slag by Fe-C Drops"* Metallurgical and Materials Transactions B: 1992, 23B, pp. 29-37

22. D. J. Min, J. W. Han and W. S. Chung, *"Rate of Reduction of FeO in Slag by Fe-C Drops"* , Metallurgical and Materials Transactions B: 1999, 30B, pp. 215-221

23. Richard H. Smith and Richard J. Fruehan, *"The Effect of Carbon Content on the Rate of Reduction of FeO in Slag Relevant to Iron Smelting"*, Steel Research, 1999 No. 8+9, pp. 283-295

24. R. J. Fruehan, "The Making, Shaping and Treating of Steel", AISE Foundation, Steelmaking Volume, 11 th Ed. 1998, pp. 525-648

25. Deo Braham and Boom Rob, "Fundamentals of Steelmaking Metallurgy", New York: Prentice Hall International, 1993

26. Subagyo, G. A. Brooks and K. S. Coley, *"Residence Time of Metal Droplets in Slag Metal Gas Emulsions through Top Gas Blowing",* Canadian Metallurgy Quarterly, 2005, Vol. 44, No. 1, pp. 119-130

27. Geoffrey Brooks and Yuhua Pan, Subagyo and Ken.Coley, *"Modeling of Trajectory and Residence Time of Metal Droplets in Slag Metal Gas Emulsions in Oxygen Steelmaking"*, Metallurgical and Materials Transactions B, 36B, 2005, pp. 525-535

28. Subagyo, G. A. Brooks, K. S. Coley and G. A. Irons, *"Generation of Droplets in Slag Metal Emulsion through Top Gas Blowing"*, ISIJ International, 2003, Vol. 43, No. 7, pp. 983-989

29. Subagyo, G. A. Brooks and K. S. Coley, *"Interfacial Area in Top Blown Oxygen Steelmaking",* Ironmaking Conference Proceedings, 2002, pp. 837-850

30. Qing Lin HE and Nicholas STANDISH, *"A Model Study of Droplet Generation in the BOF Steelmaking"*, ISIJ International, 1990, Vol. 30, No. 4, pp.305-309

31. Qing Lin HE and Nicholas STANDISH, *"A Model Study of Residence Time of Metal Droplets in the Slag in BOF Steelmaking",* ISIJ International, Vol. 30, No. 4, 1990, pp. 356-361

32. Price, *"L. D. Steelmaking: Significance of the Emulsion in Carbon Removal"*, Process Engineering of Pyrometallurgy, 1974, pp. 8-15

33. Ho Yong Hwang, PhD These, "A study of impinging gas jets on liquid surfaces", McMaster University, Hamilton, Ontario, Canada, 2008

34. R. Li and R.L. Harris: Pyrometallurgy 95 Conf. Proc., IMM, London, (1995), pp. 107.

35. Satish C. Koria and Klaus W. Lange, *"A New Approach to Investigate the Drop Size Distribution in Basic Oxygen Steelmaking",* Metallurgical and Materials Transactions B, 15B, August, 1984, pp. 109-116

36. S. C. Koria and K. W. Lange, *"Estimation of Drop Sizes in Impinging Jet Steelmaking Processes",* Ironmaking and Steelmaking, vol. 13, No. 5, 1986, pp. 236-240

37. R. C. Urquhart and W. G. Davenport, *"Foams and Emulsions in Oxygen Steelmaking"*, Canadian Metallurgical Quarterly, 1973, vol. 12, No. 4, pp. 507-517

38. Mansoor Barati, *"Kinetics of CO-CO2 Reaction with Iron Oxide Containing Slags"*, PhD thesis, McMaster University, Hamilton, On, Canada, 2005

39. D. R. Sain and G. R. Belton, "*Interfacial Reaction Kinetics in the Decarburization of Liquid Iron by Carbon Dioxide",* Metallurgical and Materials Transactions B, 7B, 1976, pp. 235-244

40. A. W. Cramb, W. R. Graham and G. R. Belton, *"Interfacial Kinetics of the Reaction of CO2 with Nickel -1. The 14CO_2-CO Exchange Reaction and the Influence of Sulphur",* Metallurgical Transactions B, 9B, 1978, pp. 623-629

41. F. J. Mannion and R. J. Fruehan, "*Decarburization kinetics of liquid Fe-Csat alloys by CO2",* Metallurgical and Materials Transactions B, 20B, 1989, pp. 853-861

42. David E. Woolley and Uday B. Pal, *"Rate of Reduction of Ferric and Ferrous Oxide from Calcia-Silica-Alumina Slag by Carbon in Liquid Iron"*, ISIJ International, Vol.39, No.2, 1999, pp. 103-112

43. D. P. Agarwal and D. R. Gaskell, "*The Self Diffusion of Iron in Fe_2SiO_4 and $CaFeSiO_4$ Melts*", Metallurgical and Materials Transactions B, 1975, pp. 263-267

44. H. J. Grabke,V. Leroy and H. Viefhaus, *"Segregation on the Surface of Steels in Heat Treatment and Oxidation",* ISIJ International, 1995, pp. 95-113

45. A. W. Cramb and I. Jimbo, *"Surface Tension Values for Use in Casting"*, 1994 Turdogan Symposium Proceedings, pp. 195-206

46. L. A. Baker and R. G. Ward, *"Reaction of an Iron Carbon Droplet during Free Fall through Oxygen"*, Journal of The Iron and Steel Institute, July, 1967, pp. 714-717

47. L. A. Baker, N. A. Warner and A. E. Jenkins, *"Decarburization of a Levitated Iron Droplet in Oxygen"*, Transactions of The Metallurgical society of AIME, 1967, Vol. 239, pp. 857-864

48. L. A. Baker, N. A. Warner, and A. E. Jenkins, *"Kinetics of Decarburization of Liquid Iron in an Oxidizing Atmosphere Using the Levitation Technique"*, Trans. AIME, 1964, Vol.230, pp. 1228-1235

49. Kevin GAO, Veena sahajwalla, Haiping Sun, Charles Whetley and Rod DRY, *"Influence of Sulfur Content and Temperature on the Carbon Boil and CO Generation in Fe-C-S Drops"*, ISIJ International, 2000, Vol. 40, No. 4, pp. 301-308

50. K.Gao, V.Sahajwalla and R.Dry, *"Carbon Boiling Phenomenon and Oxygen Absorption by Metal Drops in Direction Iron Smelting"*, ICSTI/Ironmaking conf. proc., 1998, pp. 1489-1499

51. D.G.C. Robertson and A.E.Jenkins, *"The Reaction of Liquid Iron and Its Alloys in Pure Oxygen"*, Heterogeneous kinetics at elevated temperatures, 1970, pp.393-408

52. N.H.EL Kaddah and D.G.Robertson, *"Homogeneous Nucleation of Carbon Monoxide Bubbles in Ion Drops"*, Journal of colloid and interface science, 1977, pp. 349-360

53. N.H.EL Kaddah and D.G.Robertson, *"Equilibria in Reactions of CO and CO_2 with Dissolved Oxygen and Carbon in Liquid Iron"*, Metallurgical and Materials Transactions B, 1977, pp. 569-579

54. N.H.EL-Kaddah and D.G.C.Robertson, *"The Nucleation of CO Bubbles in Molten Iron Carbon Drops Reacting with Oxidizing Gases"*, Metallurgical and Materials Transactions B: 1988, 19B, pp. 831-837

55. D.K.Panda and D.G.C.Robertson, *"Physical Modeling of Metal Drop Slag Reactions with Gas Evolution"*, Steelmaking Conference Proceedings, 1994, pp. 443-456

56. Zhijun Han and Lauri HOLAPPA, *"Bubble Bursting Phenomenon in Gas/Metal/Slag Systems"*, Metallurgical and Materials Transactions B:, 2003, 34B, pp. 525-532

57. P.A.Distin, G.D.Hallett, and F.D.Richardson, *"Some Reactions between Drops of Iron and Flowing Gases"*, Journal of the Iron and Steel Institute, 1968, August, pp. 821-833

58. P.G.Roddis, "*Mechanism of Decarburization of Iron Carbon Alloy Drops Falling through an Oxidizing Gas*", Journal of the Iron and Steel Institute, January, 1973, pp. 53-58

59. R.S.Kaplan and W.O.Philbrook, *"The Rate of CO Bubble Nucleation at Oxide Metal Interfaces within Liquid Iron Alloys"*, Metallurgical and Materials Transactions B: 1972, 3B, pp. 483-487

60. Herman S. Levine, "*Formation of Vapor Nuclei in High Temperature Melts*", The journal of Physical Chemistry, 1972, Vol. 76, No. 18, pp.2609-2614

61. Herman S. Levine, "*Homogeneous Nucleation of CO Bubbles in Fe-C-O Melts*", Metallurgical Transactions, 1973, Vol. 4, pp: 777-782

62. Herman S. Levine, *"Surface Structure Concepts in the Theory of Homogeneous Bubble Nucleation"*, Metallurgical transactions B, 1974,Vol. 5, pp: 953-955

63. Ho-Young Kwak and Si-Doek Oh (1998). "*A Model of Homogeneous Bubble Nucleation of CO Bubbles in Fe-C-O Melts*", Journal of Colloid and Interface Science, Vol. 198, pp: 113-118

64. M. Volmer, *Kinetics of Phase Formation* ATI No.81935 (F-TS-7068-RE) Translated from "Kinetic der Phasenbildung Verl-Steinkopff" Dresden, 1939, pp: 149-154

65. Yu. Kagan, "*The Kinetics of Boiling of a Pure Liquid*", Russian Journal of Physical Chemistry, 1960, January, Vol.34, No.1, pp. 42-46

66. J. P. Hirth and G. M. Pound, "*Condensation and Evaporation: Nucleation and Growth Kinetics*", Progress in Materials Science, vol. 11, The Macmillan Company, New York, 1963

67. J. P. Hirth, G. M. Pound and G. R. ST. Pierre, "*Bubble Nucleation*", Metallurgical and Materials Transactions B: 1970, Vol.1, pp. 939-945

68. J. Feder, K. C. Russell, J. Lothe and G. M. Pound, "*Homogeneous Nucleation and Growth of Droplets in Vapours*", Advances in Physics, 1966, pp:111-133

69. A. C. Zettlemoyer, "Nucleation", Marcel Dekker, Inc. New York, 1969

70. Milton Blander and Joseph L. Katz, "*Bubble Nucleation in Liquids*", AIChE Journal, 1975, September, pp. 833-848

71. Milton Blander, "*Bubble Nucleation in Liquids*", Advances in Colloid and Interface Science, 10, 1979, pp. 1-32

72. Van. P. Carey, "Liquid –Vapor Phase Change Phenomena", 2008, second Edition, Published: New York: Taylor and Francis.

73. Peter G. Bowers, Kedma Bar-Eli and Richard M. Noye. *"Unstable Supersaturated Solutions of Gases and Nucleation Theory",* Journal of Chemical Society, Faraday Transactions, 1996, 92(16), pp: 2843-2849

74. S. D. Lubetkin (2003). *"Why Is It Much Easier to Nucleate Gas Bubbles Than Theory Predicts?"* , Langmuir, 19, pp: 2575-2587

75. Amir Attar, *"Bubble Nucleation in Viscous Material Due to Gas Formation by a Chemical Reaction: Application to Coal Pyrolysis"*, AIChE Journal, 1978, July, pp. 106-115

76. Haiping Sun and Guangqing Zhang, *"Influence of silicon on decarburization rate and bloating of iron droplets in steelmaking and direct iron smelting slags"*, AISTech Conference Proceeding, ICS Proceedings, 2005, pp. 257-268

77. Kimihisa Ito and R.J.Fruehan, *"Study on the Foaming of CaO-SiO2-FeO Slags: Part I. Foaming Parameters and Experimental Results",* Metallurgical and Materials Transactions B: 1989, 20B, pp. 509-514

78. Kimihisa Ito and R.J.Fruehan, *"Study on the Foaming of CaO-SiO2-FeO Slags: Part II. Dimensional Analysis and Foaming in Iron and Steelmaking Processes",* Metallurgical and Materials Transactions B: 1989, 20B, pp. 515-521

79. R.Jiang and R.J.Fruehan, *"Slag Foaming in Bath Smelting",* Metallurgical and Materials Transactions B: 1991, 22B, pp. 481-489

80. Y.Zhang and R.J.Fruehan, *"Effect of the Bubble Size and Chemical Reactions on Slag Foaming",* Metallurgical and Materials Transactions B: 1995, 26B, pp. 803-812

81. Y.Zhang and R.J.Fruehan, *"Effect of Gas Type and Pressure on Slag Foaming",* Metallurgical and Materials Transactions B: 1995, 26B, pp. 1088-1090

82. Bahri Ozturk and R.J.Fruehan, *"Effect of Temperature on Slag Foaming",* Metallurgical and Materials Transactions B: 1995, 26B, pp. 1086-1088

83. Sung-Mo Jung and R.J.Fruehan, *"Foaming Characteristics of BOF Slags",* ISIJ International, 2000, Vol.40, No.4, pp. 348-355

84. A.K.Lahiri and S.Seetharaman, *"Foaming Behavior of Slags",* Metallurgical and Materials Transactions B: 2002, 33B, pp. 499-502

85. Abha Kapilashrami, Ashok Kumar Lahiri, Marten Gornerup and Seshadri.Seetharaman, *"The Fluctuations in Slag Foam under Dynamic Conditions",* Metallurgical and Materials Transactions B: 2004, 37B, pp. 145-148

86. Abha Kapilashrami, Ashok Kumar Lahiri, Seshadri.Seetharaman, *"Bubble Formation through Reaction at Liquid-Liquid Interfaces",* Steel Research Int: 2005, 76, No. 9, pp. 616-623

87. A. Kapilashrami, M.Gornerup, A.K.Lahiri and S. Seetharaman, *"Foaming of Slag under Dynamic Conditions",* Metallurgical and Materials Transactions B: 2006, 37B, pp. 109-117

88. J. J. Bikerman, "Foams", 1973, Spriner-Verlag New York, Heidelberg, Berlin.

89. S. J. Neethling, H. T. Lee, P. Grassia, *"The Growth, Drainage and Breakdown of Foams",* Colloids and Surfaces A: Physicochem. Eng. Aspects, 2005, 263, pp. 184-196

90. P. Grassia, S. J. Neethling, C. Cervantes, H. T. Lee, *"The Growth, Drainage and Breakdown of Foams",* Colloids and Surfaces A: Physicochem. Eng. Aspects, 2006, 274, pp. 110-124

91. Arnaud Saint-James, *"Physical Chemistry in Foam Drainage and Coarsening",* The Royal Society of Chemistry, No. 2, 2006, pp. 836-849

92. I. Jimbo, A. Sharan and A. W. Cramb, *"The Surface and Interfacial Tensions of Steel Alloys Containing Nickel or Carbon and Sulphur",* Iron and Steelmaker, 1994, pp: 48-55

93. Alan W. Cramb and Utaru Jimbo, *"Calculation of the Interfacial Properties of Liquid Steel-Slag Systems",* Steel Research, 1989, Vol.60, No. 3+4, pp. 157-165

94. Ashok Bhakta, Eli Ruckenstein, *"Decay of Standing Foams, Drainage, Coalescence and Collapse",* Advances in Colloid and Interface Science, 1997, Vol.70, pp. 1-124

95. Boryan P. Radoev, Alexei D. Scheludko, and Emil D, Manev, *"Critical Thickness of Thin Liquid Films: Theory and Experiment",* Journal of Colloid and Interface Science, 1983, Vol. 95, No. 1, pp. 254-265

96. Roumen Tsekov, *"The R4/5-Problem in the Drainage of Dimpled Thin Liquid Films",* Colloids and Surfaces A: Physicochemical and Engineering Aspects 1998, Vol. 141, No.2, pp. 161–164

97. Ganesan Narsimhan and Eli Ruckenstein, *"Hydrodynamics, Enrichment, and Collapse in Foams"*, Langmuir, 1986, Vol. 2, No. 2, pp. 230-238

98. D. Desai and R. Kumar, "*Flow Through a Plateau Border of Cellular Foam",* Chemical Engineering Science, 1982, Vol.37, pp. 1361-1370

99. Tharwat F. Tadros, "Applied Surfactant: Principles and Applications", 2005, WILEY-VCH Verlag GmbH&Co. KGaA

100. John R. Taylor, An Introduction to Error Analysis: The Study of Uncertainties in Physical Measurements, University Science Books, Second edition, 1997

Appendix A

Tables of Experimental Results

In this appendix, the experimental results of CO evaluation rates and the droplet swelling rate are given.

Table A.1 – CO evolution rate (moles/s) for different sizes of metal drop (slag compositions: CaO/SiO_2=1.2, MgO=12%, FeO=20%) at T=1773K

Droplet size (g)	*Metal Chemistry*	*Rate*10^5 (moles/s)*
0.53	C=2.70%, S=0.027%	12.14
1.01	C=2.64%, S=0.022%	20.89
1.49	C=2.70%, S=0.027%	34.79
2.04	C=2.64%, S=0.022%	40.57

Table A.2 – CO evolution rate (moles/s) for different sulphur in 1 g of metal drop (slag compositions: CaO/SiO_2=1.2, MgO=12%, FeO=20%) at T=1713K

% S	*% C*	*Rate*10^5 (moles/s)*
0.013	2.91	7.87
0.027	2.76	5.20
0.068	2.70	5.87
0.194	2.94	3.62

Table A.3 – CO evolution rate (moles/s) for different sulphur in 1 g of metal drop at T=1773K (slag compositions: CaO/SiO_2=1.2, MgO=12%, FeO=20%).

% S	*% C*	*Rate *10^5 (moles/s)*
0	2.90	7.24
0.013	2.91	22.82
0.02	2.75	20.83
0.022	2.64	20.89
0.068	2.70	21.31
0.194	2.94	10.58
0.3	2.69	6.55

Table A.4 – CO evolution rate: R*10^5 moles/s (slag Compositions: CaO/SiO_2=1.2, MgO=12%), metal drop weight = 1g

	FeO, wt %				
T ,^oC	*3*	*5*	*10*	*20*	*30*
1355				0.98	
1400	0.00	0.46	1.56	6.35	4.85
1440	0.27		2.67	11.67	13.08
1500	0.79	5.21	16.11	22.82	22.66
1600	16.46		36.17	40.41	39.74

Table A.5 – Droplet swelling data for 1g of metal drop (C=3.71%, S=0.0063%) reacting with slag of FeO=20%, CaO/SiO2=1.2, MgO=12% at T=1440^{o}C

Time, s	*Radius, mm*	*Diameter, mm*	*Area, cm^2*	*Volume, cm^3*
0	3.26	6.51	1.33	0.14
1	5.00	10.00	3.14	0.52
2	5.15	10.30	3.33	0.57
3	5.35	10.70	3.59	0.64
4	3.26	6.51	1.33	0.14

Table A.6 – Droplet swelling data for 2 grams of metal drop (C=2.64%, S=0.022%) reacting with slag of FeO=20%, CaO/SiO2=1.2, MgO=12% at T=1500^{o}C

Time, s	*Radius, mm*	*Diameter, mm*	*Area, cm^2*	*Volume, cm^3*
0.00	4.11	8.21	2.12	0.29
1.67	5.25	10.50	3.46	0.61
2.60	5.60	11.20	3.94	0.74
3.80	11.20	22.40	15.76	5.88
4.27	14.85	29.70	27.70	13.71
4.73	9.30	18.60	10.86	3.37
5.00	9.30	18.60	10.86	3.37
6.00	9.00	18.00	10.17	3.05
7.00	9.30	18.60	10.86	3.37
8.00	9.00	18.00	10.17	3.05
9.00	9.00	18.00	10.17	3.05
10.60	4.60	9.20	2.66	0.41

Table A.7 – Droplet swelling data for 1 gram of metal drop (C=2.64%, S=0.022%) reacting with slag of FeO=20%, CaO/SiO2=1.2, MgO=12% at T=1500^{o}C

Time, s	*Radius, mm*	*Diameter, mm*	*Area, cm^2*	*Volume, cm^3*
0.00	3.26	6.51	1.33	0.14
1.80	5.25	10.50	3.46	0.61
2.73	9.75	19.50	11.94	3.88
3.07	5.50	11.00	3.80	0.70
4.00	5.50	11.00	3.80	0.70
5.00	5.50	11.00	3.80	0.70
6.00	5.50	11.00	3.80	0.70
7.00	5.50	11.00	3.80	0.70
8.00	5.50	11.00	3.80	0.70
8.94	3.20	6.40	1.29	0.14

Table A.8.1 – Droplet swelling data for 1 gram of metal drop (C=2.87%, S=0.01%) reacting with slag of FeO=30%, CaO/SiO2=1.2, MgO=12%

T= 1400 ^{o}C				
Time, s	*Radius, mm*	*Diameter, mm*	*Area, cm^2*	*Volume, cm^3*
0.00	4.68	9.35	2.75	0.43
0.93	4.98	9.95	3.11	0.52
1.40	4.83	9.65	2.92	0.47
1.73	4.48	8.95	2.52	0.38
2.40	3.95	7.90	1.96	0.26
3.93	3.40	6.80	1.45	0.16
6.53	2.65	5.30	0.88	0.08
9.53	2.65	5.30	0.88	0.08
21.40	3.30	6.60	1.37	0.15
28.67	2.88	5.75	1.04	0.10

Table A.8.2 – Droplet swelling data for 1 gram of metal drop (C=2.87%, S=0.01%) reacting with slag of FeO=30%, CaO/SiO2=1.2, MgO=12%

T= 1440C				
Time, s	***Radius, mm***	***Diameter, mm***	***Area, cm^2***	***Volume, cm^3***
0.00	3.25	6.50	1.33	0.14
1.20	3.85	7.70	1.86	0.24
2.27	5.20	10.40	3.40	0.59
2.93	5.22	10.43	3.42	0.59
3.60	5.63	11.27	3.99	0.75
4.00	5.71	11.43	4.10	0.78
4.60	5.61	11.23	3.96	0.74
5.67	3.88	7.77	1.89	0.25
6.87	3.72	7.43	1.73	0.21
9.00	3.72	7.43	1.73	0.21
15.00	3.72	7.43	1.73	0.21

Table A.8.3 – Droplet swelling data for 1 gram of metal drop (C=2.87%, S=0.01%) reacting with slag of FeO=30%, CaO/SiO2=1.2, MgO=12%

T=1500C				
Time, s	***Radius, mm***	***Diameter, mm***	***Area, cm^2***	***Volume, cm^3***
0.00	2.50	5.00	0.79	0.07
0.07	3.48	6.95	1.52	0.18
0.40	4.53	9.05	2.57	0.39
1.27	5.40	10.80	3.66	0.66
1.60	5.30	10.60	3.53	0.62
2.47	5.10	10.20	3.27	0.56
2.93	5.38	10.75	3.63	0.65
3.60	5.73	11.45	4.12	0.79
4.07	5.65	11.30	4.01	0.76
4.27	5.60	11.20	3.94	0.74
5.00	4.30	8.60	2.32	0.33

Table A.8.4 – Droplet swelling data for 1 gram of metal drop (C=2.87%, S=0.01%) reacting with slag of FeO=30%, CaO/SiO2=1.2, MgO=12%

T=1600C				
Time, s	***Radius, mm***	***Diameter, mm***	***Area, cm^2***	***Volume, cm^3***
0.00	3.26	6.51	1.33	0.14
0.40	3.48	6.95	1.52	0.18
0.80	3.45	6.90	1.49	0.17
1.20	3.43	6.85	1.47	0.17
2.00	4.63	9.25	2.69	0.41
2.40	5.40	10.80	3.66	0.66
2.67	5.20	10.40	3.40	0.59
3.07	5.95	11.90	4.45	0.88
3.40	5.63	11.25	3.97	0.75
3.93	5.18	10.35	3.36	0.58
4.67	4.95	9.90	3.08	0.51
5.27	4.03	8.05	2.03	0.27
7.33	3.05	6.10	1.17	0.12
11.00	2.85	5.70	1.02	0.10
18.67	2.65	5.30	0.88	0.08
22.13	2.70	5.40	0.92	0.08
25.07	2.65	5.30	0.88	0.08

Table A.9 – Droplet swelling data for 1 gram of metal drop (C=2.13%, S=0.046%) reacting with slag (FeO=20%, CaO/SiO2=1.2, MgO=12%)

T= 1500C				
Time, s	***Radius, mm***	***Diameter, mm***	***Area, cm^2***	***Volume, cm^3***
0.00	3.26	6.51	1.33	0.14
0.93	7.18	14.35	6.47	1.55
1.07	7.98	15.95	7.99	2.12
2.13	5.20	10.4	3.40	0.59
4.47	5.15	10.3	3.33	0.57
5.60	5.05	10.1	3.20	0.54
6.07	4.75	9.50	2.83	0.45
7.40	4.20	8.40	2.22	0.31
7.93	3.00	6.00	1.13	0.11
8.73	3.05	6.10	1.17	0.12

Table A.10 – Droplet swelling data for 1 gram of metal drop (C=2.62%, S=0.06%) reacting with slag of FeO=20%, CaO/SiO2=1.2, MgO=12%

T= 1500C				
Time, s	***Radius, mm***	***Diameter, mm***	***Area, cm^2***	***Volume, cm^3***
0.00	3.26	6.51	1.33	0.14
0.13	3.26	6.51	1.33	0.14
1.13	5.35	10.7	3.59	0.64
2.20	10.23	20.45	13.13	4.48
2.73	8.63	17.25	9.34	2.69
4.60	7.03	14.05	6.20	1.45
5.20	5.95	11.9	4.45	0.88
9.87	3.05	6.10	1.17	0.12
15.60	3.05	6.10	1.17	0.12
19.60	3.05	6.10	1.17	0.12
25.60	3.05	6.10	1.17	0.12

Appendix B

Error Analysis

In general, the uncertainty in the measurement can be divided into two types: [100] one is random error, which is involved in the repeated measurements; and these kinds of uncertainty can be estimated reliably by repeating the measurements several times. For example, N measurements were made on the same quantity, x, the best estimate is their mean:

$$\bar{x} = \frac{1}{N}\sum_{1}^{N} x_i \tag{A.1}$$

The standard deviation represents the average uncertainty in the individual measurement, is calculated by:

$$\sigma_x = \sqrt{\frac{1}{N-1}\sum (x_i - \bar{x})^2} \tag{A.2}$$

And the standard deviation of the mean:

$$\sigma_{\bar{x}} = \frac{\sigma_x}{\sqrt{N}} \tag{A.3}$$

The random error could be calculated as:

$$\delta_{\bar{x}} = 100\% \frac{\sigma_{\bar{x}}}{\bar{x}} \tag{A.4}$$

Not all of the experiments have been repeated in this study. The random errors are around 5% in this study based on the results of these repeated tests shown in Table A-1.

Table A-1: CO evolution rate and the estimated errors under different experimental conditions.

	FeO	***C***	***S***	***T***	***Rate × 10^5 moles/s***	***Average***	***Error %***
1st	30	2.92	0.0087	1400	5.41	5.13	5.44
2nd	30	2.87	0.01	1400	4.85		
1st	30	2.87	0.01	1500	20.79	21.73	4.30
2nd	30	2.87	0.01	1500	22.66		
1st	30	2.92	0.0087	1600	40.38	40.06	0.80
2nd	30	2.87	0.01	1600	39.74		
1st	20	2.64	0.022	1500	20.89	20.86	0.14
2nd	20	2.75	0.02	1500	20.83		

Another type of uncertainty is systematic error, such as in this study, the calibration of the pressure transducer and the leakage of the furnace at high temperature. Efforts have been made to minimize these errors, such as calibrated the pressure transducer periodically, and checked the leakage of the furnace each time before the experiment and sealed all the pipe connections, etc. As discussed in the previous random error part, the uncertainty in the experimental measurements is around 5% of the best estimation on the evolution rate.

Appendix C

Publications

1. E. Chen, and K.S. Coley, "Kinetic study of droplet swelling in BOF steelmaking", Ironmaking & Steelmaking , Volume: 37, Issue: 7, 2010, pp: 541-545

2. E. Chen, and Kenneth Coley, "Kinetic study of droplet swelling in BOF steelmaking", Proceedings of the VIII International Conference on Molten Slags, Fluxes and Salts, Santiago, Chile, January 2009, pp.803-813

3. E. Chen, and K. Coley, "Gas Slag Reaction Kinetics in Slag Cleaning of Copper Slags", Canadian Metallurgical Quarterly, Vol.45, No.2, 2006, pp: 167-174.

4. Michael POMEROY, Elaine CHEN, Kenneth. S. COLEY and Glendon BROWN, Kinetic study of droplet swelling in BOF steelmaking. The 6th European Oxygen Steelmaking Conference, Stockholm, Sweden, 2011, September 7-9.

5. M. Barati, E. Chen and K. Coley, "A Comparison of the Kinetics of the CO/CO2 Reaction, with EAF Steelmaking Slag and in Copper Making Slag", VII International Conference on Molten Slag Fluxes and Salts, Cape Town, South Africa, 2004, pp: 393-398